University of Rome "Tor Vergata"

Faculty of Engineering

Philosophy Doctorate in Learning and Sensor Systems Engineering

PERSON DEPENDENT AND INDEPENDENT THERMO HYGROMETRIC COMFORT SENSORS: STUDY, DESIGN, BUILDING, CALIBRATION AND TESTS

Tutor:
Prof. Paolo Coppa

Cotutor:
Ing. Carlo Andrea Malvicino

Candidate:
Ing. Gianni Pezzotti

December 6th 2004

Index

A. General Introduction

B. SENSOR OF INDIVIDUAL COMFORT

PERSON DEPENDENT AND INDEPENDENT THERMO HYGROMETRIC COMFORT SENSORS: STUDY, DESIGN, BUILDING, CALIBRATION AND TESTS.

A. General Introduction

The systems up today developed for surveying conditions of thermo hygrometric comfort generally give a unique total result involving all the comfort variable (e.g. Bruel & Kier Thermal Comfort Meter type 1212), or can measure single ambient variable independently, as air velocity (anemometer) , relative humidity (hygrometer), air temperature (thermometer) and mean radiant temperature (thermopile, or other radiation detectors).

Goal of the present work is to develop systems which can provide some comfort variables of people occupying the compartment of a vehicle, both individually and unprejudiced. Surely comfort conditions of vehicle passengers are much different from ones of people living in traditional environments (e.g. hall the hotel, rooms, classrooms, offices, etc), and even in defined particular ambient, as surgery departments and stay rooms in hospitals.

The two fundamental requirements above described correspond to the two different activities developed:

- First consists of realization of a sensor of individual comfort of passengers (driver or accompanying persons) in the car compartment. The prototype realized consists of a low temperature pyrometer used for measuring the skin of the forehead of the driver, attached to the rear view mirror;
- The second consists of a sensor of independent comfort to be used as an help to the test driver, able to supply during the same test independent information of three comfort variable: air temperature, mean radiant temperature and air velocity.

A1. General consideration about thermo hygrometric comfort

The complete description of the thermo regulatory control system of the human body is reported in the appendix 1. This constitutes the basis for every heat balance involving environment and human beings. Nevertheless the equations reported in appendix don't take into account local

discomfort, which is easy to be found in a small and full of air changes as the car compartment. In fact this is the reason of the difficulty in realizing a good thermal comfort regulation system in a car.

A2. Goals of the activity

The principal purpose of all the activity carried on is the realization of sensors for measuring variables governing the thermal comfort or thermal sensation itself. This corresponds to the two different devices studied, designed, realized, calibrated and tested:

1. Realization of a sensor of individual comfort of passengers (driver or accompanying persons) in the car compartment. The prototype realized consists of a low temperature pyrometer used for measuring the skin of the forehead of the driver, attached to the rear view mirror;
2. Realization of a sensor of independent comfort to be used as an help to the test driver, able to supply during the same test independent information of three comfort variable: air temperature, mean radiant temperature and air velocity

B. SENSOR OF INDIVIDUAL COMFORT

B.1.0 Introduction

The designed and built device is a pyrometer (containing an optical system, a mechanical support and a sensor radiation) to detect the comfort grade, from the forehead temperature of a passenger living in the compartment. It is specifically designed to measures the exitance of the infrared radiation emitted by the passenger forehead skin, taking into account that the human skin is an almost perfect blackbody perfect that emits the maximum possible radiation at a defined temperature.

Objective of the research is therefore to build a device of small size, in order to be installed inside a car, in a location where it can be easily focused on the passenger forehead skin. The best location to do so is the rear view mirror, where the realized instrument can be mounted and adjusted in a different way for each person. The forehead is the external part of human body with a more constant temperature, almost independent on the environment temperature (see paragraph A.1.). But internal temperature is considered by some authors [1][2] as dependent on the hot and cold sensations of the person.

The principal requirements for a so described individual comfort sensor are:

- Optical system with minimum dimensions, but enough high to guarantee good measurement accuracy,
- Measurement of infrared radiation in the wavelength range between 3 and 15 μm, which corresponds to the ambient temperature emission,
- Pyrometer target on the forehead, with an area of about 4 cm^2, and a working distance of about 375 mm (distance between the rear view mirror and the mean position the test driver forehead, datum supplied by the Fiat Research Centre).
- Range of measure temperature between 34 to 38°C, considering that the forehead temperature changes from 34 to 36 °C as T_{air} ranges between 22 and 35°C.

B.2.0 Optical System

The design of the optical system (used to convey the maximum possible quantity of radiation to the sensor) is based upon the specified requirements: mirror diameter of 50 mm, focal distance of 375 mm and magnification 0.1, in order to obtain a target of 20 mm x 20 mm being the sensor 2 x 2

mm^2. With the purpose of minimizing the spherical aberration, it has been decided to adopt an objective with an unique mirror aspherical(see figure 2). From an optical design the best solution resulted an elliptic shaped concave mirror, which by principle does not present this type of aberration.

Figure 1: Optical system

B.2.1 Characteristics of the mirror

The principal characteristic of mirror are the shape and the material: the elliptic concave mirror is made in aluminium, with reflecting surface coated with gold (see figure 6); for avoiding oxidation and increasing reflectance of radiation in the temperature range considered (20°C to 45 °C). The wavelength range of the detected radiations does not require a too high superficial finishing, but is enough the one obtainable with a good machining (about 0,5 μm).

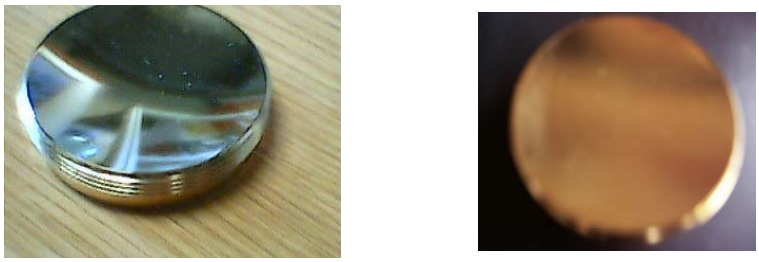

Figure 2: mirror

B.3.0 Radiation Sensor (Melexis thermopile)

General description of this device, its characteristics and performances and reported in appendix 2

B.3.1 Thermopile

For experimental two different thermopile types have been used, available from the IR sensor market. They were supplied by the two producers Cal Sensor and Melexis (see figure 3)

a. b.

Figure 3: Detail thermopiles: a Call sensor b. Melexis

Technical Data Thermopile "Cal Sensors": mod. TP-25, sensibility area 4 mm^2 and window of CaF_2 for radiation in field of wavelength between 0,2 to 11 μm. i.e figure 3a

Technical Data Thermopile "Melexis": mod. MLX90247D, sensibility area 4.81 mm^2, con FOV 100° and aperture diameter 3.5mm radiation in field of wavelength between 0,2 to 11 μm; with common mode connection for best protection of the thermopile. i.e figure 3b

B.3.2 Used Instrumentation for measurements

Data Acquisition Systems National Instruments (NI) DAQPAD MIO16X
Blackbody made Tor Vergata figure 4a
Dual blackbody source 2600 series -SBIC figure 4b
Bipolar Operational Power supply/Amplifier –Kepco 100V/1A
DC power Supply 40V/1A-PE1537 Philips
System amplification with battery alimentation
IR thermometer module Melexis MLX90601B

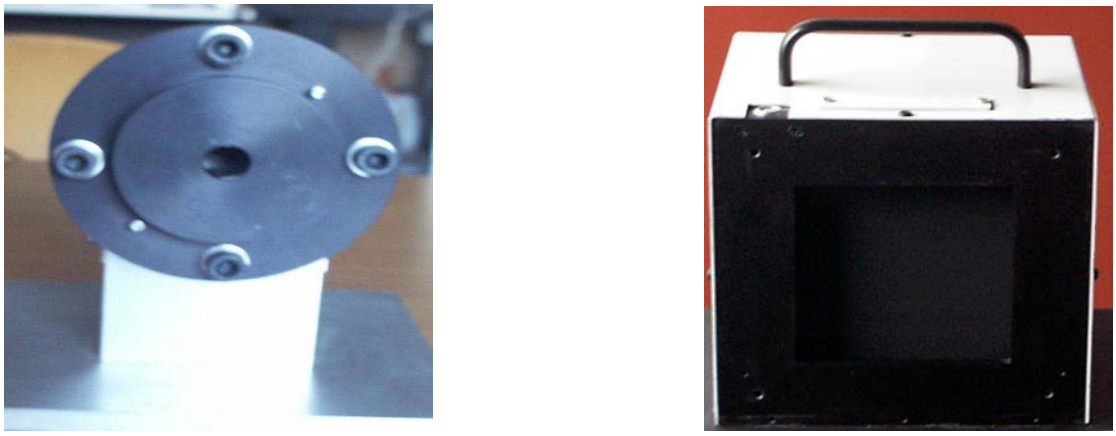

a. b.

Figure 4: blackbodies for measurements: a. Tor Vergata b. SBIC

B.3.3 Analysis thermopile

General procedure of signal measurement:

- Set blackbody temperature initially at 10°C to 60 °C, with 5°C steps.
- Recording of thermopile signal

In the figure 5 are represented the results.

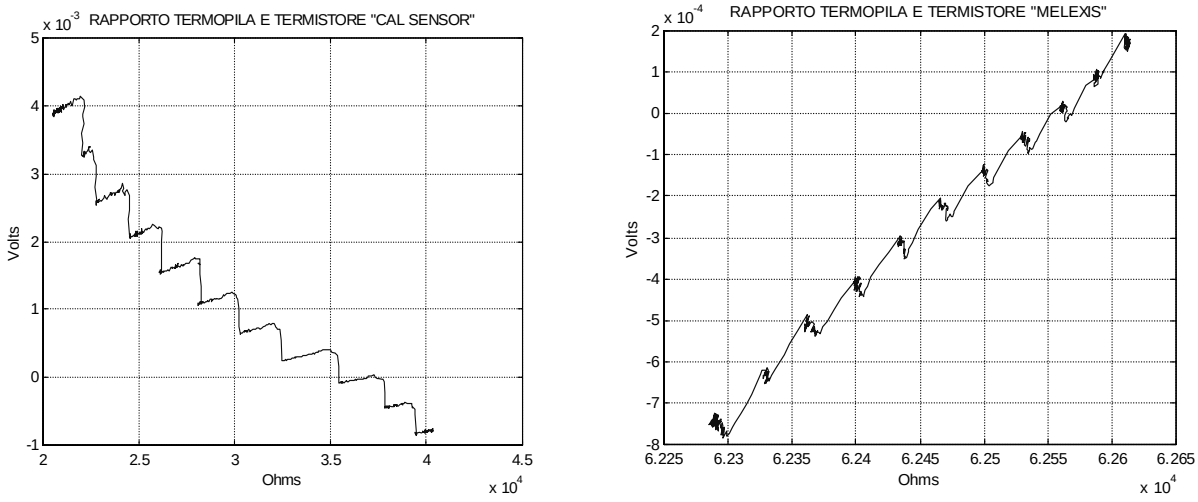

a. b.

Figure 5: Relation between IR signal and thermistor for different values of temperature a. Call sensors b. Melexis

B.3.4 Operational amplifier for thermopile

The gain($\Delta Vo/\Delta Vi$) for the Cal Sensor device is 1000 and for Melexis 10000; with operational amplifier OP-27 (see figure 6)

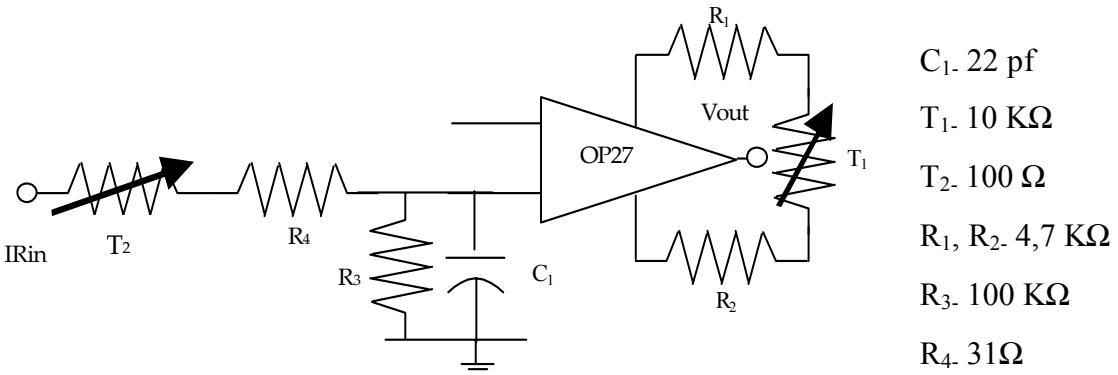

Figure 6: Amplification system

B.3.5 Calibration of the thermopile

The output signal of the thermopile is a function of its hot junction temperature (dependent on irradiance to the surface), and the one of the cold junction, that commonly is kept at ambient temperature. This last is measured with a thermistor inserted inside the thermopile. The relationship between temperature and resistance of the thermistor is given by the supplier.

In order to avoid signal variations due to ambient temperature fluctuations, it is possible either to maintain the sensor in a thermostatic environment, or to evaluate its influence through a proper calibration. This dependence is called cross sensitivity. In the present case this last solution has been adopted.

Calibration of the cross sensitivity has been carried out detecting the signal of the thermopile when irradiated only by the radiation of a blackbody (e.g. when it is located directly in front of a wide blackbody, with an area of 20x 20 cm^2 , see figure 7) and contemporarily changing the ambient temperature (through the hot air of the air conditioning plant or an auxiliary heat supplier). This operation has been repeated for the following temperatures of the blackbody: for the Cal Sensors TP 30°C, 33°C, 35°C, 37°C, 38°C, 40°C e 41°C, and for Melexis thermopile 35°C, 37°C, 38°C, 40°C, 41°C e 43°C.

The figure 8a and 8b present all the results: it is apparent that all regression lines for diverse black body temperatures present the same trend.

Supposing hence that the slope of the temperature signal versus the cold junction temperature be linear, and equal for the diverse temperatures of the hot junction, the best determination of the slope is carried on through a polynomial multiple regression, supposing the output signal S_T be linearly

dependent on the resistance of the thermistor R_{TM} , while the dependence on the blackbody temperature T_{BB} is supposed to be parabolic. That is the following model has been used:

$$S_T = b_0 + b_1 R_{TM} + b_2 T_{BB} + b_3 T_{BB}^2 \quad (1)$$

the parameters b_i are calculated through a least square multiple regression. Their values and uncertainties resulted:

$b_0 = -11.554 \pm 0.0891$

$b_1 = 4.875 \pm 0.0181$

$b_2 = 0.631 \pm 0.00502$

$b_3 = (-7.230 \pm 0.0689)\ 10^{-3}$

data standard uncertainties 0.019 V

the value b_1 represents the desired result. By it the correction of the signal is possible in order to obtain values independent on the cold junction temperature, and hence on the ambient temperature.

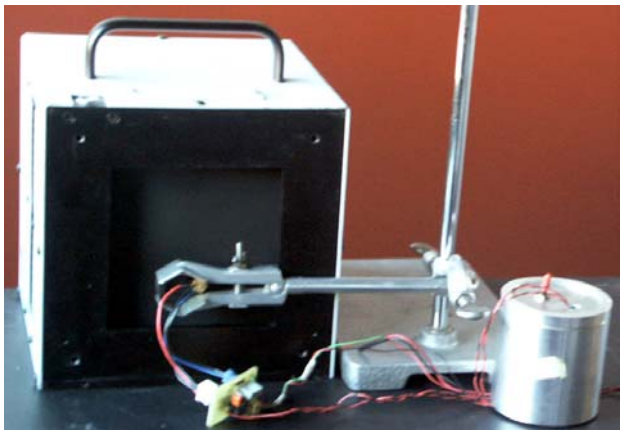

Figure 7: Calibration thermopile with blackbody

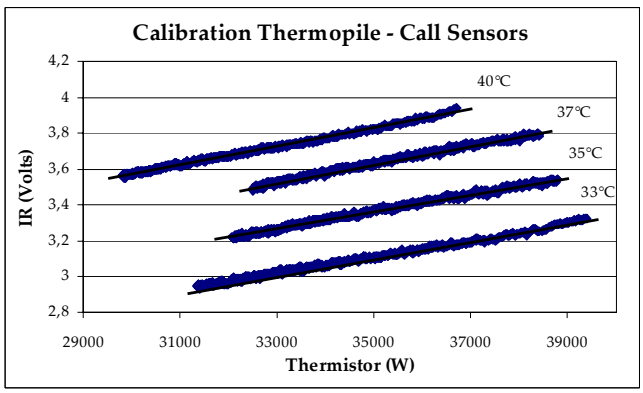

a.

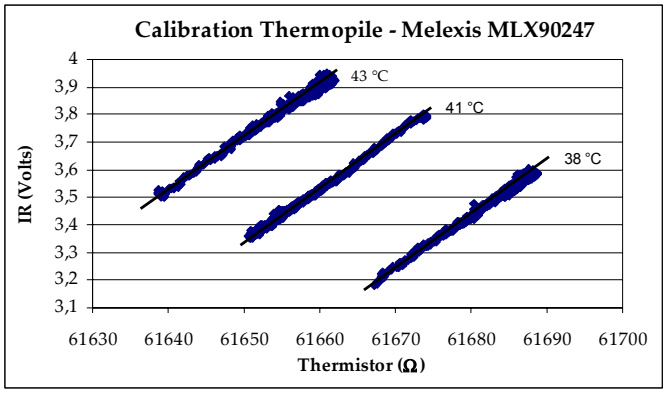

b.

Figure 8: Calibration thermopiles: a. Call sensors b. Melexis

It must be taken into account that other Melexis thermopiles are supplied with a chip able to directly compensate temperature with a chopper system. This automatic compensation has been verified with the same procedure adopted to evaluate the cross calibration just described

B.3.5 Thermometer module Melexis MLX90601B

General description of this device, its characteristics and performances and reported in appendix 2

B.3.6 Calibration thermometer module Melexis MLX90601B

Calibration of these two devices (thermopile integrated with chip for acquisition feeding and processing) has been carried out with the same procedure above described, i.e. multiple linear regression of thermopile signal versus black body temperature and ambient temperature as measured by the thermistor resistance. Results are reported in fig. 9. It appears immediately that no or little dependence of results on ambient temperature exists, indicating a good performance of the compensation algorithm used by the chip.

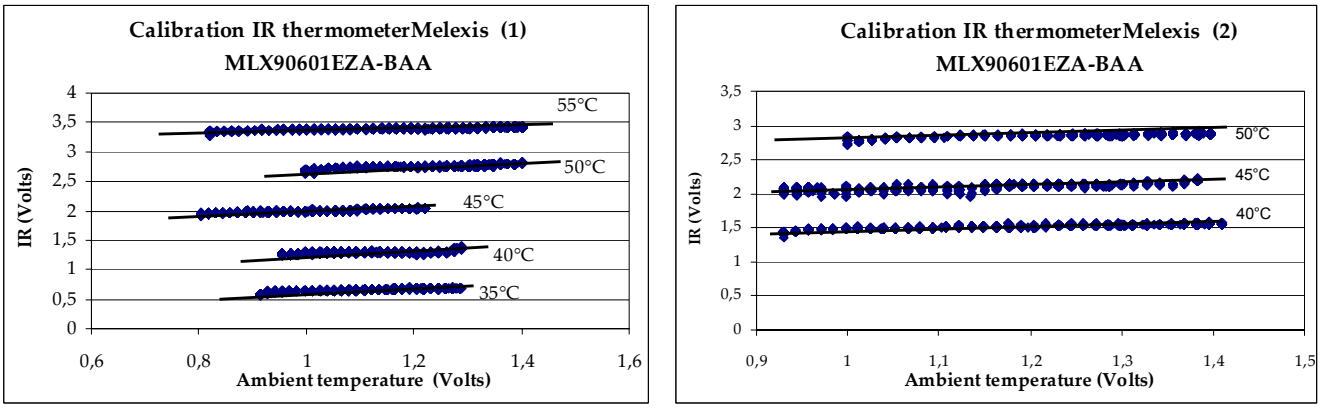

a. b.

Figure 9 : Chip Melexis MLX90601B: a. Calibration of chip 1 - b. Calibration of chip 2

Results of the multiple regression are, using again relation (1):

b_0 = -1131.52 ± 2.654

b_1 = (-1.846 ± 0.00411) 10^{-2}

b_2 = -0.344 ± 0.00784

b_3 = (6.329 ± 0.0951) 10^{-3}

prevision uncertainty of data = 0.00792 V

B.3.7 Alternative tests on thermometer module Melexis MLX90601B

Further tests have been carried out to verify the temperature compensation of this chip, sketched in figure 10 a.

Fig. 10 b report the results obtained in the test: output signals of the chip are the thermopile values and the ambient temperature. Thermopile was locate just on the aperture of a blackbody designed and realized by the Heat Transfer and Thermal Measurement laboratory of the University of Rome "Tor Vergata". Working range of this black body was 30-60°C. The test consists in changing the blackbody temperature and contemporarily perturbing ambient temperature, e.g. directing a heater just on the chip. In fig. 14 b the yellow line is the ambient temperature as measured by a type E thermocouple, and the black one is the signal of the thermistor (in V): clearly they appear strongly correlated. On the contrary the line red (thermopile signal, in V) is correlated to the blue line (type J thermocouple control of the blackbody). As a conclusion, the compensation algorithm provided by the Melexis chip appears quite good.

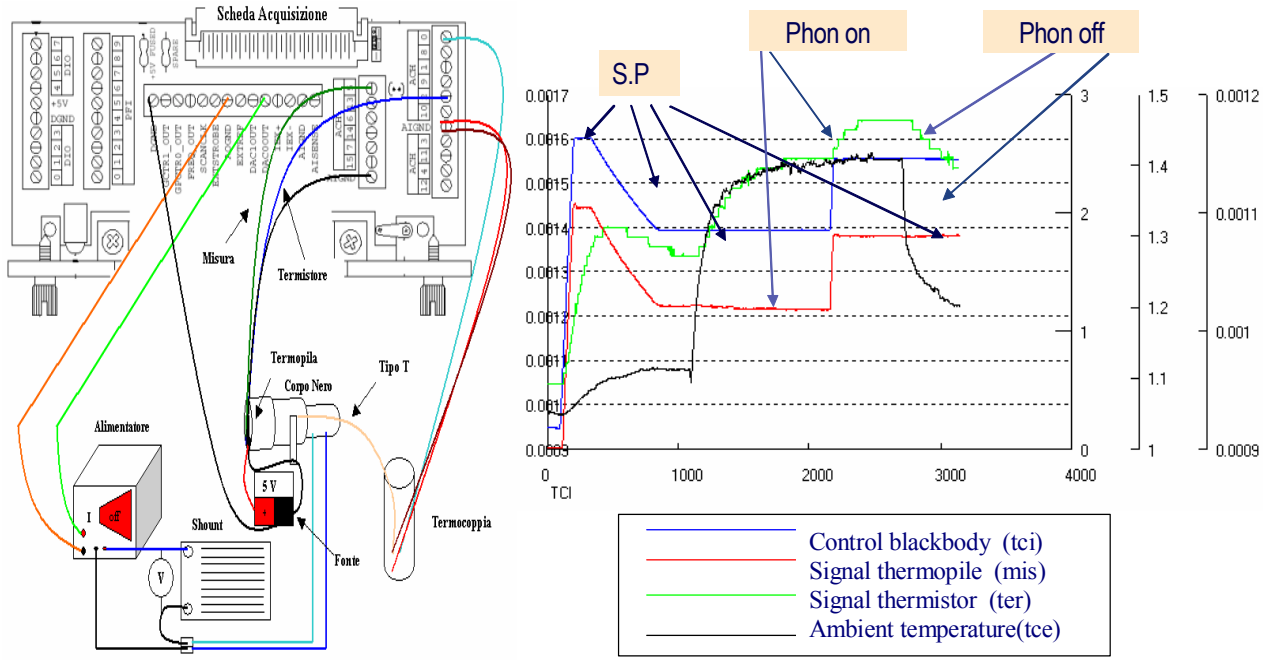

a. b.

Figure 10: Alternative Test: a. Measurement circuit b. Graphic of results

B.4.0 Tests on the pyrometer for measurement of the forehead skin temperature

B.4.1 Description

The optical system is made in order to condense the maximum quantity of infrared radiations in the sensor. Figure 11 illustrates the target distance(from pyrometer 337mm) with an imagine obtained of 20x20m.

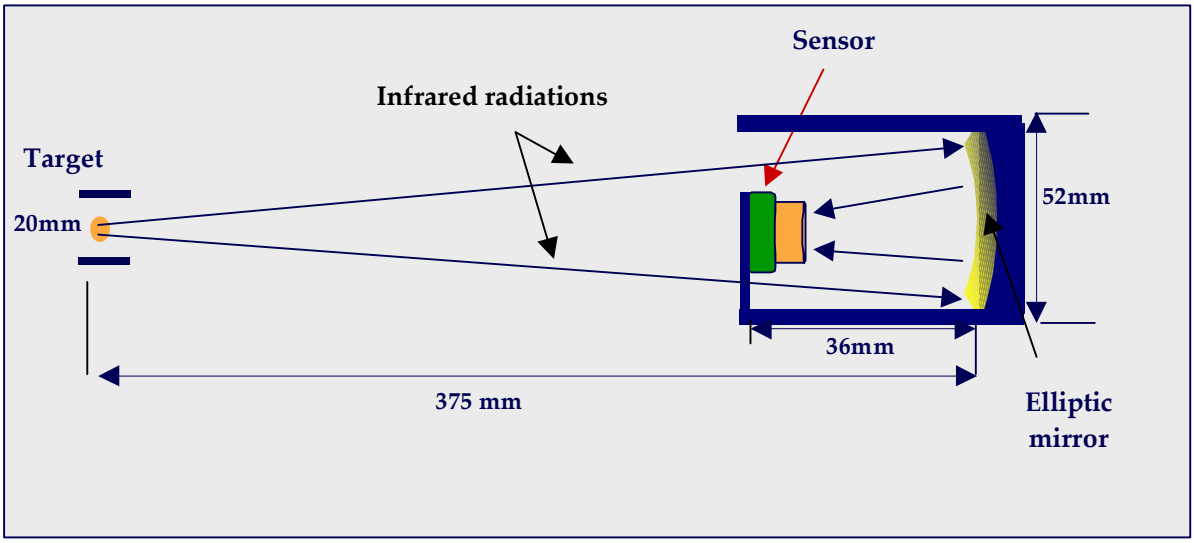

Figure 11: Operation pyrometer

B 4.2 Pyrometer with thermopile and amplification system

Figure 12 illustrates the pyrometer (see paragraph 4.1) and the amplification system using as thermopile of the Call Sensors firm (see paragraph B.3.4 and B.3.5)

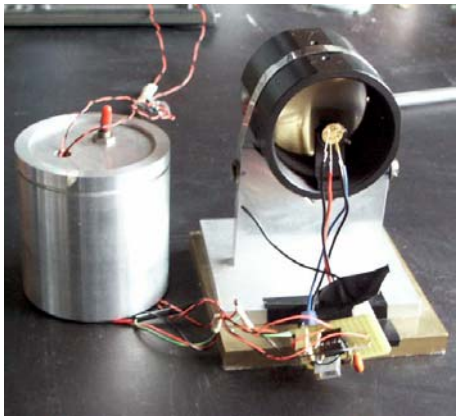

Figure 12 : Pyrometer with thermopile Call sensor

B.4.2.1 Used Instrumentation for measurements

Data Acquisition Systems: National Instruments (NI) DAQPAD MIO16X

Dual blackbody source 2600 series –SBIR

System amplification with battery alimentation

B.4.2.2 Pyrometer calibration

The first calibration tests have been realized by the above described pyrometer, using the Call Sensor thermopile as detector. Tests have been carried out at different distances between blackbody and detector, in order to verify if the pyrometer could give results independent on the ambient temperature radiation. Effectively no difference were found between tests at different distances between 1.3 m and 0.3 m .

Results of multiple regression on tests with variable ambient temperature, using the same equation previously applied are:

$b_0 \pm s_{b0}$= -2.653 ± 0,0396

$b_1 \pm s_{b1}$= (1.396 ± 0,00133) 10^{-4}

$b_2 \pm s_{b2}$= (-6.22 ± 0,221) 10^{-2}

$b_3 \pm s_{b3}$= (3.809 ± 0,0319) 10^{-3}

prevision uncertainty of data = 0.0209 V

the calibration results are reported in figure 13

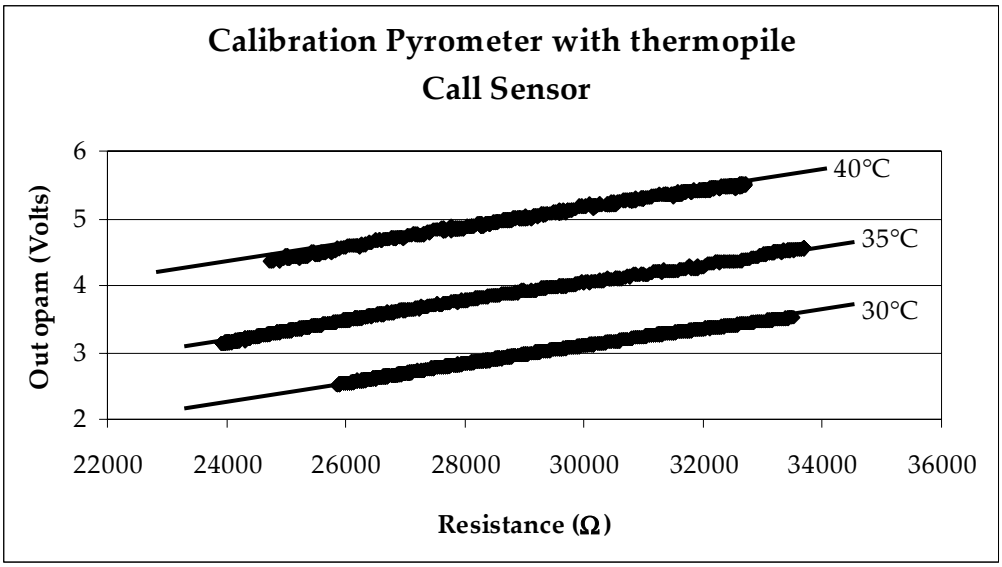

Figure 13: Calibration results

It must be noted that calibration of pyrometer takes contemporarily into account the effect of both ambient temperature on thermistor and ambient radiation on the detector. In fact the detector is also hit by radiation coming from the inside of the pyrometer body, due to FOV which is wider than the angle subtended from the mirror to the sensor. Besides, also the not perfect reflectivity of the mirror

could increase the influence of ambient temperature radiation on the detected signals. Anyway the cross calibration takes into account all the previously listed factors.

B 4.3 Pyrometer Melexis MLX90601B

The pyrometer with the detector (integrated in an electronic chip) considered the most suited for the applications, as dimensions and versatility, is shown in Fig. 14 (see paragraph 4.1). The represented chip is the Melexis MLX90601B (see appendix 3 for a description of characteristics, performances and working)

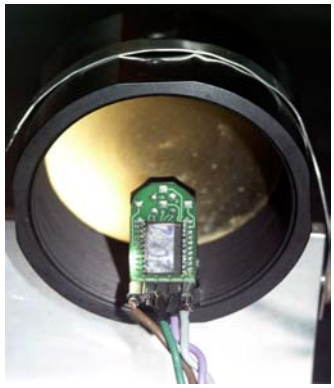

Figure 14: Pyrometer Melexis MLX90601B

B.4.3.1 Used Instrumentation for measurements

Data Acquisition Systems: National Instruments (NI) DAQPAD MIO16X
Dual blackbody source 2600 series –SBIR
DC power Supply 40V/1A-PE1537 Philips
IR thermometer module Melexis MLX90601B

B.4.3.2 Pyrometer calibration

The calibration tests have been realized for the pyrometer, using the thermometer module Melexis MLX90601B as detector. Tests have been carried out at change ambient temperature between 17÷26°C with set temperature blackbody at 55 °C and chip, in order to verify if the pyrometer could give results independent on the ambient temperature radiation. the calibration results are reported in figure 15

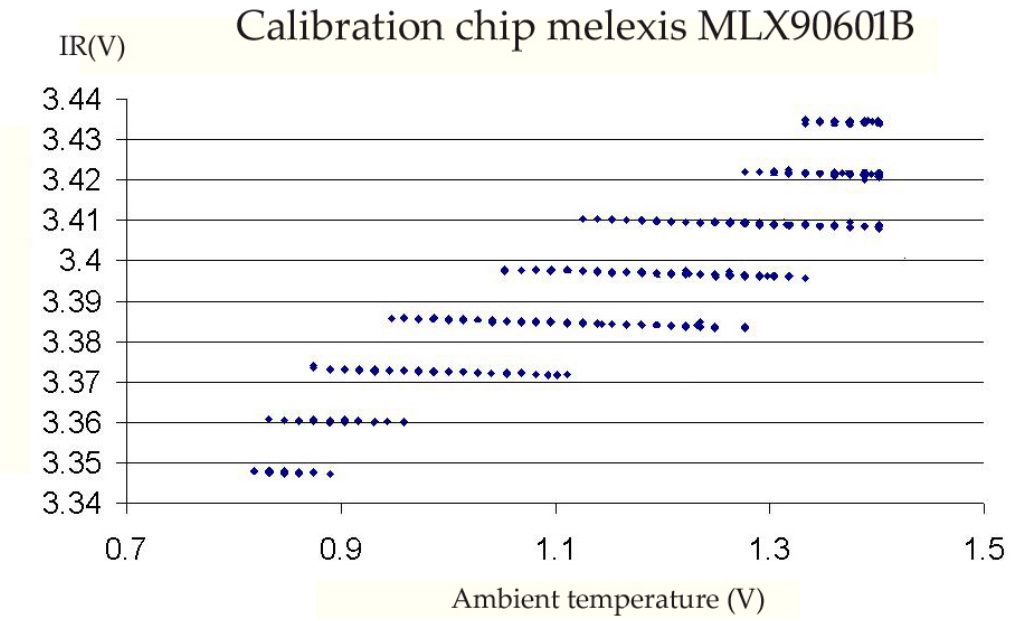

Figure 15: Calibration chip Melexis

This chip has a working range, supplied by the producer, of 30÷55 °C. Taking into account that the measurement range of the skin is 33÷37 °C, the working range as supplied is too large, resulting in an output lower than 0.5 V. This is the reason why it has been decided to use the other chip (the programmable one).

B.4.4 Pyrometer using programmable Melexis MLX90601KZA-BKA as detector

General description of this device, its characteristics and performances and reported in appendix 4

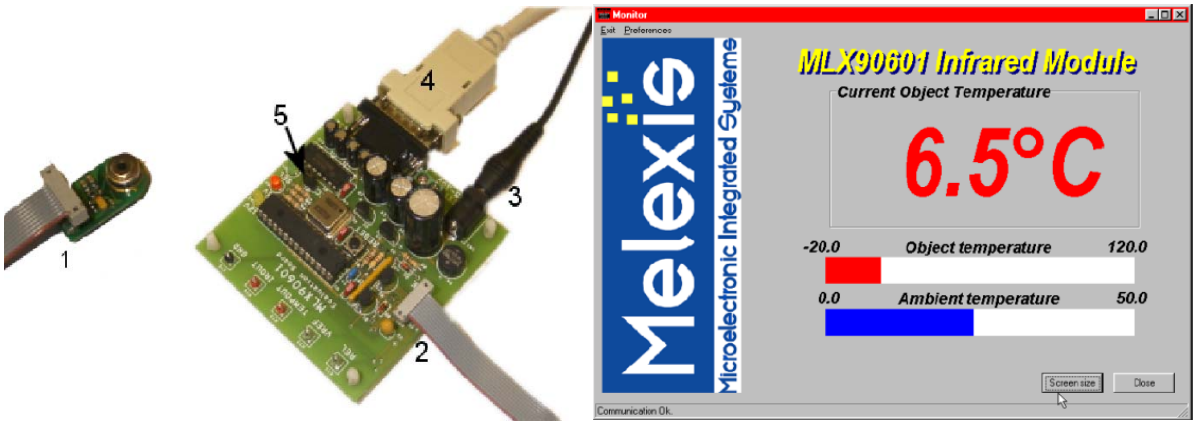

Figure 16: the Melexis MLX90601KZA-BKA: a. Board connection b. Software for visualising

B.4.4.1 Used Instrumentation for measurement

Dual blackbody source 2600 series –SBIR

Evaluation board V2 MLX90601 (Appendix 5)

B.4.4.2 Pyrometer calibration

An overall calibration of the pyrometer has been carried out , taking into account, as previously described, all the sources of influence of ambient temperature (cold junction of the thermopile, too wide FOV of the sensor, and non perfect reflectivity of the gold coated mirror). I.e. the pyrometer has been focused on the black body at variable temperature, and the signal has been recorded trying to keep ambient temperature as constant as possible.

Figure 17 reports the results of these tests. Taking into account that a relationship

$S_{pyr}=f(T_{bb},\ T_a)$

exists between the three quantities, $S_{pyr,}$ $T_{bb,}$ and T_a being the variables

Spyr Target Temperature - signal of thermopile

T_{bb} BlackBody Temperature

T_a Ambient Temperature – signal of thermistor

This relationship has been evaluated again phenomenologically by a lest square polynomial (2° order) multiple regression, i.e.

$$S_{pyr} = B_1 + B_2 \cdot T_{bb} + B_3 \cdot T_a + B_4 \cdot T_{bb}^2 + B_5 \cdot T_{bb} \cdot T_a + B_6 \cdot T_{bb}^2 \cdot T_a \qquad (1.1)$$

In order to get the black body temperature from the pyrometer signal and the ambient temperature, the previous equation must be inverted, i.e. :

$$S_{pyr} = (B_4 \cdot T_{bb}^2 + B_6 \cdot T_{bb} \cdot T_a^2) + (B_2 \cdot T_{bb} + B_5 \cdot T_{bb} \cdot T_a) + B_1 + B_3 \cdot T_a \; ; \qquad (1.2)$$

$$0 = T_{bb}^2 \cdot (B_4) + T_{bb} \cdot (B_2 + B_5 T_a + B_6 T_a^2) + B_1 + B_3 \cdot T_a - S_{pyr} \; ; \qquad (1.3)$$

$$T_{BB} = \frac{-(\mathrm{B2} + \mathrm{B5\,Ta} + \mathrm{B6Ta}^2) \pm \sqrt{(\mathrm{B2} + \mathrm{B5\,Ta} + \mathrm{B6Ta} + \mathrm{B6Ta})^2 - 4 * (\mathrm{B4} + \mathrm{B6Ta}) * (\mathrm{B1} + \mathrm{B3} * \mathrm{Ta} - \mathrm{Spyr})}}{2 * (\mathrm{B4})}$$

$$T_{BB} = \frac{3.3002 - 0.4325\,\mathrm{Ta} \pm \sqrt{(-3.3002 + 0.4325\,\mathrm{Ta})^2 + 4 * (0.02986 + 6.2029\mathrm{E}-03\mathrm{Ta}) * (128.194 - 7.8578 * \mathrm{Ta} - \mathrm{Spyr})}}{2 * (-0.02986 - 6.2029\mathrm{E}-03\mathrm{Ta})}$$

(1.4)

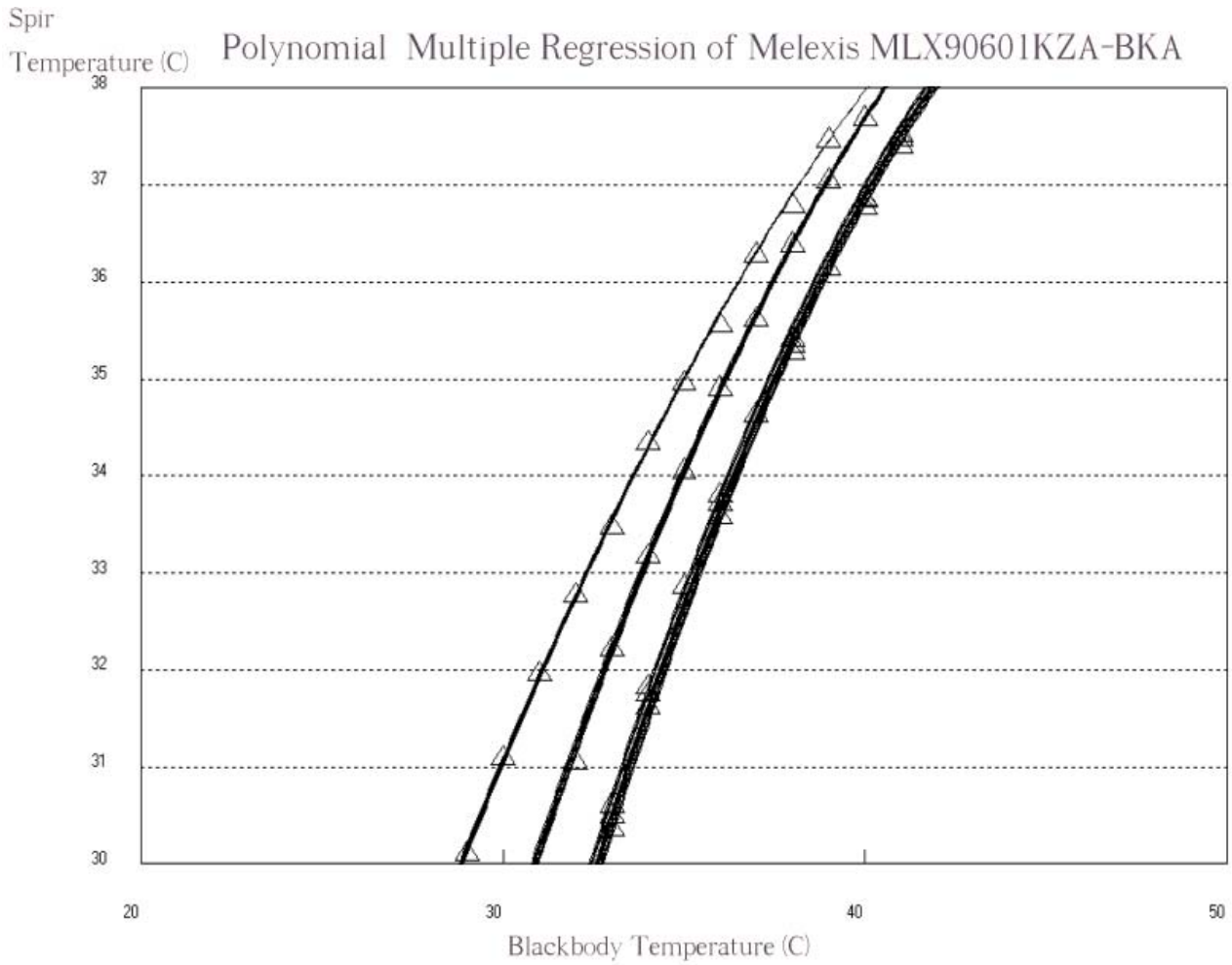

Figure 17: Multiple regression

In Fig. 17 the curves obtained (at different T_a) are plotted as $S_{pyr,}$ versus T_{bb}.

Parameter evaluation by least square algorithm leads to the following results:

- $B_1 \pm \Delta B_1 =$ *128.19 ±5.39*
- $B_2 \pm \Delta B_2 =$ *-3.30 ±0.41*
- $B_3 \pm \Delta B_3 =$ *-7.86 ±0.37*
- $B_4 \pm \Delta B_4 =$ *-0.03 ±2.1E-03*
- $B_5 \pm \Delta B_5 =$ *0.43 ±4E-02*
- $B_6 \pm \Delta B_6 =$ *(-6.2 ±.84) E-03*

with a prevision uncertainty of data of 0.081V, and a corresponding temperature uncertainty of 0.15°C.

B.4.5 Pyrometer preliminary tests

Preliminary test on the pyrometer are shown in fig.18. The radiation source (forehead skin of several people, as the one in figure) has been placed between 375mm to 400mm, and according to the optical design , the detected area ranged between 20x 20 mm^2 and 25x25 mm^2. Anyway it was possible to detect the forehead skin temperature.

Figure 18: Preliminary test

B.5.0 Experiments inside the vehicle

When the pyrometer was mounted on the rear view mirror, it appeared immediately that the working distance declared by the Fiat Research Centre was not suited to the car under test (FIAT Nuova Panda). So it was necessary to mount the device 10 cm far from the mirror, by means of suited extension bars (Fig. 19). A distance of 475 appears more suited to the effective driving style of the major part of drivers.

a. b.

Figure 19: Pyrometer on the rear view mirror: a. Pyrometer b. Pyrometer with extension bars

B.5.1 Used Instrumentation for measurement

Circuit for alimentation in the car
Evaluation board V2 MLX90601

B.5.2 Experiment results in winter

Winter experiments have been carried out with a group of people of different sex , during the month of February in the following conditions:

Figure 20: Test Fiat Nuova Panda

- Used vehicle: Fiat Nuova Panda version 2004 (kindly put at disposal by the FIAT agency in Rome, ROMANA Auto, owner Prof. Tavernese)
- Pyrometer installed on the rear view mirror of vehicle (Fig. 19)
- Sample of 18 people (13 men and 5 women)
- Calibration range of the programmable chip Melexis MLX90601KZA-BKA , for forehead temperature: 30-40°C
- Working temperature range of the pyrometer (different from the previous value as suggested by the Melexis testing procedure): temperature forehead (33.5 to 38.5°C) ; ambient temperature range as measured by the thermistor: 0°- 40°C

During the winter 2004 different comfort conditions aboard of a vehicle were tested on a group of people instructed to give an information of their hot-cold feeling according to the Fanger list (-3

very cold to +3 very hot, 0= neutral). Changing the inside temperature using the manual air conditioning regulation, the driver gives a personal judgment inherent the felt comfort expressing a vote between +3 and -3. This would result in the so called DMV (declared mean vote)

For each vote expressed by the driver all information, shown in figure 21, are recorded by the pyrometer for 15 consecutive seconds. It is also possible to set this recording time for longer time.

The range time that elapses between cooling/heating of the vehicle and the following cold/hot sensation felt by the driver, defined *acclimatization*, could be a problem. In fact the battery level of the laptop (Pentium IV) is limited to 50 minutes maximum and it is possible to make only two tests for each person. Another drawback could be the traffic density in Rome during the tests and the great number of the data that the Melexis EEPROM sends to the laptop.

During the working of the Melexis program (figure 21), the ambient temperature, labelled with T_a the acquired data and forehead temperature of the driver, labelled with T_{obj}, are continuously sent to the computer and visualized. The acquisition card makes an auto-check to verify that everything works well (confirmed by what is written at the end of the data file, see Fig. 21).

Even if during the test time (15 s) T_a could be considered , T_{obj} can change(for example in a test it varied between 34.32°C and 35.22°C).

This variation of recording demonstrates that it is very important that the driver forehead should be steady. But this request is impossible for a good and safe driving. In fact the thermopile during the motion of the driver head detects the emission from any parts of the its face: the nose, with a temperature lower of 3°C compared to the forehead temperature [13], or from the eyes whose temperature is very near to the internal one. Besides, eye temperature of people wearing glasses results much lower.

A possible ideal control system [17] could involve a device for *objective following* (in this case represented by the forehead of the driver) or an algorithm that takes in account only data with highest values, corresponding to the correct pointing of the pyrometer.

Martedi 20 gennaio 2004
ora 9:45

Nome: Ivano P.
Maschio (bianco) 30 anni

Prove fatte -> (-3,-1,-2;0,1,2,3)
Cambio Velocità ->[(-1) (+1)]

Livello Comfort 1

****** Measuring Module 13952 ******

Detected IR offset in EEPROM: 21364
Detected ambient offset in EEPROM: 2684

Time	TOUT	Ta	IROUT	Tobj	OVH	OVL	FE
0000000.000	1546	15.10	736	34.40	N	N	Y
0000001.192	1546	15.10	1410	35.22	N	N	Y
0000001.933	1545	15.09	1166	34.92	N	N	Y
0000002.674	1546	15.10	1176	34.94	N	N	Y
0000003.415	1545	15.09	1109	34.85	N	N	Y
0000004.156	1546	15.10	1207	34.97	N	N	Y
0000004.897	1545	15.09	675	34.32	N	N	Y
0000005.638	1546	15.10	1370	35.17	N	N	Y
0000006.379	1546	15.10	1271	35.05	N	N	Y
0000007.120	1545	15.09	1113	34.86	N	N	Y
0000007.861	1546	15.10	1128	34.88	N	N	Y
0000008.602	1546	15.10	671	34.32	N	N	Y
0000009.343	1546	15.10	921	34.62	N	N	Y
0000010.085	1546	15.10	1056	34.79	N	N	Y
0000010.826	1545	15.09	1002	34.72	N	N	Y
0000011.567	1545	15.09	1324	35.12	N	N	Y
0000012.308	1545	15.09	1201	34.97	N	N	Y
0000013.049	1545	15.09	1055	34.79	N	N	Y
0000013.790	1546	15.10	1044	34.77	N	N	Y
0000014.531	1545	15.09	1167	34.92	N	N	Y
0000015.272	1545	15.09	894	34.59	N	N	Y

Module 13952: control measurements completed successfully

Figure 21: Results data

To avoid this trouble in our tests the driver has been forced to drive in straights and without difficulties roads. Moreover during the data elaboration (see figure 22) only data in a defined temperature range were taken into account. In evaluating the mean forehead temperature, only the values that didn't change more than 0.3°C one each other about are counted.

A first filtering of data is carried on: for instance in Fig. 22 an ideal range, between 34.8°C and 35.1°C, is considered.

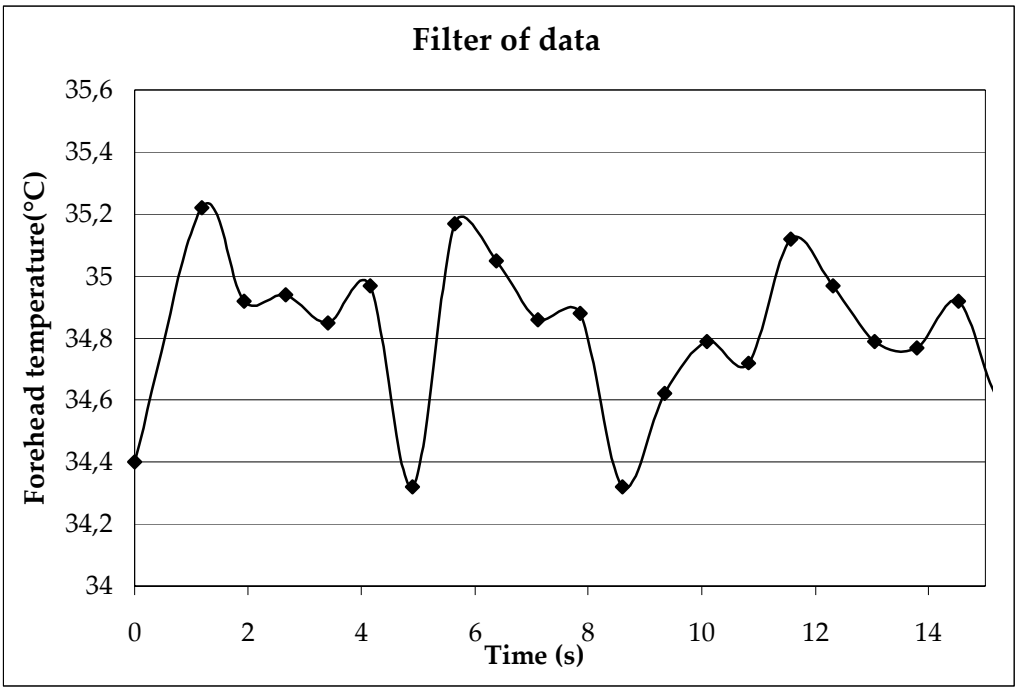

Figure 22: Filtering of data

First acquired data are processed with equation 1.4 in order eliminate the avoid ambient temperature influence. Than different plot have been shown in order to search a correlation between variables. From the analysis of all data, for the winter case, the following consideration can be deduced:

- Analysis of the declared medium vote (DMV) vs ambient temperature: in figure 23 the positive trend is evident, indicating an increment of the DMV as the ambient temperature increases. This is a trivial result, because logically the perception of very hot to very cold depend from ambient temperature. But the shown results indicate also the spreading of data about this correlation

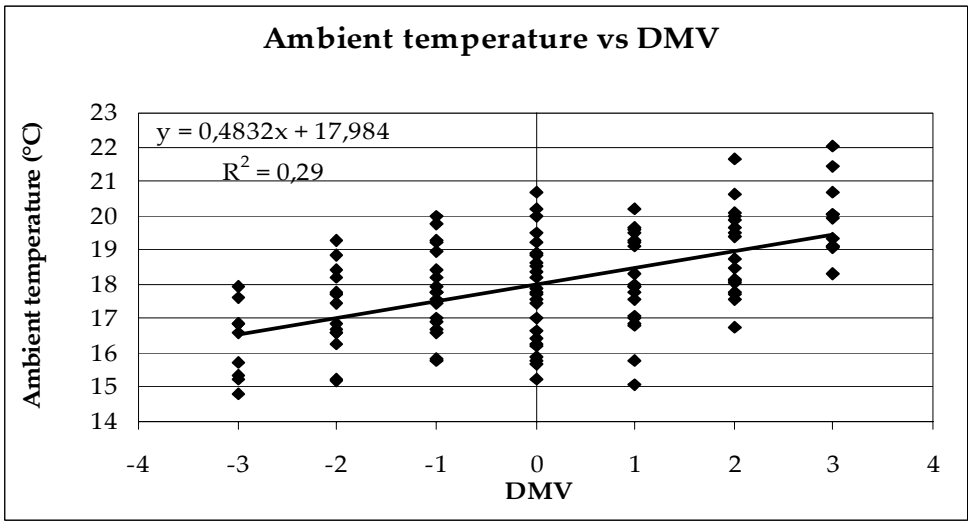

Figure 23: Ambient temperature vs DMV

- Data of the forehead temperature versus DMV (Fig. 24) don't show any trend, that is it is not possible to evidence any correlation between DMV and forehead temperature.

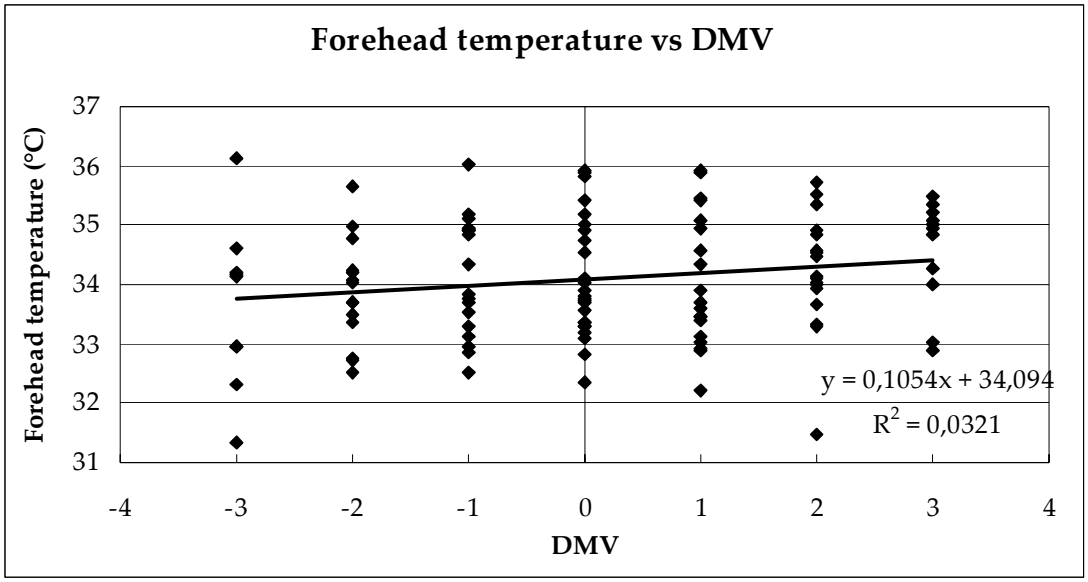

Figure 24: Forehead temperature vs DMV for winter tests

- No dependence of the ambient temperature on the forehead one(see figure 25), is verified.

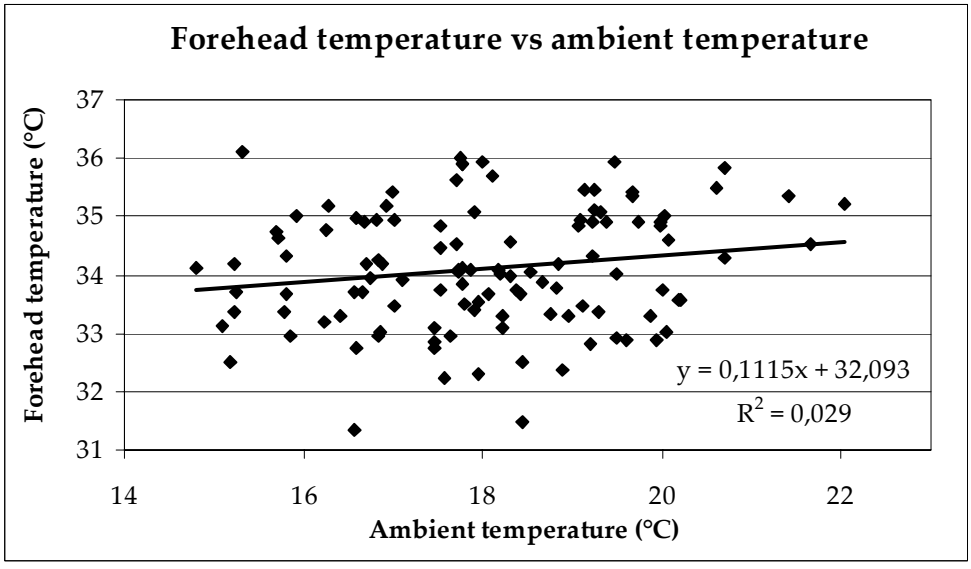

Figure 25: Forehead temperature vs ambient temperature for winter tests

- The correlation between the ambient and the forehead temperature does not exist even at constant DMV (e.g. in figure 26 the same behaviour is reported with DMV=0, but the same condition happens for all the other DMVs).

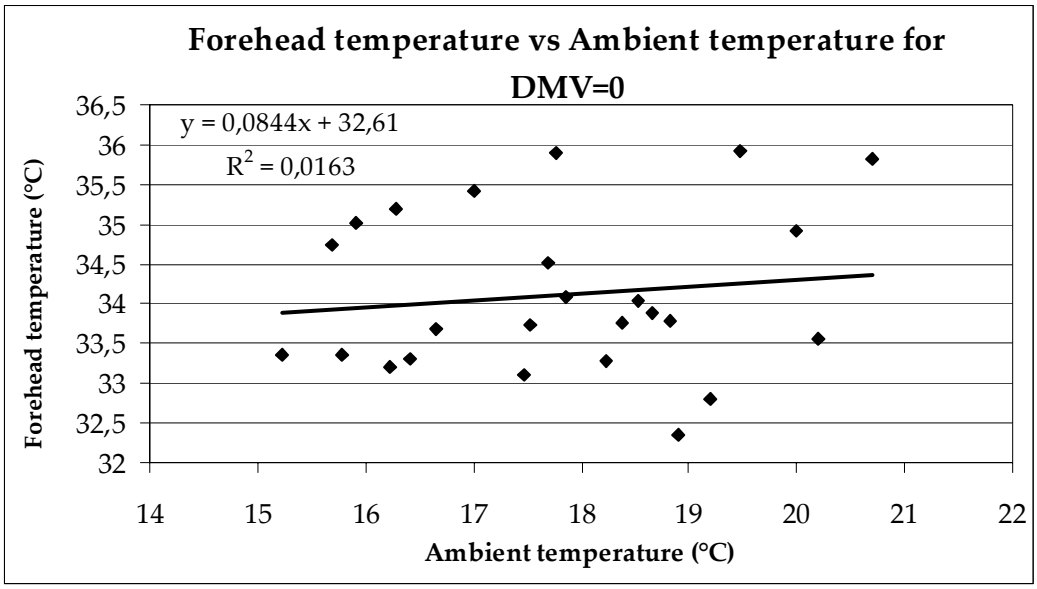

Figure 26: Skin temperature vs. ambient temperature at DMV=0(comfort)

B.5.3 Experimental results in summer

Other experiments have been carried out during summer on a different group of people, with different sex. Tests were carried out during the month of June 2004, which resulted particularly hot. In the following, the characteristics of the performed tests are listed:

Figure 27: Test Fiat Punto

- Used vehicle: Fiat Punto Multijet version 2004 (from Romana Auto)
- Pyrometer installed on the rear-view mirror of vehicle
- Sample of 20 people (14 males and 6 femmes)
- Calibration of the programmable chip Melexis MLX90601KZA-BKA: 25-40°C (forehead temperature)
- Pyrometer working range (different from the previous value as prescribed by Melexis test procedure); forehead temperature: 30 to 38°C and ambient temperature: 0°- 40°C.

As a first consideration, the flux of the air conditioning system caused an effect in the skin temperature: when the skiing is invested by the air flow, the transpiration increases. Hence the test has been realized in two different conditions: with the air flux directly in the face of the driver or in upward direction.

- Both in the case when the air is in the upward direction, toward the compartment ceiling (figure 28a), and when the flux air is directed in face of the driver (figure 28b), no correlation between the DMV and the forehead temperature was found. The same situation as the winter case resulted.

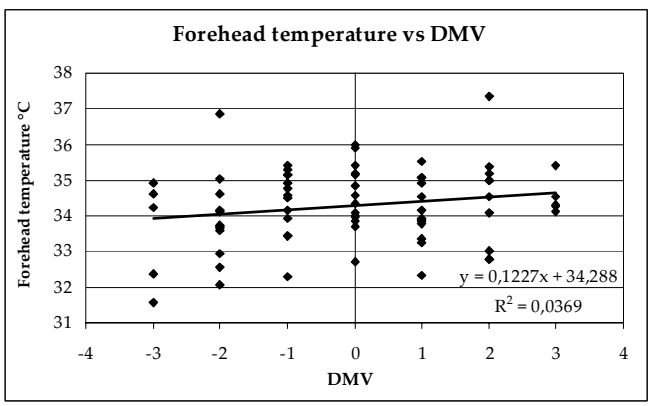

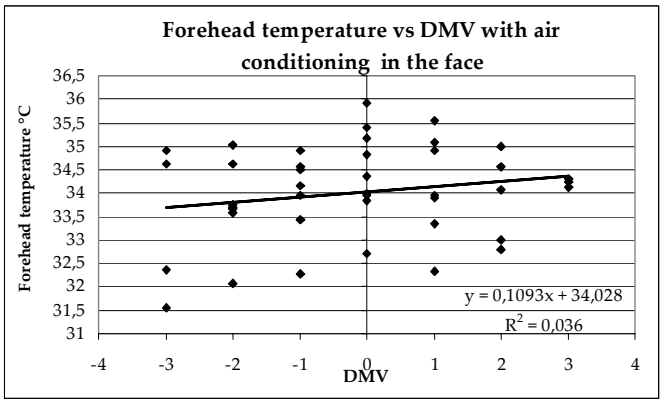

a. b.

Figure 28: Summer results: a. Forehead temperature b. With air conditioning

- Contrarily to the winter case, in the summer case a correlation between forehead skin temperature and ambient temperature can be found. Clearly this correlation must be searched only at fixed comfort feeling. Fig. 29 shows this condition for DMV=0 (comfort condition). Similar results have been obtained in both cases: with air flux on the driver face and without.

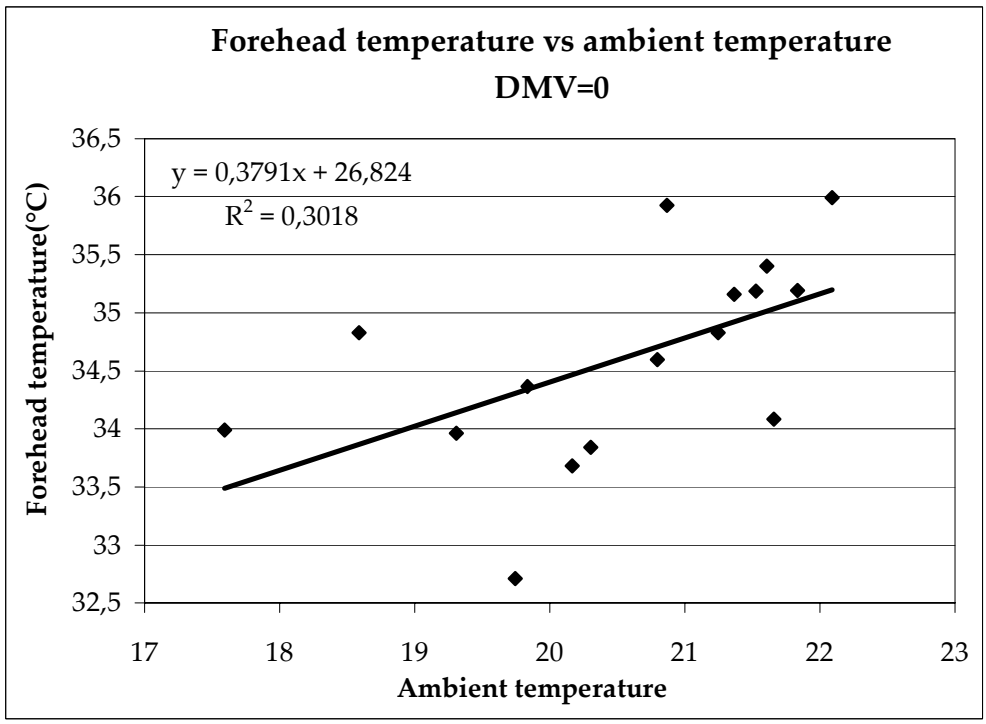

Figure 29: Skin temperature vs. ambient temperature at DMV=0(comfort)

- In agreement with using of Fanger theory (for which a PMV between +1 and –1 can be allowed), even if the ambient temperature is the same, the DMV can vary between +1 ÷ –1

(e.g. figure 30). The example reported in the figure was carried out at a ambient temperature ranging between 20.8°C and 20.9°C. The same consideration holds for all the made tests.

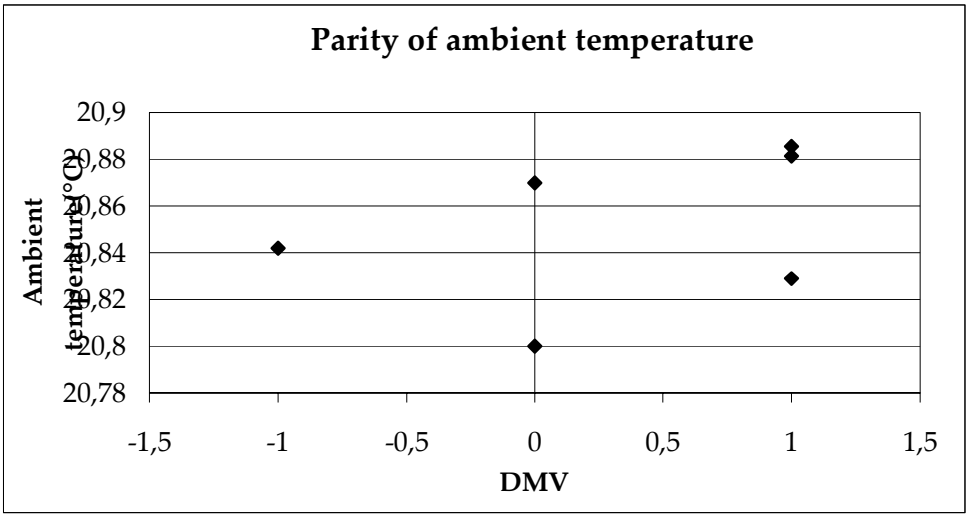

Figure 30: Dispersion of DMV at almost equal ambient temperature.

- Also for what concerns forehead temperature, at quasi constant ambient temperature a dispersion appears of about 3 °C, always with DMV ranging from –1 and +1.

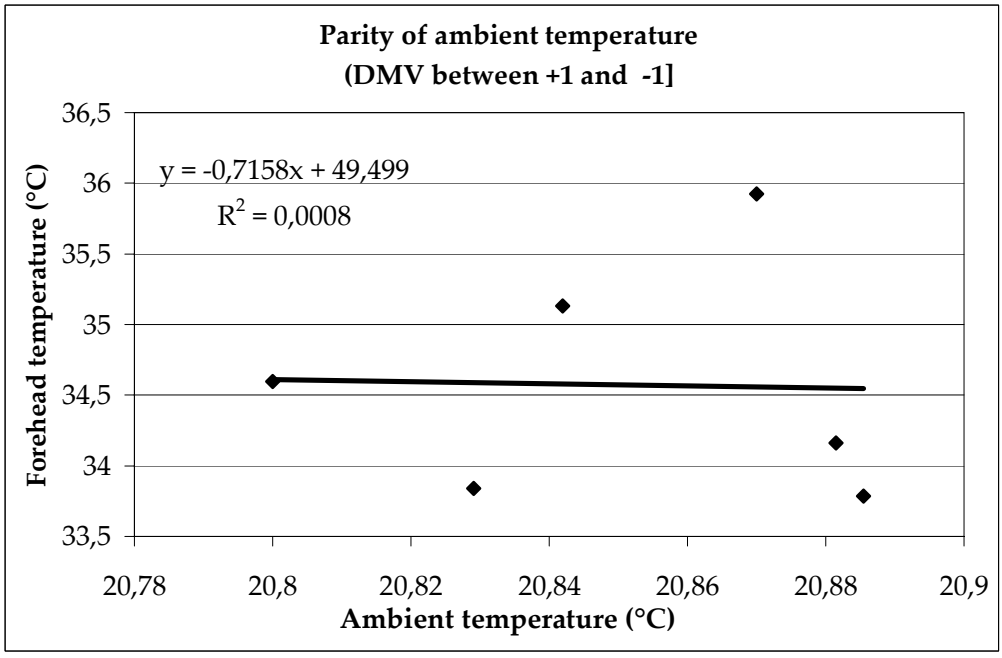

Figure 31: Forehead vs ambient temperature, at quasi constant ambient temperature, with (DMV between -1÷+1)

B.5.4. Affinity and difference between winter and summer tests

Naturally the mean ambient temperature in the vehicle changes according to the season.

Comparing data in figures 24 and 28, both in comfort conditions, the average value of forehead temperature results about 34°C in winter, and . 34.4°C or 34.2°C.in summer without or with air in the driver face.

Therefore this test demonstrates that the temperature of the skin of a person, subjected directly to external air currents, is function of the air flux. This effect has been studied (in 1992) by Japanese researchers (for example Taniguchi, Aoki and Tanaka [7]) which estimated the temperature variation on the lay simulating the skin of a manikin subjected to strong hot/cold air fluxes with velocities that reached 60 Km/h.

After these considerations, the average forehead temperature can be considered quasi constant at a value of 34°C. Note that this temperature is some degrees lower than the rectal one (internal body temperature) that in general is considered about 37°C (this value is reported in figure 1 in the appendix 1, Fig. 1).

From the data analysis. we notice that there is not a correlation between the skin temperature and comfort level, and it is not possible to establish a general rule, at least taking into account the number of the examined people.

Naturally there is a correlation between the comfort level and the ambient temperature in which the driver is living.

A peculiarity in the relation that links the T_a with T_{obj} on equal DVM is highlighted analysing the recorded data. While in summer tests there is a good correlation between the two temperatures (T_{obj} increase with the growth of T_a) in the winter tests this correlation disappears.

To explain this it is necessary to consider that the human body releases heat through the effective thermal exchange and the perspiration.

As mentioned in the introduction, the fundamental elements to give an interpretation to this behaviour are:

- The $\Delta T = T_{obj} - T_a$;
- The skin transpiration that improves the heat release.
- The vasoconstriction that happens when the ΔT is enough high, and decreases the temperature of skin in in winter
- The vasodilatation, which increases the skin temperature increasing the heat transfer to the air, if air temperature is lower of the body temperature.

It is necessary to note that in the winter we have to consider the thermal resistivity of the clothes I_{cl} also to perspiration, while in summer the body surface is more exposed to the air. In summer I_{cl} is equal to 0.5 [1] (this value could increase if the person sweats) , that is the clothes are lighter and both the transpiration and the thermal heat transfer takes advantage [19]. That results in an efficiency in increasing heat transfer from the body to the air with increasing the skin temperature, at least till when skin temperature is higher than air temperature.

In winter the body exposition is reduced, and the I_{cl} is between 1 and 2 for temperate weather [2]. In this case the transpiration is obstructed, because of the thickness of clothes. Consequently the thermal heat transfer is more difficult, and the automatic self regulatory system of body temperature searches for methods of increasing heat transfer different from skin temperature increasing, i.e. sweating.

Another parameter taken into account is the direction of cold-hot feeling versus time. If a value of –1 is given to this direction, with the meaning of temperature decreasing, and +1 is given to the temperature increasing, all data of Fig. 24 can be divided in two parts, one with direction +1 and the other –1. One could expect that a thermal inertia of the human body could influence results, so dividing data according to this parameter should result in an improving of correlation between skin temperature and DMV. This has been made in Fig. 32 and 33. But again no correlation was found, in both cases.

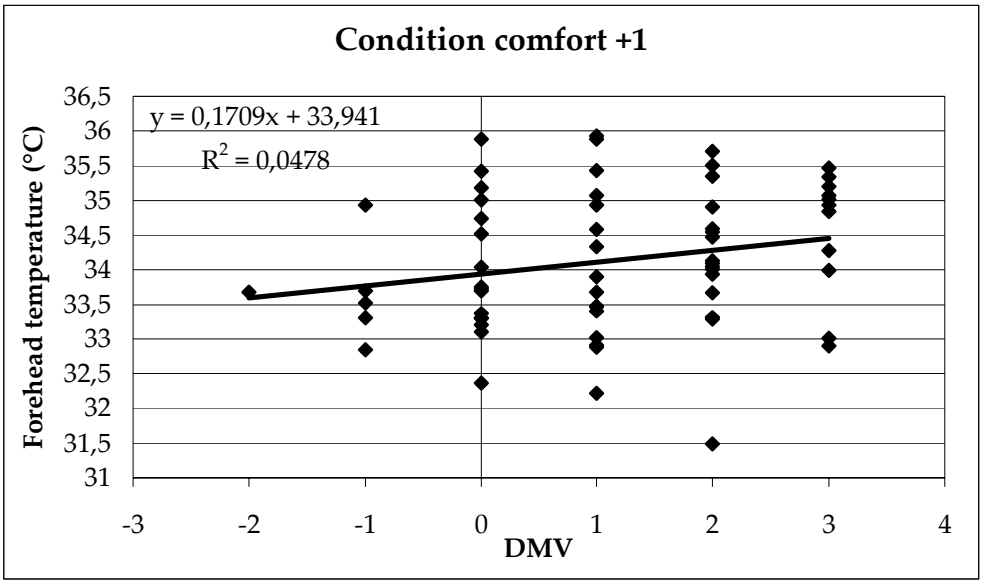

Figure 32: Forehead temperature vs DMV for comfort +1

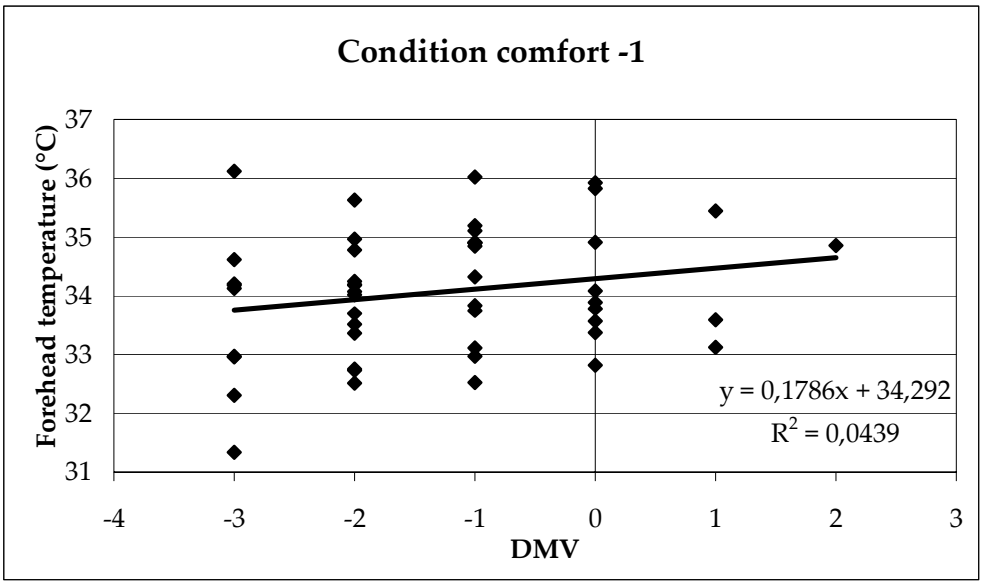

Figure 33: Forehead temperature vs DMV for comfort -1

Moreover, it is necessary to stress that every man is different from each other, reacting differently in different situations, and this is the reason why a big dispersion exists even when some correlation is found. No differences were found between men and women, in agreement with Fanger experiments. In general it is believed that a woman feels cold more than a man, but this depend uniquely from the lighter dresses generally worn by them (lower value of I_{cl}). The general Fanger theory is reported in appendix 1.

Taking into account that a not particularly stressed driver has M=1.5 , i.e. 75 W/m^2 , if there is no heating loss due to evaporation and sweating (indicated with E+RES), heat transfer for radiation and convection must be equal to 75 W/m^2 approximately. In the case of temperature increasing anyway evaporation increases, either for transpiration or sweating, and a further term must be taken into account. But, as already said this is very much influenced by the cloth thickness, and a more detailed explanation of the obtained results should take into account all the possible phenomena happening at and through the skin.

B.6.0 Conclusions

From the obtained results, we can notice the importance of the environment in which this test was developed, i.e. vehicle. In fact the conditions inside the vehicle are rarely well controlled. For example the mean radiant temperature can be highly different by the air temperature, some anomalous fluxes of air can be enter through the windows or from the air conditioning system, and the small dimensions of the vehicle must be taken into account.

Up today the automotive industries build cars equipped by high-technology devices to increase the comfort level of the driver. Nevertheless the vehicle characteristics always introduce the climatization problems described before.
Moreover the control of these parameters is complicated by other conditions as the difference of thermal and ventilating charges to which the vehicle is subjected and in some way the results obtained by tests cannot describe the real situation.
In this work a system to appreciate the individual answer of the tested people is carried out to measure the forehead temperature of each person using a low-temperature pyrometer.
The first experimental test have demonstrated that is possible to measure the surface temperature of the face skin of passengers in the vehicle with an accuracy of 0,15°C.

During the test we found some different problems to be solved:

- The difficult in aiming the pyrometer given by the continuous movement of the head and vibrations of the mirror, even if the level of damping of the Fiat cars tested was good;
- The deposit of pollution on the elliptic mirror of the optical system;
- The restricted range in which the thermal sensor can be used (only due to the electronic card used, as supplied by the manufacturer);
- The sensibility of the thermopile also to the temperature of the pyrometer body, due to its field of view (FOV).

Strength and advantages of the system are:

- The capacity to realize measurements without contact with the measured body;
- The satisfactory velocity response during measurement (about 0,3s);
- The little obstruction in the passenger compartment. In the tests carried out this has caused problems to the visibility of the driver, but find a more suited adjustment is only a problem of industrialization.

When the instrument is not used on black bodies, as the skin, the emissivity ε of the tested surfaces must be known.
In conclusion, the experimental tests performed show that the forehead temperature of the passenger compartment in a moving vehicle are not correlated with the declared comfort vote by the occupants.
Different authors [2,7,11,13,14,16] discussed about this correlation for people living in a normal room, and found that in some cases this correlation exists. Evidently the passenger compartment in the vehicle presents extreme conditions that can invalidate the control.

If the conditions would be controlled in a more accurate way (i.e. reducing or eliminating infiltrations, distributing more homogeneously the flux of air and lowering the difference between wall and air temperature), a correlation could be found.
In the present work, also the differences in winter and summer correlation between skin and ambient temperature have been verified, at equal comfort conditions. This correlation exists only in the summer tests, where the clothes are lighter and more skin is directly exposed to air, and an increase of skin temperature results efficient for preservation of the thermo hygrometric comfort.
Contrarily in the winter case the same mechanism is not effective because of the reduced skin surface exposed in the air. This limits the possibility to the thermoregulation system of interviewing, and in this case only like evaporation (transpiration and sweating) that increase heat transfer from skin to air.

The instrument anyway could be profitably used for other applications, in the field of skin temperature measurements, and again in the following conditions:

- focal distance between 375mm and 400
- temperature range: between 30 to 40°C
- skin emissivity from 0.97 to 1 (similar to a perfect blackbody)

These application could be for example the control of people passing through gates of airports, in order to discover the presence of hyperthermia (fever), which is often correlated to particular diseases as SARS or infection from Ebola virus. Or continuous monitoring of forehead temperature of patients in reanimation or intensive therapy departments.

D. INDEPENDENT SENSOR OF TEMPERATURE, RADIATION AND AIR VELOCITY

C.0.1 Introduction

The thermo hygrometric comfort condition (i.e. experience of hot or cold) depends on four ambient variables: air temperature, mean radiant temperature, air velocity and relative humidity. Commercial instruments for estimating a global feeling of comfort are available, based on thermal balance in systems simulating the skin behaviour, or simple gauges for measuring separately the four quantities. Goal of the present work was to design, realize and test a single instrument able to measure independently during the same test three of the four quantities, which have major influence on the comfort sensation: air temperature, mean radiant temperature and air velocity.
Besides, a portable device is desired, which could be adapted as a medallion on the suit of test drivers of vehicles, in order to give an estimation of the thermal comfort conditions in the passenger compartment.

C.1.0 Studied cases

Three different approaches to solve the above described problem have been followed. The progression of the research was due to improve the resolution of the studied sensors to the wanted quantities.
Initially A single metal wire was studied (see figure 34 a), because a heated metal wire is a very good detector of air velocity (e.g. the hot wire anemometer). Successive tests and theoretical evaluation showed its inadequacy to detect mean radiant temperature (T_{mr}). So a flat sensor (PT100 temperature flat sensor) was tested (Fig. 34 b) : a difference at different T_{mr} was found, bat again not so high to guarantee a good measuring device, likely due to the small sizes of the sensor (3 mm x 7 mm). Finally it was decided to develop one other sensor by the Heat Transfer Laboratory of The dept. of Mechanical Engineering of the University of Rome “Tor Vergata” , with the help of the Electronic Dept. of the same University (Pro. D’Amico) and the Microsensors Laboratory of the CNR, Research Area of “Tor Vergata” (Mr. Petrocco). In Fig. 34 c this sensor is depicted: it is much wider (25 mm x 50 mm)

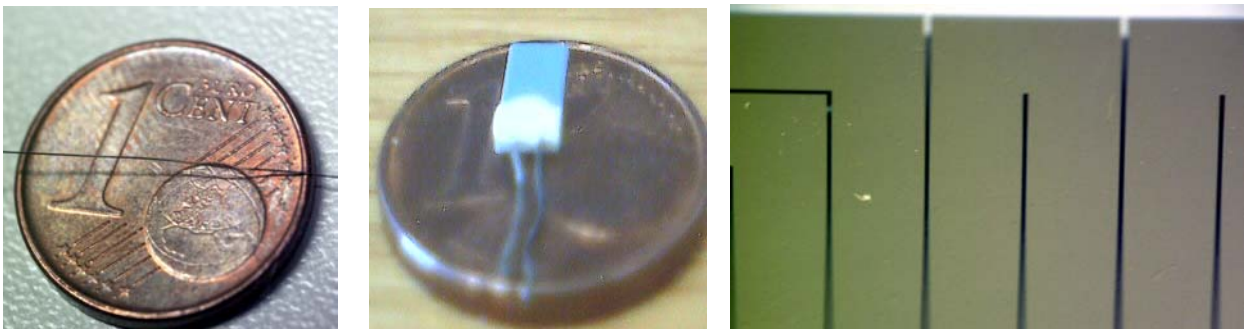

a. b. c.

Figure 34: studied cases: a. nickel wire b. PT100 c. detail of the flat sensor gold

C.2.0 Nickel wire

A nickel wire with diameter 0.7mm (see fig. 35) , can easily measure ambient temperature when not heated, and air velocity if heated to a defined temperature. The present tests were carried out to recognize if it was possible to measure also mean radiant temperature.

Recognizing the mean radiant temperature has been evaluated by comparing the difference between steady state r transient data of the sensor, when it is bright or blackened with a painting at high emissivity (e.g. a opaque black painting, of colloidal graphite, Aquadag, which both present generally emissivity higher than 0.95).

Figure 35: Nickel wire

C.2.1 Important considerations in measurement preparation.

A special configuration was adopted to carry on measurements on nickel wire: the wire was stretched within two cooper wires in V shape (see figure 36). These two holders have three purposes: the first to sustain the wire, the second to stretch it avoiding its relaxation during heating,

and the third constitute a four wire resistance meter, leading the current by two of them (at opposite sides) and detecting the voltage drop by the other two.

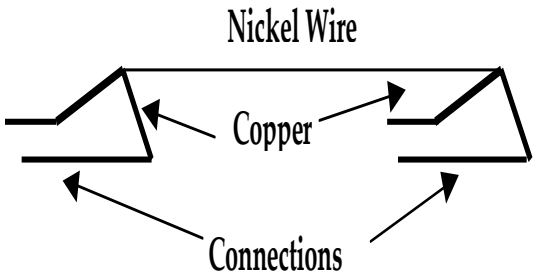

Figure 36: Configuration of the nickel wire

C.2.2 Calibration curve for the nickel wire

Before measurements, the nickel wire must be calibrated in order to detect the relationship between its electric resistance and temperature.

This calibration is carried on changing the temperature of the wire (measured in a calibration bath by a Platinum resistance thermometer *PRT-25,* standard of the laboratory), and contemporarily measuring the wire electrical resistance with four wire technique (Kelvin bridge) as above mentioned. Fig. 39 represents a sketch of the calibration set up.

During calibration the nickel wires are positioned around the tip of the platinum resistance thermometer (PRT-25), and inserted into a properly realized comparator (a glass pipe with an inlet and outlet of the liquid coming from the thermostat, i.e. a mixture of 50% distilled water and 50% ethylene glycol; Result of calibration is the relation between electric resistance and temperature of wire.

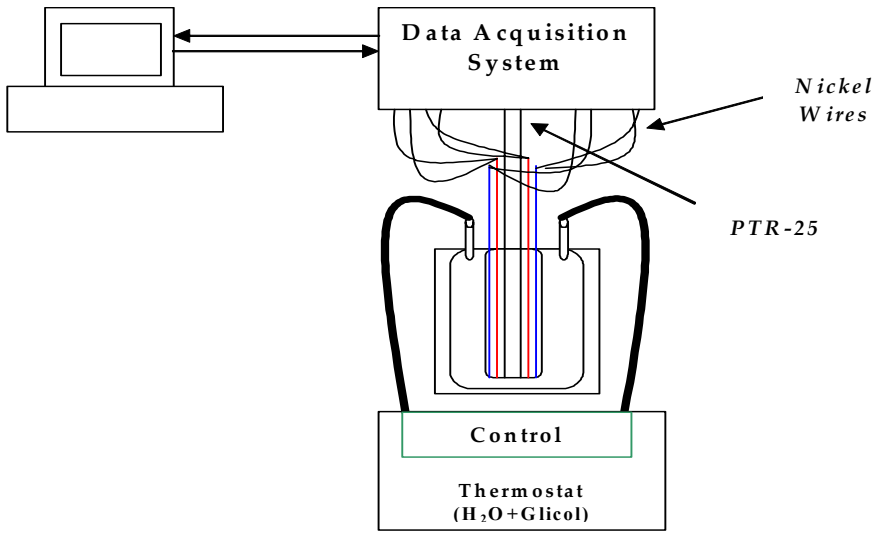

Figure 37 Calibration process nickel wire

C.2.2.1 Instrumentation used for calibration:

2700 Multimeter/Data Acquisition Systems -Keithley Integra series

Platinum resistance Thermometer (PTR-25) standard, calibrated by IMGC – CNR (national metrological laboratory, Torino, Italy)

Thermostat -Julabo F33

Instrumentation used during tests:

Data Acquisition System National Instruments (NI) DAQPAD MIO16X

Bipolar Operational Power supply/Amplifier –Kepco BOP100-1M 100V/1A

Standard resistance (manganine shunt) 0.1Ω

C.2.2.2 Calibration results

The nickel wire presents a linear behaviour between resistance and temperature, at least in the temperature range investigated (-5°C÷55°C). As a result also the sensitivity $\frac{\partial T}{\partial R} = 0.392$°C/Ω has been obtained, with standard uncertain Sy/x=1.6 10^{-3}Ω. In figure 42 the calibration of the nickel wire is reported.

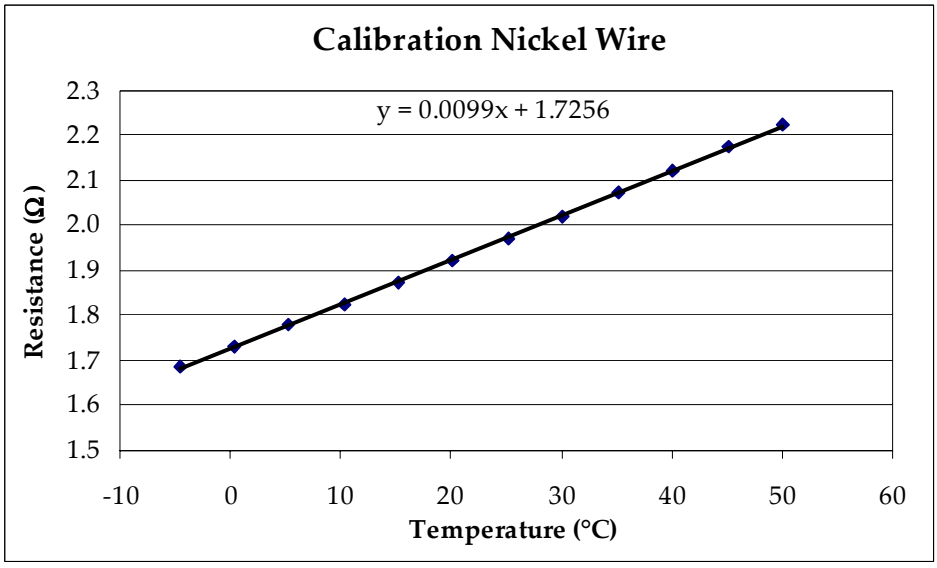

Figure 38:Calibration nickel wire

C.2.3 Description of the experimental set up for transient test on nickel wires (Fig. 39)

Through the DAC function of the data acquisition system (with an output variable between 0 and 10V), the power supply is commanded to give a constant current variable in the range 0÷1A. This power is used to feed the circuit constituted by the wire and the shunt resistance in series.

At the beginning the DAC signal is set to send a bias current of 10mA for a time interval of 5s. This negligible current is enough to detect the resistance of the wire, without increasing its temperature by self heating. After this stationary first step, an increase of the DAC output is given to the power supply for an interval of 15 s. In both tests the If register the shunt and nickel wire voltage drop is recorded, and the wire resistance is evaluated by the following relation:

$$R_{Wire} = \frac{V_{Wire} \cdot R_{Shunt}}{V_{Shunt}} \quad (2).$$

Temperature of the wire is obtained from its resistance by means of the performed calibration.

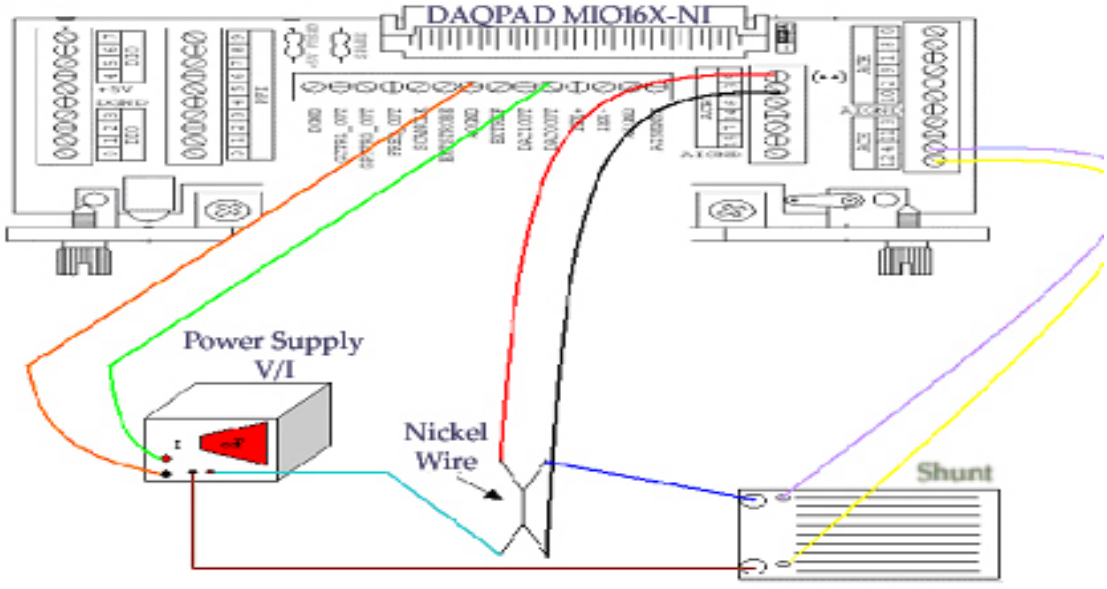

Figure 39: circuit for test nickel wire

C.2.4 Nickel wire results

Both free and forced convection were tested on wire, the first protecting the wire with transparent case (Fig. 40 a and 41b), and the second investing the wire with the air flux from a fan.

The results of the experiments in free convection also with air conditioning are reported in the figure 41a . The temperature behaviour represented is influenced by a overshoot in voltage, likely

due to a retard in developing natural convection, and hence a major temperature increasing a the beginning of heating.

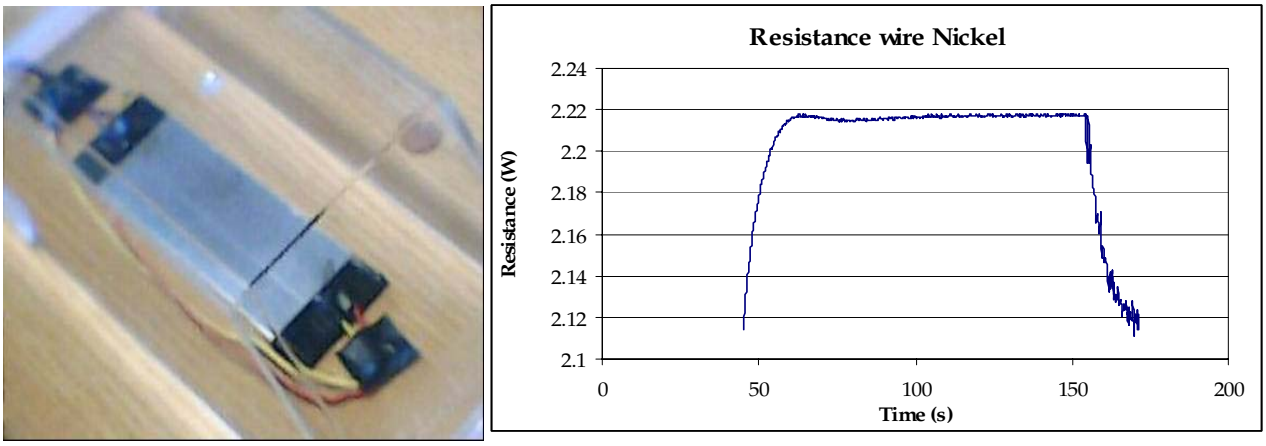

a. b.

Figure 40: wire nickel: a. forced convection b. Behaviour of the wire nickel

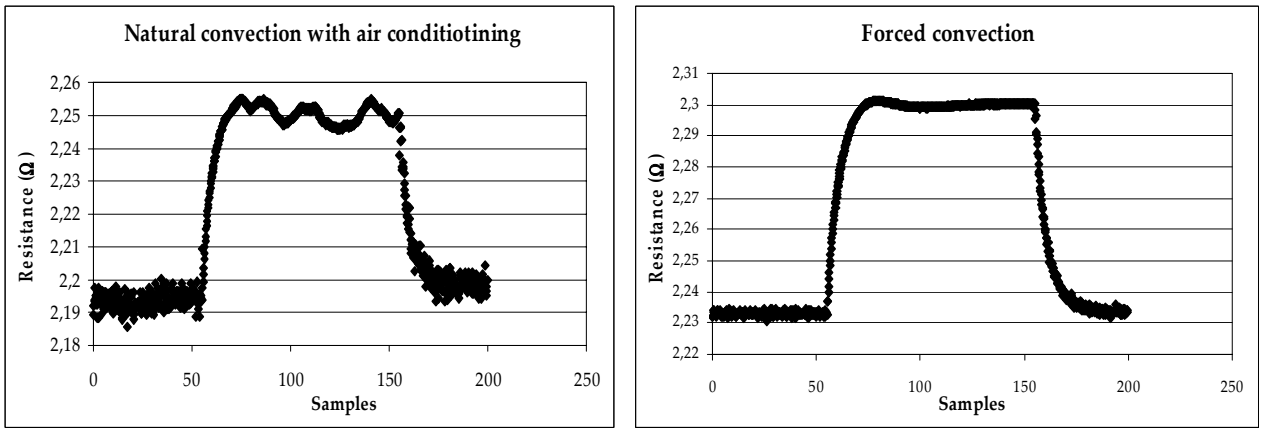

a. b.

Figure 41: test nickel wire: a. Natural convection b. Forced convection

C.2.4 Theoretical temperature versus time behaviour of the wire.

The theoretical trend of temperature of wire during heating can be estimated a priori by the simple solution of a lumped parameter problem, balancing the three heat fluxes involved in the description of the phenomenon. These three fluxes are: $\dot{Q}_1$, heat produced by the current flow into the wire; $\dot{Q}_2$ variation of the internal energy of the wire during heating, and $\dot{Q}_3$ thermal heat transferred to the ambient air by convection.

$$\dot{Q}_1 = \dot{Q}_2 + \dot{Q}_3 \quad (3) \therefore \quad \dot{Q}_1 = RI^2 \quad (4) \quad \dot{Q}_2 = mc_p \frac{dT_w}{dt} \quad (5) \quad \dot{Q}_3 = hA_w(T_w - T_a) \quad [h] = \frac{\mathrm{W}}{\mathrm{m}^2\mathrm{K}} \quad (6)$$

where:

R- wire average electric resistance; *I*-electric current*; h* the convection coefficient (free or forced).*;* A_w-wire external surface; T_w- wire temperature, T_a- ambient air temperature

If *h* is considered independent on temperature, the above written balance constitutes a first order linear differential equation that can easily be solved, leading to the relation

$$T(t) = T_a + \frac{RI^2}{hA_w}\left(1 - e^{-\frac{hA_w}{mc_p}t}\right) \quad (7)$$

h values are influenced by the phenomenon governing heat transfer:

- in free convection $h = f(T_w - T_a)$ $\begin{cases} \text{Laminar flow} \Rightarrow h \propto \Delta T^{1/4} \\ \text{Turbulent flow} \Rightarrow h \propto \Delta T^{1/3} \end{cases}$
- in forced convection *h* is dependent on air velocity *w*, as predicted for example by the empirical correlation (e.g. the one of Eckert and Drake)

  $Nu = \mathrm{Pr}^{0.38}(0.43 + 0.5\,\mathrm{Re}^{0.5})$ (8)

  which leads to the following values

  $h = f(w)$ $\begin{cases} 200\ \mathrm{W/m^2K} & \text{for free convection} \\ 500\ \mathrm{W/m^2K} & \text{for forced convection and } w = 5\ \mathrm{m/s} \end{cases}$
- when radiation is present, a radiation component of the convection coefficient h_r can be evaluated according to the following relations:

  $$\dot{Q}_3 = h_r A_w(T_w - T_a) = A_w\sigma\varepsilon_w\left(T_w^4 - T_a^4\right) = A_w\sigma\varepsilon_w(T_w - T_a)\cdot\left(T_w^3 + T_w^2T_a + T_wT_a^2 + T_a^3\right) = \\ = A_w\sigma\varepsilon_w(T_w - T_a)\cdot 4T_w^3 \quad (9)$$

  and h_r results

  $h_r = \sigma\varepsilon_w 4T_w^3$ (Irradiation) (10)

Fig. 46 b reports the computed temperature behaviours for three different air velocity, i.e. $w = \frac{5m}{s}; \frac{1m}{s}; \frac{0.2m}{s}$.

When radiation is taken into account, it can be computed that the radiation component h_r assumes a value about 6 W/m^{2}K, influencing only 3% of the value of natural convection. This is the reason why this system (the wire) is a very good tool to evaluate the ambient temperature and the velocity

of air, but is influenced very little by the mean radiation temperature. The measurement of this last hence must be carried out by other techniques. The reason of the negligible amount of the h_r as respect to convective part of h is related to the high values of h in the case of convection as computed by the empirical relations. Really, it is not h_r to be very small (its value is about the same of flat surfaces) but h_{conv} to be hugely high for wires.

Experiments carried out with two wires, one bright (without coating) and the other covered with a black painting, didn't show any difference in h, confirming the negligible amount of h_r .

This is the reason why further experiments were carried on flat surfaces.

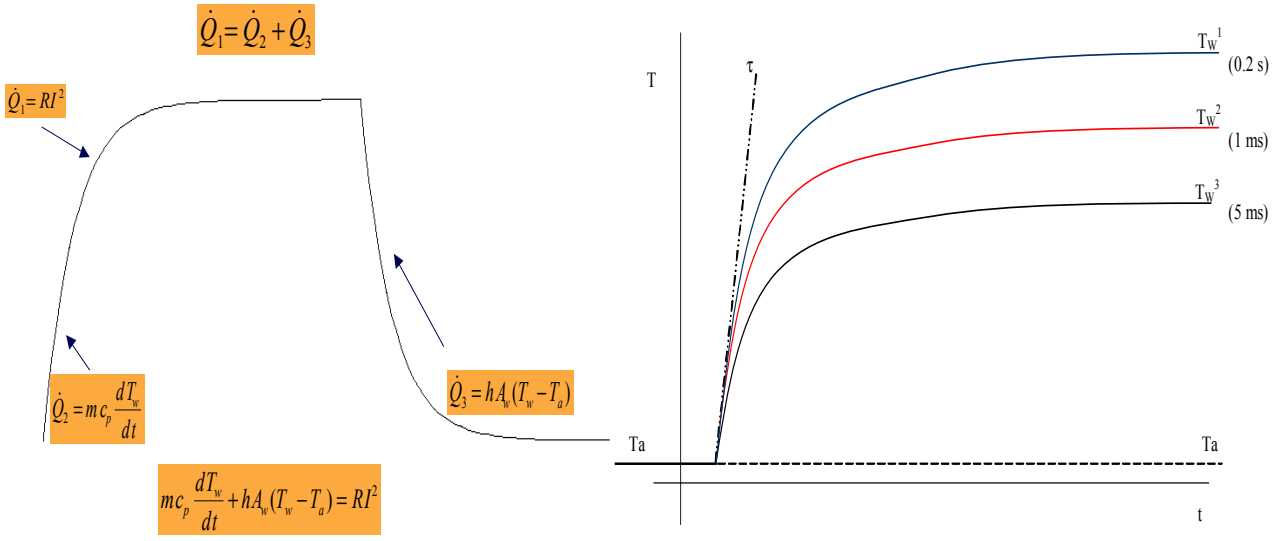

a. b.

Figure 42: Theoretical behaviour of the wire: a. Theoretical trend of temperature b. Behaviour air velocity

C.3.0 PT100

As a first trial, a two flat PT100 was tested, again one as supplied by Centro Ricerche FIAT (see fig. 43), and the other insulated (in order to avoid short circuit inside the Pt winding) and blackened.

Sizes of the devices were 7x3 mm^2-(rectangular shape), and 1mm thickness, with the platinum on the upper flat surface.

Figure 43: Flat PT100

C.3.1 Important considerations for measurement preparation

In order to put into evidence as possible the differences between the two sensors (the bare one and the blackened) an accurate resistance measurement must be made. This is done with the four wire resistance. Two couples of leading wires have been tin soldered to the connection of the PT100, (see figure 44), getting the two current and the two voltage terminals of the resistance. In order to increase the radiation effect, the two sensors were both glued to an aluminium base (30 x 60 mm^2), one blackened together with the sensor.

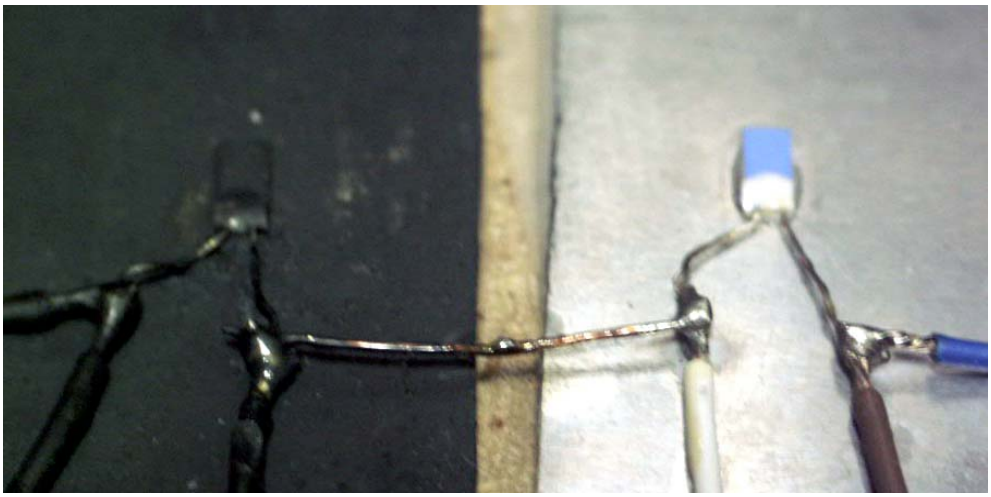

Figure 44 Blackened and bright PT100

C.3.2 Used device

Data Acquisition System: National Instruments (NI) DAQPAD MIO16X
Bipolar Operational Power supply/Amplifier –Kepco BOP 100V/1A
Standard resistance (shunt) 0.1Ω

C.3.3 Description of the experimental set up (Fig. 45)

Through the DAC of the acquisition system, a voltage signal (0-10V) is sent to the power supply, which respond with current in the range 0÷1A. Also in the present case, at the beginning the two sensors are fed with a low current bias (10mA) for five seconds. Then the DAC voltage is increased to 60mA for 15 seconds The voltage drop on the on the shunt and PT100s are recorded by the data acquisition system, and the PT100 resistance is evaluated again by the following relation:

$$R_{PT100} = \frac{V_{PT100} \cdot R_{Shunt}}{V_{Shunt}} \quad (11)$$

Temperature is obtained with a standard relation between resistance and temperature, as supplied by international rules (e.g. ITS90)[15]. Only a check of the 0°C resistances of the sensors were measured.

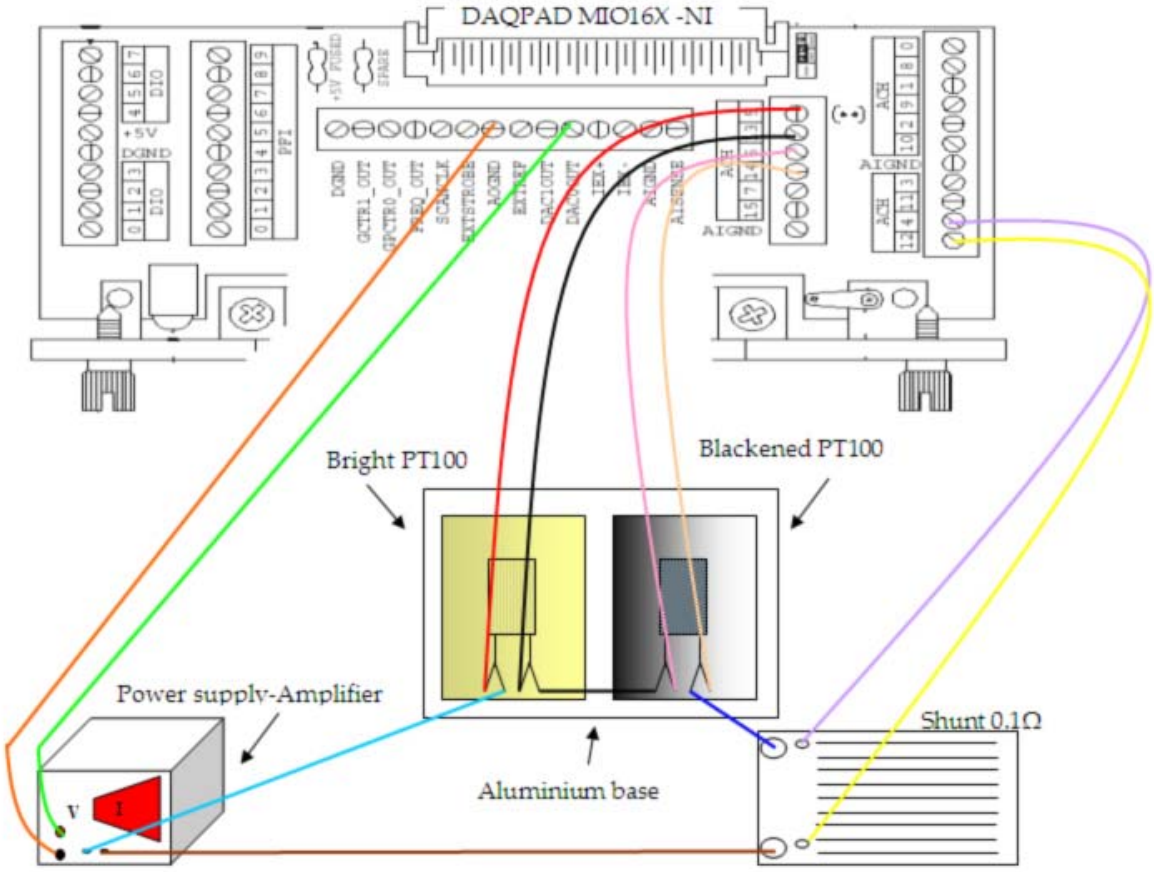

Figure 45: Circuit for test

C.3.3 PT100 results

As a result of the tests, a first difference between the blackened and the bright PT100 was obtained. Both a curvature change in the temperature behaviour between the two sensors (the bright one and the blackened one) and a difference in asymptotic temperature was noted, demonstrating a variation of the convection coefficients, and hence of their radiation component. In figure 46 the results of the two PT100s (blackened and bright.) are reported, and the above mentioned differences are evident.

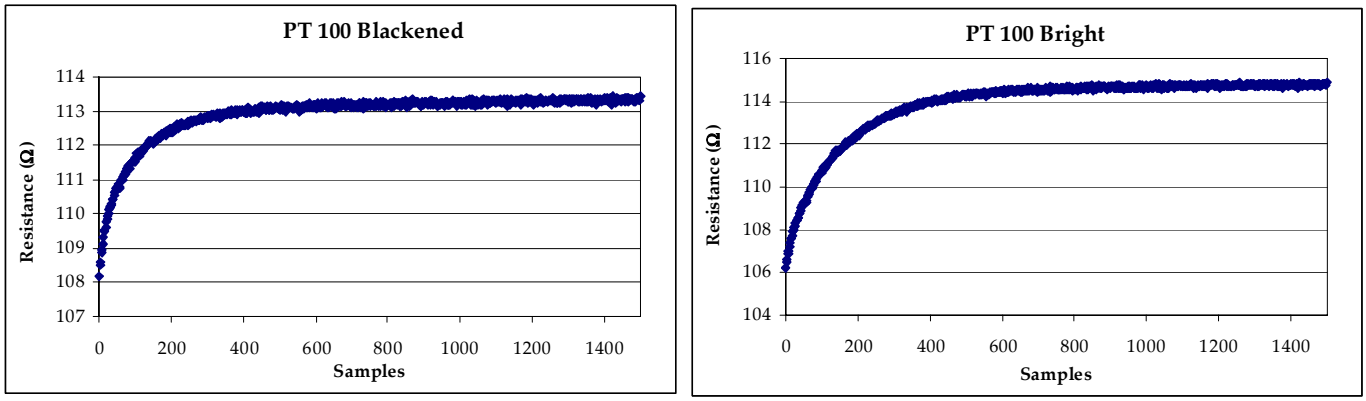

a. b.

Figure 46: Results PT100: a. Blackened b. Bright

C.3.4 PT100 Behaviour

Most of the considerations made about the Nickel wire can be repeated at the same level for the PT100s. But now the radiation component of the convection overall coefficient cannot any more be considered negligible, and influence thermal behaviour as described.

From the experience of these tests, it has been decided to built a new type sensor, constituted by a bigger flat surface, with a metal coating to detect temperature and to lead current in order to be heated. Again transient behaviour is considered quicker and more accurate to evaluate convection coefficient, because of lack of anomalous natural convection behaviours, even in steady state.

C.4.0 Flat sensor

As previously said, it has been decided to develop new comfort sensors, flat and enough wide to avoid the edge effect (as in the case of wire), in order also to amplify the differences between bright and blanked sensing elements noticed on the PT100s.

The principal characteristic of the new flat sensor realized are:

- double nature (it is divided in two parts: a blackened and a bright part),
- dimensions of a medallion, with an area of 250mm^2, each part 25 mm x 50 mm;
- the sensible element is a deposit of conducting metal (gold or platinum), insulated from the substrate; with a resistance enough low (5-10 ohm) to allow good voltage drop measurements with the usual data acquisition systems.

C.4.1 Mask computing and design

The double sensor must be wide enough to don't be influenced by the size effect (as the wire), so a total size of 50 x 50 mm^2 was chosen (one half for each part, bright and blackened). Besides it must have a bifilar winding, in order to reduce the inductance and consequent ambient electric noise. In order to have an enough low resistance, only few double pass were designed. The complete description of the two version of the sensor (gold and platinum deposit) is reported in the following:

Gold deposit (Fig.47):

Path for soldering : 5mm
Path width =4mm
Separation between paths =0.18mm
Separation between sensors= 0.20mm
Total average length (L)= 299.99mm

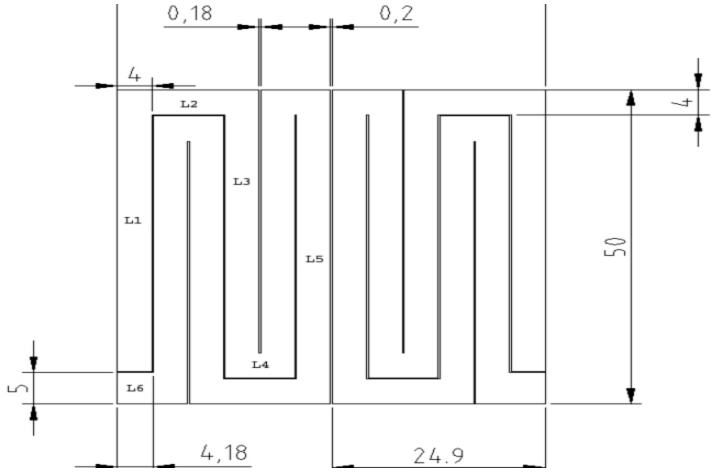

Figure 47: Mask for gold deposit

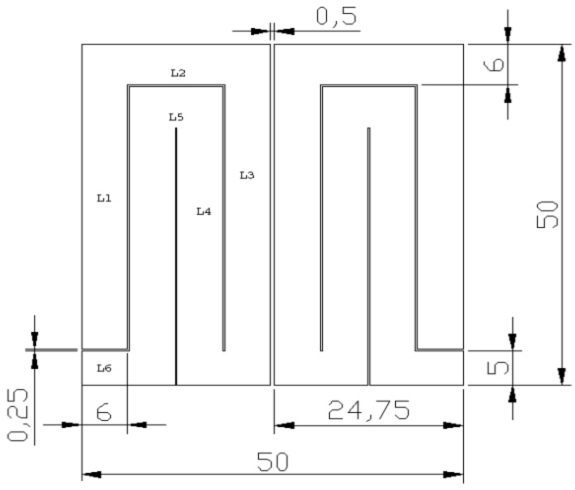

Figure 48 platinum mask

Platinum deposit (Fig.48):

Path for soldering : 5mm
Path width =6mm
Separation between paths =.25mm
Separation between sensors= 0.5mm
Total length (L)=201.5mm

The Sensor with the platinum deposit has been designed with a wider track, because of the higher electrical resistivity of this material, compared to the gold one.

In the following the resistances of the two obtainable sensor have been calculated, assuming the resistance of the deposit equal to the bulk material one, even if it is well known that this seldom happens.

Notation:

Cross section of the deposit: $S = r*l$ where r thickness e l width; δ density

$R=\rho*L/S$ where ρ= resistivity; L= total length of the deposit

For the gold deposit, the above relations give

l =0.004 m; L = 0.2999m; r = $2.5\cdot10^{-6}$ Å; δ =$2.200\cdot10^{-8}$;S = $1.000\cdot10^{-8}$

Final result for gold coating resistance R = 0.6598Ω

For the platinum deposit, the above relations give

l =0.005 m; L = 0.2015m; r = $2.5\cdot10^{-6}$ Å; δ =$1.048\cdot10^{-8}$;S = $1.500\cdot10^{-8}$

Final result for platinum coating resistance R = 1.4078Ω

C.4.2 Fabrication process

Fabrication of the flat sensors (gold and platinum deposit) were carried out with the two above described masks, and with the reported thickness, by the CNR Roma laboratory of sensors and microelectronic of the Research Area of Tor Vergata (Prof. D'Amico and Mr. Petrocco)

C.4.2.1 Gold deposit

Gold has been deposited on a normal glass(for windows) substrate, 1.87 mm thick, cut in the shape 70 x 70 mm^2.

Process of deposition:

1. Cleaning of the substrate with a soap solution, then with acetone and finally with isopropyl alcohol
2. Spinning: the base, after cleaning with a jet of nitrogen gas, is covered with resist solution 5214, than centrifuged at 4000 rpm in vacuum for 60 s. The resulting thickness of the resist layer after application is 1.5 μm
3. Drying: in an electric oven at 90°C per 10 min.

4. Exposition: the mask is positioned to the upper surface of the glass base, then its is ultraviolet irradiated for 8 s.
5. developer: the coated and exposed base is developed in a bath for 20 s, after being cleaned with deionizer water
6. Gold evaporation: first 300 Å of chrome are deposited, as grabber, then 2500 Å of gold are deposited
7. Lift-off: with acetone to quit remaining gold in the paths.

The first deposit test were 800Å, 1000Å and 2500Å, with resulting true resistances(measured after completion of the deposit) 45Ω, 22.5Ω, 8Ω. As a result a relation was found between the measured deposited gold resistances and the ones calculated from bulk , and were 3.5, 13.91, 12.1.

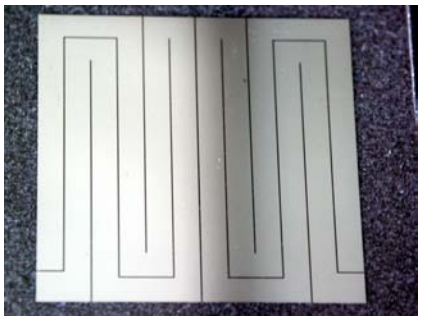

Figure 49: Gold deposit on window glass

C.4.2.2 Platinum coating

The trials of deposition of platinum on glass gave unsatisfactory results, probably due to the presence of impurities (Si , NaOH or other pollutants) in the window glass. The coating resulted irregular in thickness and shape and sometimes interruption of the circuit happened (see Fig.50). Also using a substrate of optical glass, NaOH free and with well controlled composition, didn't give accurate results. This is the reason why platinum was at last deposited on a silicon substrate, 0.5 mm thick , with the surface previously electrically insulated with 1 μm oxidation.

The procedure of the platinum deposition on the Si wafer was the same as the one already mentioned for the gold deposition on glass.

Even the Pt deposition on Si wafer result in good shape without damages, and resistance appeared suited, testing this sensor it was noted that during heating a resistance variation occurred, probably due to Si contamination f the deposit. In order to get anyway a utilizable device, it was decided to keep tha sensor in a warm bath till when no variation of resistance was noted. This happened after two days at 80°C, and the total resistance of the deposits changed from about 3 to 2 Ω.

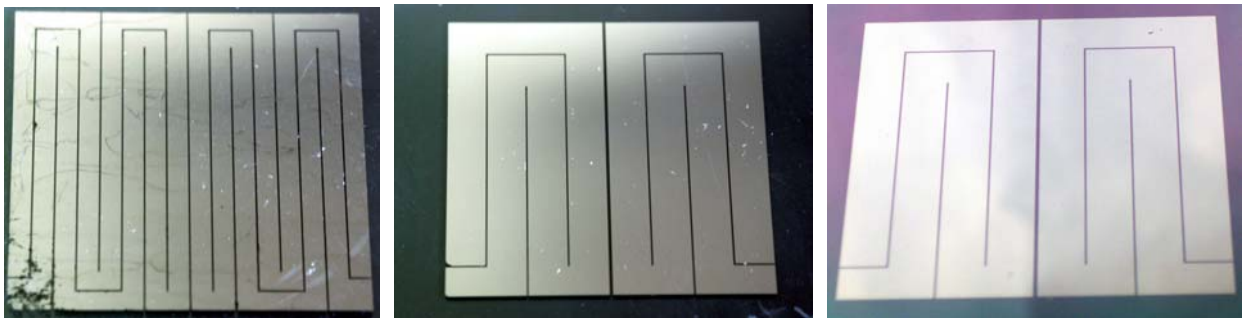

a. b. c.

Figure 50: Deposit platinum on materials different: a. Platinum on window glass b. Platinum on optical glass c. Platinum on silicon wafer

C.4.2.3 Important advices for sensor preparation

Before utilizing the sensor, connection to feeding must be provided, and particular care must be taken in order to avoid possible drawbacks. The suggested procedure is:

a. Four copper bases (the same used for connection of strain gauges) must be glued to the glass or silicon base, outside the coated surface, External electrical connection will be made through these bases in order to avoid stress on coating where the connecting wires are soldered. The four bases are used to solder four wires, in order to get a four wire resistance
b. Tin soldering of the terminal path of the sensors and the copper bases, and external connection wires to the bases (Fig.51)
c. A layer of expanded polystyrene (30 mm thick) is glued to the bottom face of the substrate, in order to thermally insulate the sensor from the background (table during tests, or driver suit during its field working)
d. One sensor of the couple is blackened

Figure 51 represents one double sensor ready for measurements.

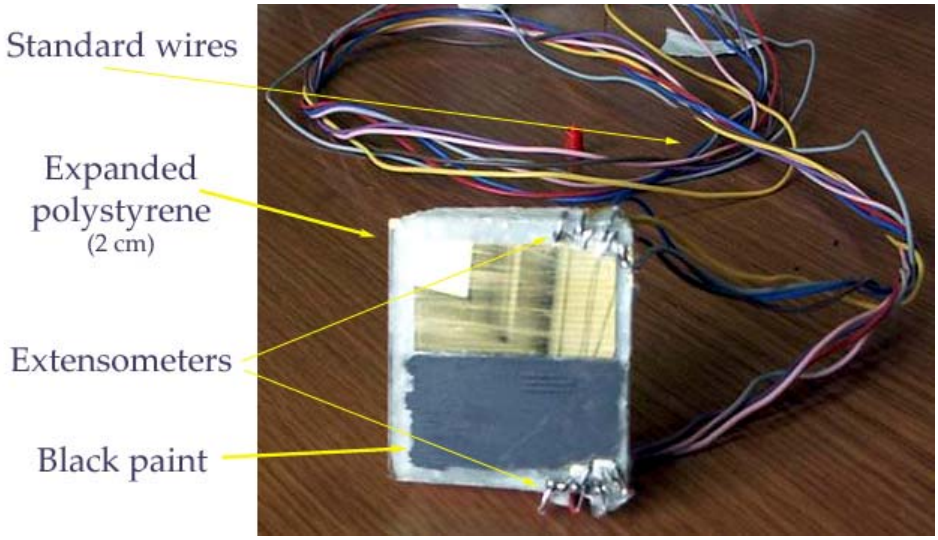

Figure 51: Flat sensor ready for measurements

C.4.3 Calibration of different sensors

All the realized sensors must be calibrated in order to get the relation between the electrical resistance and the temperature. This relation is then used during the utilization of the sensor to get the desired temperature behaviours. Generally this relation is quasi linear, at least in a limited temperature range, but an accurate evaluation must be performed taking several data in order to check this linearity and to get the uncertainty in calibration.

The calibration process consists in changing the sensor temperature (within a proper ambient where the temperature is considered uniform, as a thermostat) and obtaining the corresponding resistance values. Temperature is measured by means of a primary (for the laboratory) standard thermometer. i.e. a Platinum resistance thermometer S1061-1 (PT470), supplied calibrated at triple point of water and 100°C, which according to ITS90[15] are a sufficient number of point for the desired temperature range. This kind of calibration is called “by comparison with a standard instruments”.

During calibration the sensors are inserted into the thermostat bath (see Fig 52), inside a plastic envelope to avoid contamination with the thermostatic fluid (50% distilled water and 50% ethylene glycol); connections are kept outside the bath.

Calibration have been carried out for all the sensors realized, and for each sensor the two coatings have been calibrated, the bright one and the blackened one.

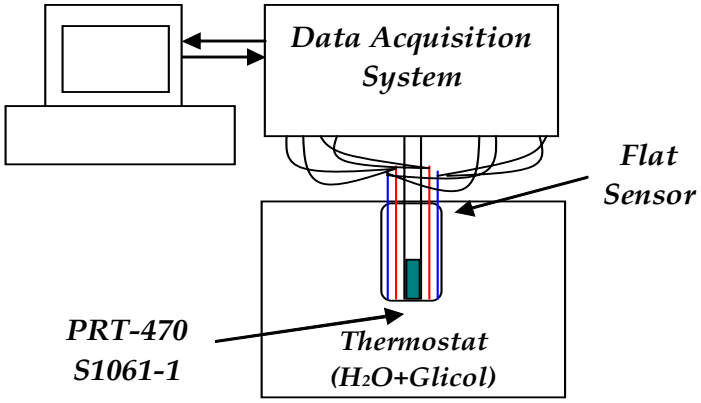

Figure 52 : Diagram for calibration flat sensors

C.4.3.1 Used Instrumentation for measurement

2700 Multimeter/Data Acquisition Systems -Keithley Integra series

Platinum resistance thermometer S1061-1 Minco Products

Thermostat -Julabo F33

C.4.3.2 Calibration results for flat sensor gold coating

The flat sensor gold presents a linear behaviour between resistance and temperature, at least in the temperature range investigated (-10°C÷80°C). As a result also the sensitivity has been obtained, with standard uncertain, in resistance and in temperature (see table 1). In figure 53 the calibration of the flat sensor gold blackened and bright is reported.

Flat sensor coated with gold				
Type	R (0.01°C)	$\partial T/\partial R$ (°C/Ω)	$S_{y/x}$ (Ω)	$S_{x/y}$ (°C)
Blackened	7.531	0.0235	$8.1\ 10^{-3}$	0.4261
Bright	7.467	0.0238	$1.0\ 10^{-2}$	0.3484

Table 1:Results calibration flat sensor gold

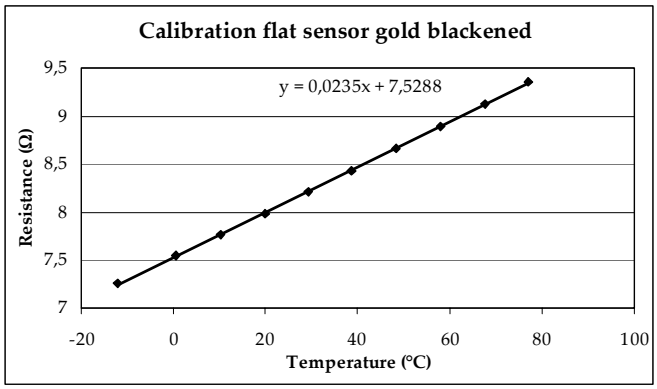

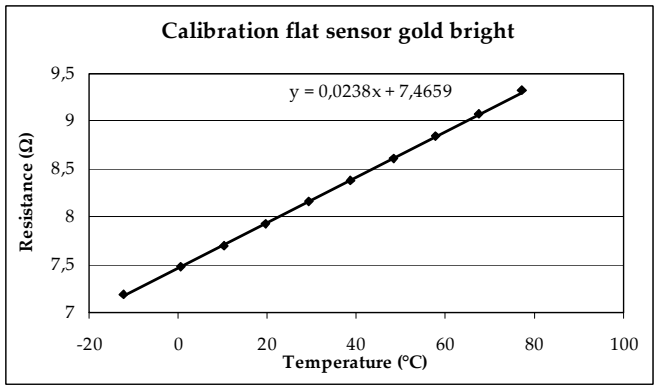

a. b.

Figure 53 Calibration results for flat sensor with gold coating a. Blackened b. Bright

C.4.3.3 Results for flat sensor with platinum coating

Also the flat sensor with platinum coating presents a linear behaviour between resistance and temperature, at least in the temperature range investigated (0°C÷70°C).). As a result also the sensitivity has been obtained, with standard uncertain (see table 2). In figure 54 the calibration results of both of two part of the flat sensor (bright and blackened) is reported.

Flat sensor coated with platinum				
Type	R (0.01°C)	$\partial T/\partial R$ (°C/Ω)	$S_{y/x}$ (Ω)	$S_{x/y}$ (°C)
Blackened	35.784	0.0614	$3.7\ 10^{-2}$	0.6061
Bright	38.999	0.0658	$3.3\ 10^{-2}$	0.512

Table 2:Results calibration flat sensor platinum

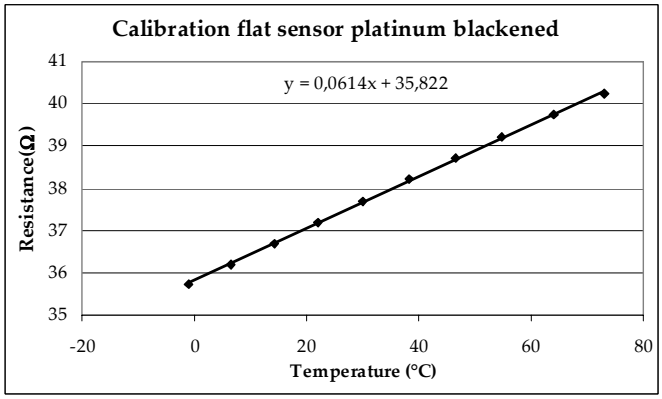

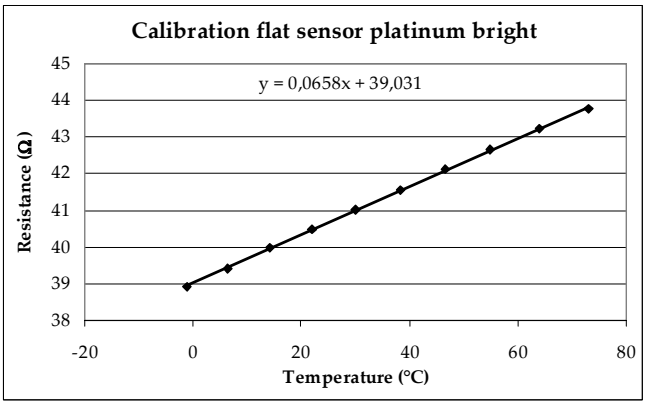

a. b.

Figure 54 Calibration results for flat sensor with platinum coating a. Blackened b. Bright

C.4.4 Description of the experimental set up

Through the DAC function of the data acquisition system (with an output variable between 0 and 10V), the power supply is commanded to give a constant current variable in the range 0÷1A. This power is used to feed the circuit constituted by the flat sensor (gold or platinum) and the shunt resistance in series (see figure 55) .

At the beginning the DAC signal is set to send a bias current of 50mA for a time interval of 5s. This negligible current is enough to detect the resistance of the flat sensor, without increasing its temperature by self heating. After this stationary first step, an increase of the DAC output is given to the power supply for an interval of 20 s. In both tests the shunt and flat sensor voltage drop is recorded, and the flat sensor resistance is evaluated by the following relation:

$$R_{Sensor} = \frac{V_{Sensor} \cdot R_{Shunt}}{V_{Shunt}}, \quad (12)$$

Temperature of the flat sensor is obtained from its resistance by means of the performed calibration

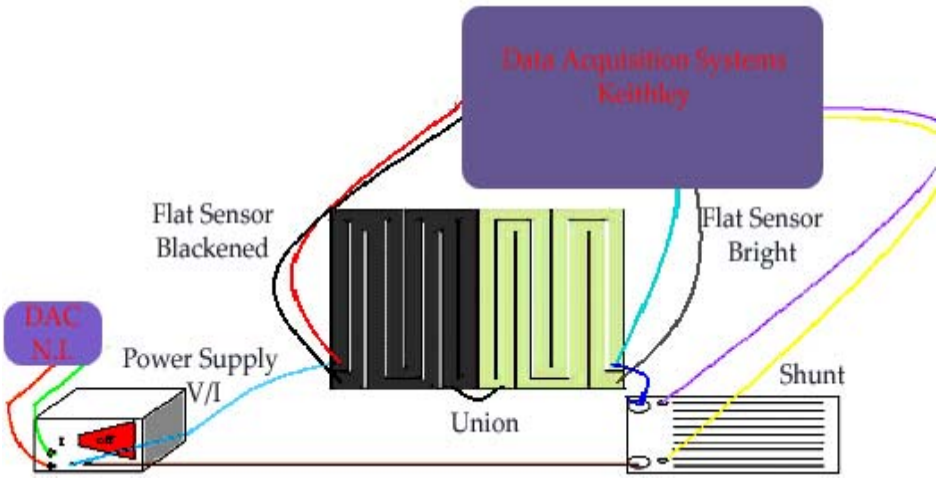

Figure 55: Description of the experimental set up

C.4.4.1 Gold coated flat sensor results

When the flat sensor with gold coating was fed with a current of 0.9A for 20 seconds, an increase of the resistance resulted. By means of the calibration performed, this resistance is converted in temperature values. So for an increases of temperature of 28.9 °C, the average resistance during the 20 seconds time of the test, resulted 8.43Ω for the blackened sensor and with and 8.37Ω for the bright one. Really, the temperature increase was slightly different for the two sensor, 28.89 for the blackened and 28.91°C for the bright. Results are represented in figure 56

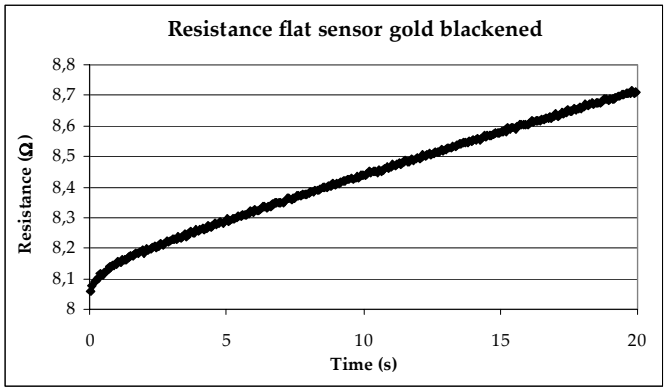

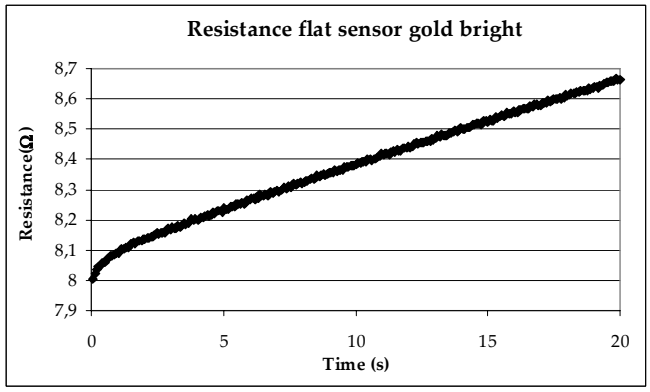

a. b.

Figure 56 Resistance for flat sensor with gold coating a. Blackened b. Bright

4.4.2 Platinum coated flat sensor results

The same results of the Platinum coated sensor just described have been obtained with the flat sensor whit platinum coating: mean resistance of the blackened sensor of 39.09Ω with an increase of temperature of 32.17°C, and 42.60Ω for the bright sensor while temperature raised of 33.52°C. Results are reported in figure 57

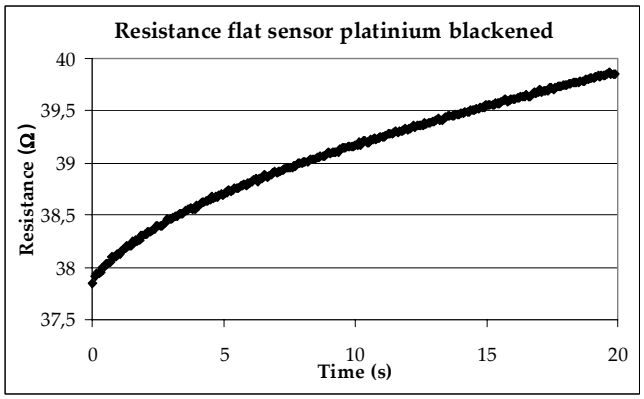

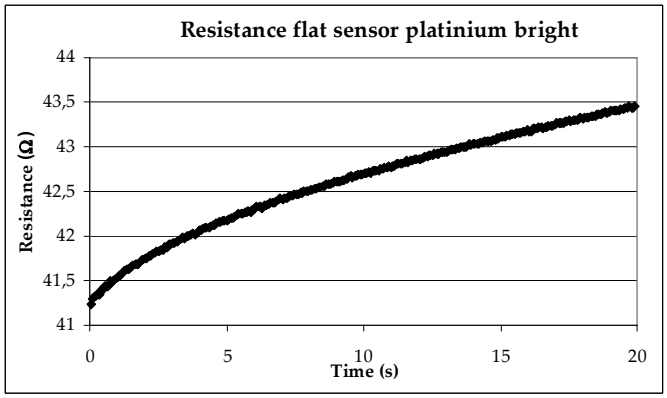

a. b.

Figure 57 Resistance for flat sensor with platinum coating a. Blackened b. Bright

C.4.4.3 Theoretical model for gold coating

The behaviour model for flat sensor with gold coating is obtained by the heat conduction in a slab, with a constant production of heat at a defined time on a surface of the slab and insulation at the other surface. As a general trend the temperature behaviour of the sensor resembles the one of the the Nickel wire and PT100s. But this behaviour leads to a temperature increases of about 500°C in

more then 8 minutes, and this time is too long for a quick and easy test. Besides, it is difficult to maintain constant conditions (convection, radiation, etc) for a long time. So a small time length is used for tests, i.e. 20 s. During this time the typical exponential behaviour of the lumped parameter trend is not recognizable, only a quasi linear trend is visible in the experimental data (see Fig. 56). Nevertheless differences from the lumped parameter solution can be found at the beginning of heating, when conduction n the glass is present, and the lumped parameter model cannot any more be considered valid. It must be noted that when a test is made with a sensor, the temperature behaviour is influenced by: thermal conductivity of the support (glass) λ_{glass}, thermal diffusivity of the same glass α_{glass}, convection of heat transfer coefficient h., beside naturally thickness of the glass plate L. Nevertheless, when different test are carried out with the same sensor, only h varies , while the other quantities remain unchanged (at lest if test are in similar temperature range).
According to the assumed hypothesises (insulation at x=0; heat production at constant rate at x=L, transient state), the analytical solution of the general heat conduction equation is

$$T(L,t) = T_f + \frac{RI}{hA}\left\{1 + \sum_{j=1}^{\infty} \frac{2\sin\lambda_j L \cos\lambda_j L \cdot e^{-\alpha\lambda_j^2 t}}{\cos\lambda_j L \cdot \sin\lambda_j L + L\lambda_j}\right\} \quad (13)$$

being $T(L,t)$ the temperature of the gold coating, while λ_j are the multiple solutions of the trigonometric equation

$$\tan\lambda L = \frac{hL}{k\lambda L} = \frac{hL}{k}\frac{1}{\lambda L} = \frac{Bi}{\lambda L} \quad (14)$$

This solution has been obtained with the standard method of partial derivative differential equations [3],

C.4.4.4 Least square regression

The analytical solution can be used as a model for a least square regression procedure, considering two unknown parameters to be evaluated the temperature before heating (equal to the fluid temperature T_f) and the convection coefficient h. In the procedure the following quantities have benn considered as constants:

Common Variable

L = 0.00187 m	Thickness of window glass
λ_g = 0.77 W/m K	Thermal Conductivity of window glass
I = 0.897 A	Electric Current

$\alpha = 33.5 \cdot 10^{-9}$ Thermal diffusivity of window glass [m²/s]

$A = 0.00125$ Sensor area =0,05m x 0,025m [m²]

Taking as an example the test shown in fig. 56a, (flat sensor, gold coated, blackened), to evaluate the power supplied to the sensor ($R \cdot I^2$), the mean electric resistance is computed as average of all the acquired data (during 20 s), and resulted

$R = 8{,}430\ \Omega$

Regression best estimation of the unknowns leads to

$h \pm \Delta h = (8.18 \pm 0.34)\ \mathrm{W/m^2K}$

the prevision uncertainty on original data (temperature) is $s_{T/t} = 0{,}16$ °C, which can be considered enough accurate.

The computed behaviour from the model is plotted overlapped to the experimental data in fig. 58a. In fig. 58b the residual analysis is shown: a residual model uncertainty still exists (recognizable from the systematic behaviour of residual), probably due to the non perfect correctness of the assumptions made, e.g. perfect insulation on the bottom of the glass and constancy of h. Anyway the correspondence of the theoretical model to the experimental data can be considered quite good.

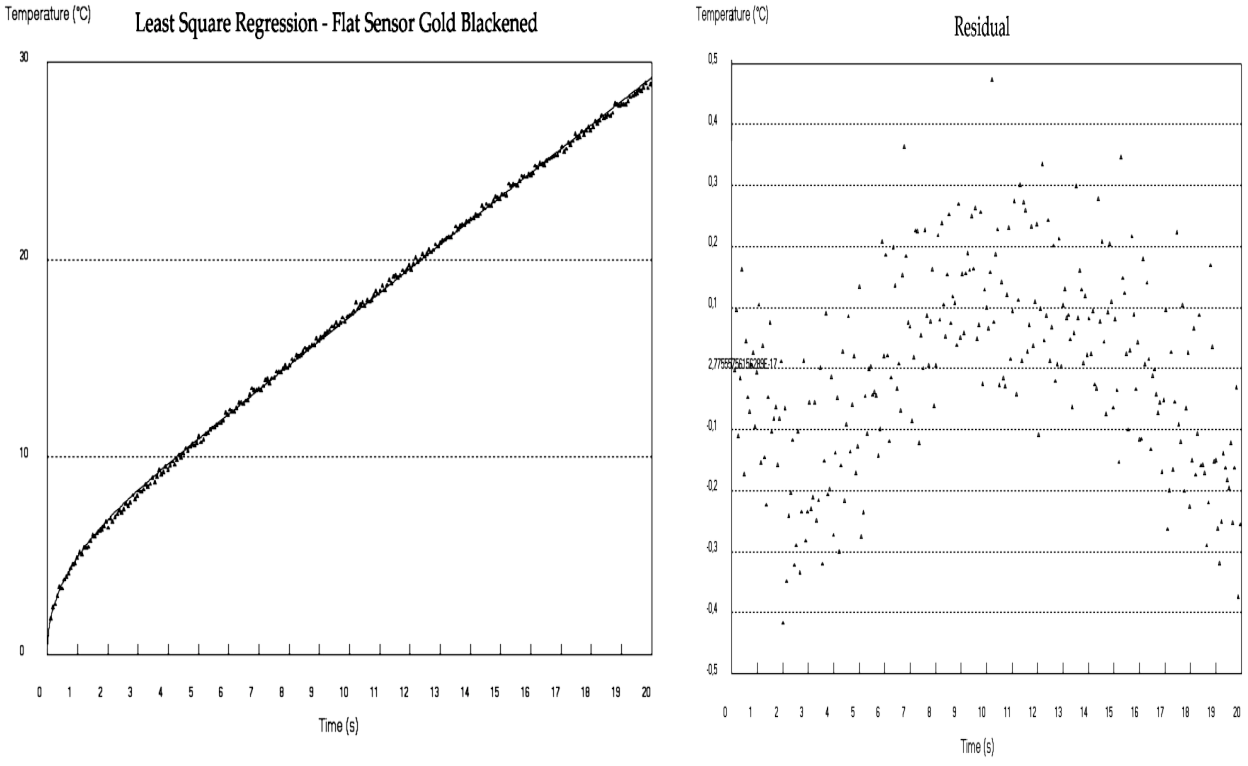

a. b.

Figure 58: Regression results for flat sensor with blackened gold coating a. LSR b. Residual

For the other part of the sensor (the unblackened one) the following data and results are obtained:

R = 8.378Ω ' Mean electric resistance during heating

h = (6,15 ± 0,32) W/m^{2}K

prevision uncertainty on temperature data = 0,15°C

From the results(Fig 59) , a meaningful difference can be noted between the h value obtained for the blackened and the unblackened coating. As can be expected, the value of the blackened one is higher , because it includes also the radiative component, which in the case of unblackened is not present (or at least influences much less the value). The shown results have been obtained in natural convection, when an increasing of temperature ob about 27 °C, with the heated surface upward and the sensors in horizontal position. A wider resume of other results is reported in the following paragraph (4.5 and 4.6).

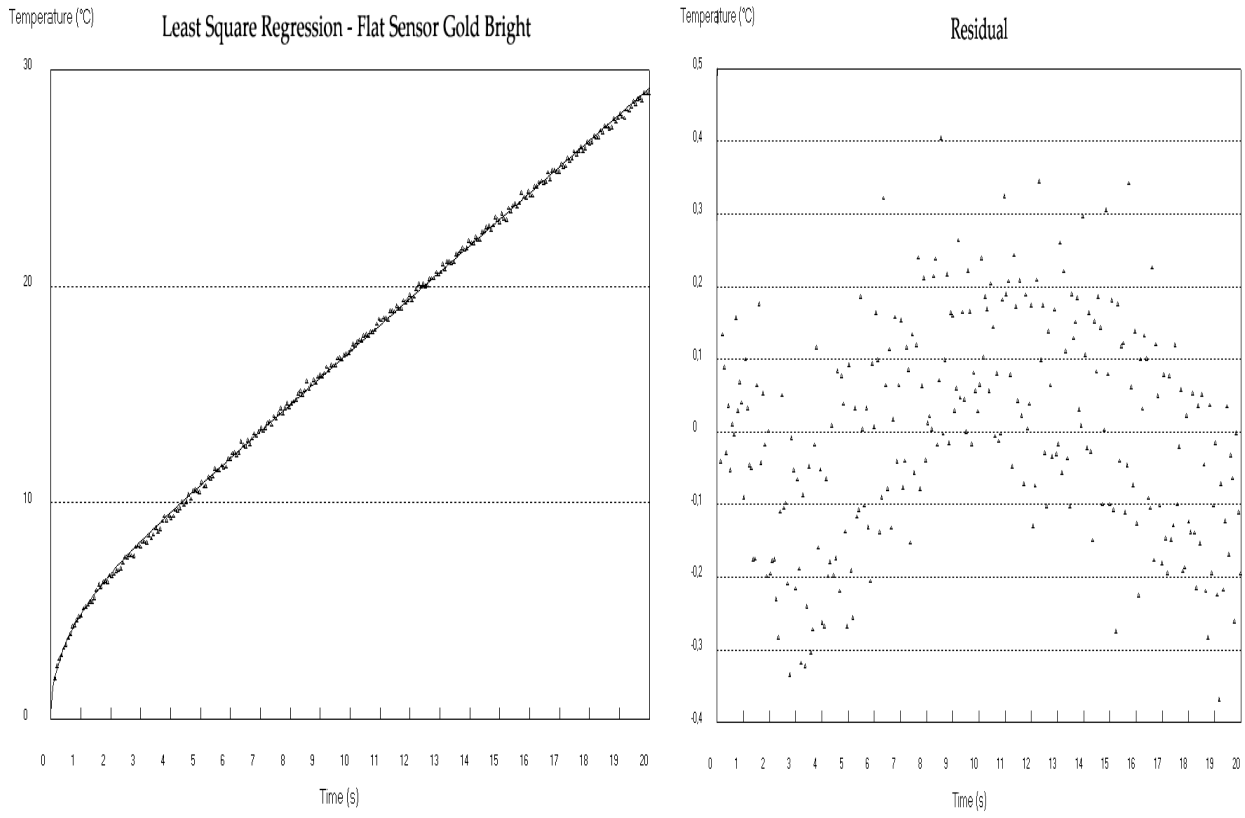

a. b.

Figure 59: Regression results for flat sensor with bright gold coating a. LSR b. Residual

C.4.4.5 Theoretical model for platinum coating

The sensor with platinum coating has been modelled with a phenomenological behaviour. Taking into account that the thickness of the silicon wafer is small (0,5mm), and the thickness of the silicon

oxide produced on the surface as insulator is even negligible (1μm), the temperature behaviour can be described by a double lumped parameter model, assuming also a 0°C of temperature increase at the beginning of heating. The resulting equation is

$$T(t) = b_1(1 - e^{b_3 t}) + b_2 t \quad (15)$$

in this equation the beginning of the exponential behaviour is describe by a linear trend ($b_2 t$) because of then same reason of the behaviour shown for the gold coating, and the measuring time results so small that no or little curvature is recognized in the final trend of this behaviour..

C.4.4.6 Least square regression

The tests have been carried out with the same experimental set up for the gold coated sensors (Fig. 45). In figure 49 the experimental data acquired, to use in the LSR, are reported, together with the behaviour of relation (15), when a current of 900mA circulates in the circuit.
For the both parts of the sensor, blackened and bright, the same condition and data processing have been used.
Least square regression results for the platinum coated sensor blackened (Fig. 60a) are

$b_1 \pm \Delta b_1 = 10.35 \pm 9.8 \cdot 10^{-2}$
$b_2 \pm \Delta b_2 = 1.116 \pm 5.9 \cdot 10^{-3}$
$b_3 \pm \Delta b_3 = (29.6 \pm 4.3) \cdot 10^{-3}$

Prevision uncertainty of data = 0.17 °C

Being difficult to recognize a parameter connected to the value of h in the used analytical model, it has been decided to use as an indicator of the effective of the convection coefficient in the temperature behaviour the maximum temperature reached after 20 s. From the reported experimental data (Fig. 60b), this value resulted

$\Delta T_{t=20} = 32.65$ °C

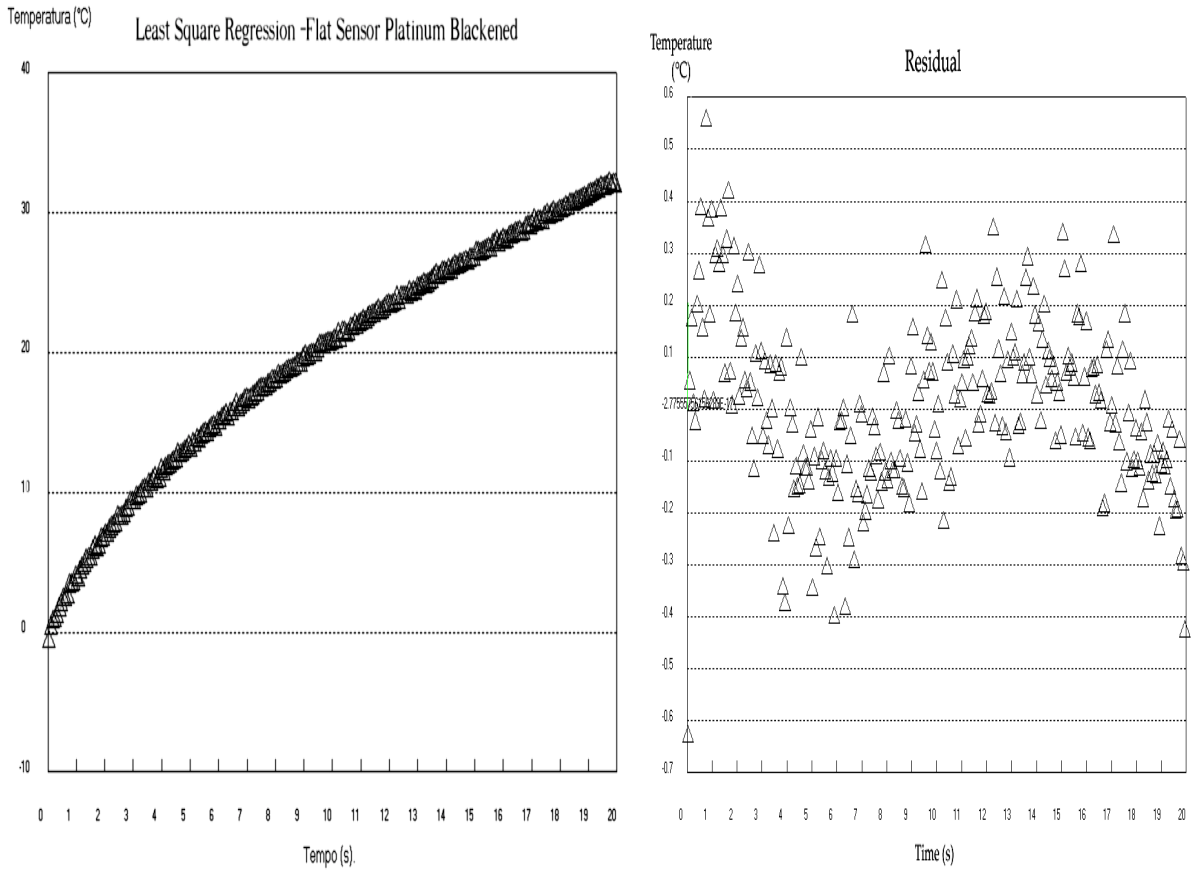

a. b.

Figure 60 Regression results for flat sensor with blackened platinum coating a. LSR b. Residual

For the other part of the platinum coated sensor (unblackened platinum) the results of the least square regression are (see fig. 61a)

$b_1 \pm \Delta b_1 = 11.0674 \pm 0.0\ 8985$

$b_2 \pm \Delta b_2 = 1.1393 \pm 0.0054715$

$b_3 \pm \Delta\, b_3 = (30.5505 \pm 3.9028)\ 10^{-3}$

Estimated uncertainty of data is = 0.16 obtained from the regression program.

ΔT after 20 second is 33.83 °C

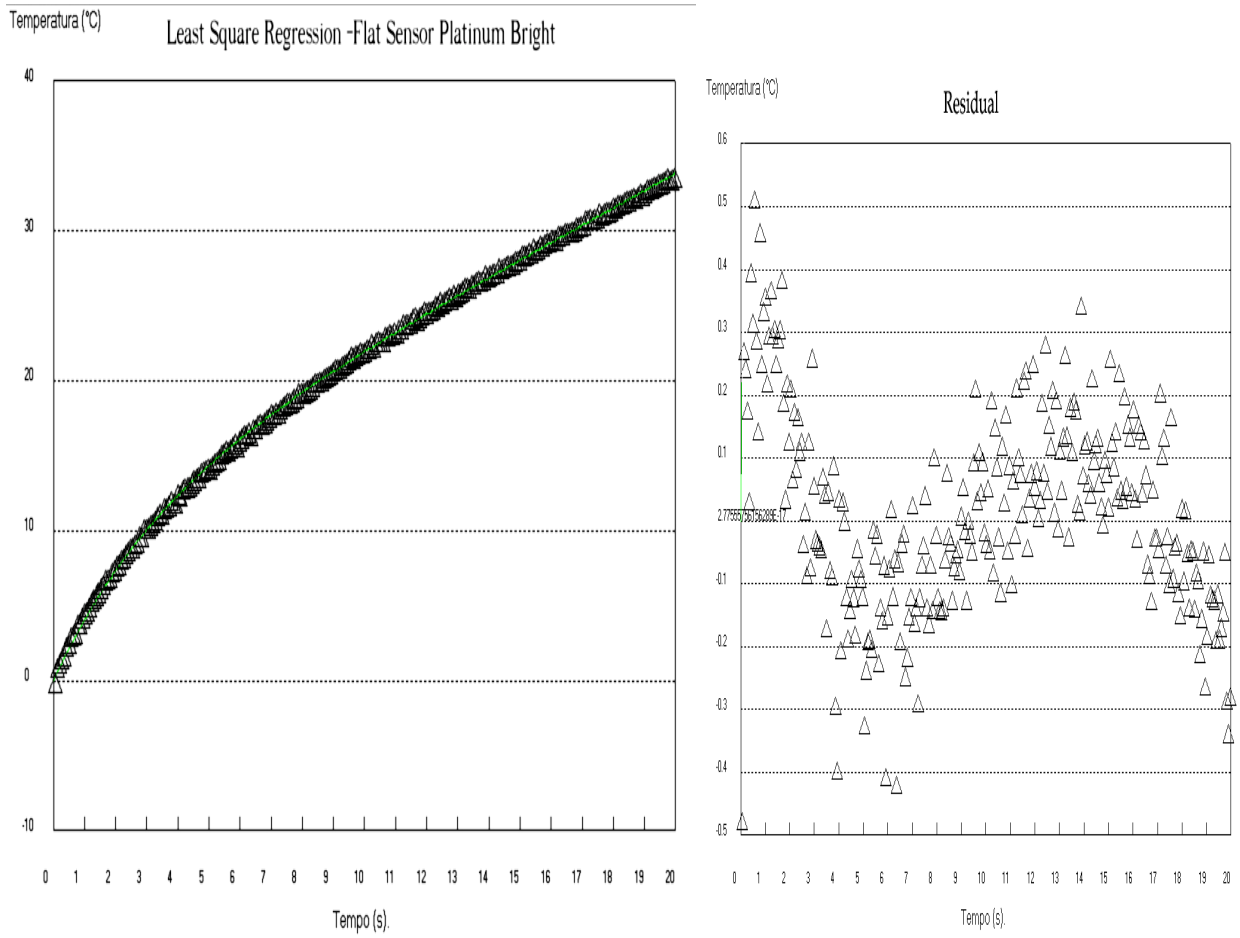

a. b.

Figure 61 Regression results for flat sensor with bright platinum coating a. LSR b. Residual

Again a difference is noted in the maximum reached temperature during the test, after 20 s, in the two cases (blackened and unblackened).

In the following paragraphs an evaluation has been carried out of the influence of the air velocity and the mean radiant temperature on the results obtained by the least regression method on sets of tests performed on the above described sensors.

C.4.5 Influence of the air velocity

Convective heat transfer coefficient (h) of the sensor changes with velocity of air: the higher is the velocity, the higher is h value. For the gold sensor the relation between h and velocity is directly given from the results. On the contrary, as already noted, for the platinum coated sensor, the behaviour t of maximum reached temperature ($T_{20'}$) is plotted versus different air velocities. As can be expected, ΔT_{max} is lower as air velocity increases.

C.4.5.1 Description and characteristics of the measurements

Before test beginning, the air velocity is measured with a fan anemometer (see Fig. 62), and the same measurements were carried out for all the tests, both on gold and platinum coated sensors. , Measurements were made feeding the electric circuit with a current of 50mA for 5 seconds, then with a current step of 900mA for 20 seconds. In both tests the shunt resistance and sensor voltage drop is recorded, and the flat sensor resistance is evaluated.

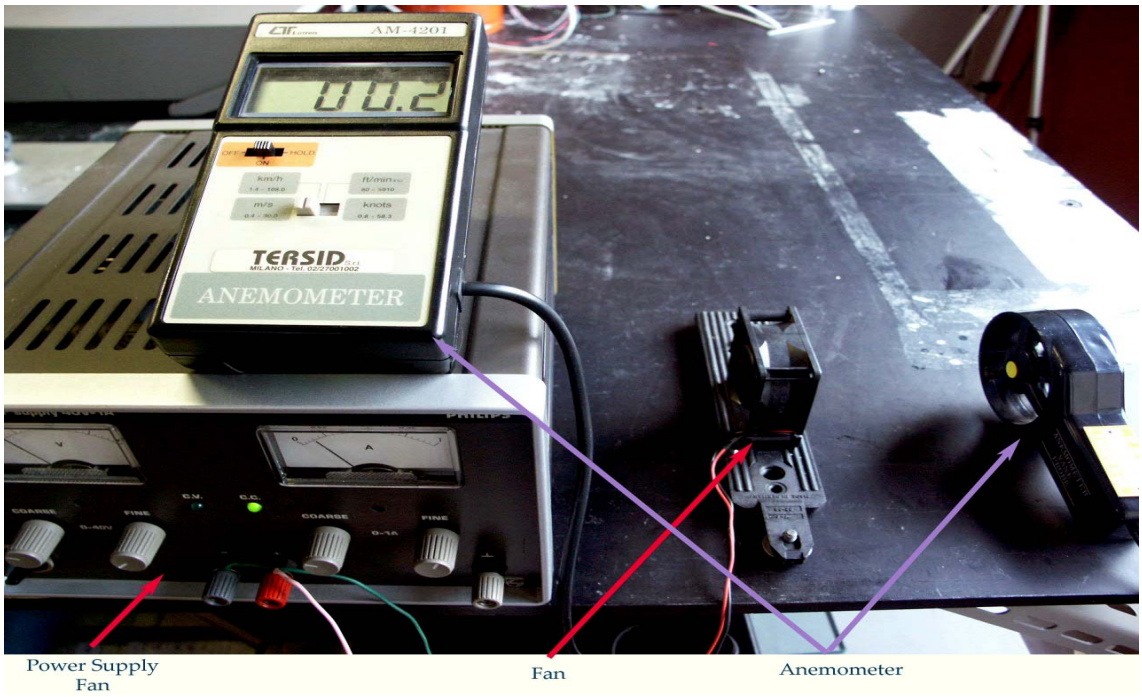

Figure 62: Measurement of air velocity

C.4.5.2 Used Instrumentation for measurements

2700 Multimeter/Data Acquisition Systems -Keithley Integra series

Bipolar Operational Power supply/Amplifier –Kepco 100V/1A

DC Brushlessfan Model FBM-06A12HF DC12V/0.2A)

Anemometer Vane Probe AM-4201-LTLutron

Standard shunt resistance 0.1Ω

C.4.5.3 Results for flat sensor gold coated

All sensors of gold (blackened and bright) are particularly sensible to direction of air velocity. The most effective influence on *h* is obtained when the sensor surface is positioned perpendicularly to the air flux (normal flux), as can be expected .

Characteristic curve of air velocity vs coefficient convection are represented in the below reported figures 63 a and b. Results of *h* obtained by the least square regression above described are reported as a function of the air velocity as measured by the fan anemometer. *h* value big increasing begins when air velocities are higher than 1.0 m/s.

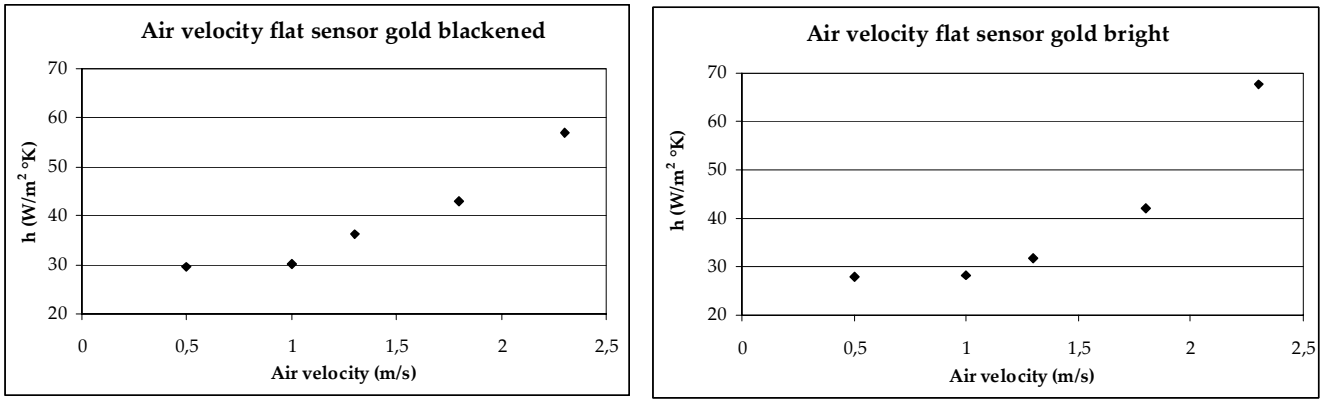

a. b.

Figure 63. Characteristic curve the air velocity vs coefficient convection for flat sensor gold: a. Blackened, b. Bright

C.4.5.4 Results for flat sensor platinum coated

Also platinum sensors (blackened and bright) are particularly sensible to direction of air velocity. And again the highest effect on ΔT is obtained when the sensor is in normal flux.

Characteristic curve of air velocity vs delta temperature are represented in figure 64

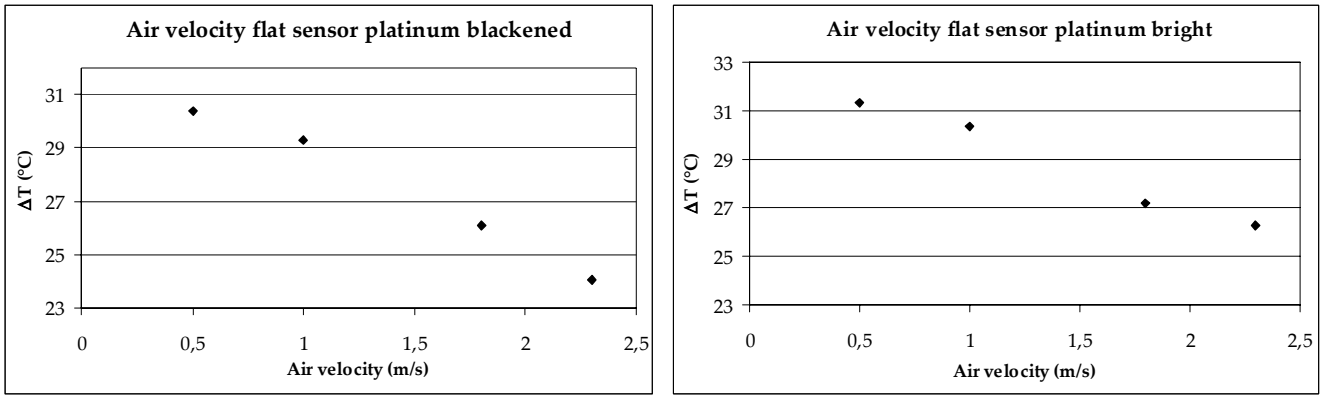

a. b.

Figure 64. The characteristic curve the air velocity vs delta temperature(ΔT) for flat sensor platinum: a. Blackened, b. Bright

C.4.6 Influence of the mean radiant temperature (*T*mr)

One of the parameters, the Mean Radiant Temperature, requires a more detailed explanation. The Mean Radiant Temperature of an environment is defined as *that uniform temperature of an imaginary black enclosure which would result in the same heat loss by radiation from the person as the actual non-uniform enclosure*. **[10]**

Measuring the temperature of all surfaces in the room is very time consuming, and even more time consuming is the calculation of the corresponding angle factors.

Convective heat transfer coefficient is influenced also by the radiation. In fact a radiative component of the convection heat transfer coefficient can be defined in the following way.

Radiation heat exchange from a surface (e.g. the sensor) at a temperature T_s to an environment T_{amb} is given by the usual relation

$$\dot{Q} = \varepsilon_s \sigma A_s \left({T_s}^4 - {T_{amb}}^4 \right) \quad (16)$$

being ε_s the emissivity of the surface, σ the Stephan Boltzmann constant. And A_s the surface area.

This equation can be written as

$$\dot{Q} = \varepsilon_s \sigma A_s \left(T_s - T_{amb} \right) \left({T_s}^3 + {T_s}^2 \cdot T_{amb} + T_s \cdot {T_{amb}}^2 + {T_{amb}}^3 \right) \quad (17)$$

if the two temperature are not too each other different

$$\dot{Q} \approx \varepsilon_s \sigma A_s \left(T_s - T_{amb} \right) \cdot 4 {T_m}^3 \quad (18)$$

being T_m the average temperature of T_s and T_{amb} . If the same thermal heat transfer is written as

$$\dot{Q} = h_r A_s \left(T_s - T_{amb} \right) \quad (19)$$

the radiative heat transfer coefficient component results

$$h_r = \varepsilon_s \sigma \cdot 4 T_m^{\,3} \quad (20)$$

So if a difference in the emissivity exists between the two parts of the sensors, the blackened and the bright one), also e difference should results in *h*, and consequently in the recorded temperature behaviour [8].

C.4.6.1 Determination of the mean radiant temperature

A radiation sensor, as a thermopile, gives information about the radiation coming from the surface where it is pointed on. It is possible to say that the thermopile measures the mean radiant temperature of the surfaces where it is faced. If all the environment is at the same temperature, the thermopile measures the mean radiant temperature, wherever it is faced. When there is a surface in the ambient at a different temperature, the mean radiant temperature must be calculated by averaging the different temperatures of the different surfaces, according to the definitions of T_{mr}.

In order to simulate a surface with a significant different temperature form the others, in the present work it has been used a glass plate, placed in from of a halogen lamp kept at constant temperature, and hence emitting constantly in time. To have a uniform temperature on the plate, a translucent membrane is put on its.

Thermopile used had been previously opportunely calibrated, see fig 65, to link the signal output to T_{mr}. The perform this calibration, the thermopile is placed on the aperture of the cavity of a black body (the same used for calibration of the pyrometer for forehead skin measurement), and the signal is recorded as the black body temperature was changing, recorded by a calibrated type J thermocouple. The relation reported in Fig. 66 is the one to be used to convert the thermopile output signal in T_{mr}.

Mean radiant temperature is then calculated by measuring the mean radiant temperature of the glass (covered by the plastic) and the one of the other surfaces in the environmental. In this case only two surfaces (at different temperatures) contribute to T_{mr}. In fact, from the definition of T_{mr}.it results:

$$\left(T_{mr}^{\,4} - T_s^{\,4}\right)\sigma\varepsilon_s A_s = \sum_{i=1}^{n} A_s F_{s-i}\sigma\left(T_i^{\,4} - T_s^{\,4}\right) \quad (21)$$

being $F_{i\text{-}j}$ the radiation configuration factor between the surfaces *i* and *j* [9]. Taking into account that

$$\sum_{i=1}^{n} F_{s-i} = 1 \quad (22)$$

T_{mr} results

$$T_{mr} = \sqrt[4]{\sum_{i=1}^{n} F_{s-i} T_i^{\,4}} \quad (23)$$

with in the present case n=2 (the glass plate and the other surfaces. So the first step in computing the mean radiant temperature is to compute $F_{s\text{-}i}$ (from the completeness relation $F_{s\text{-}1}$ is equal to (1- $F_{s\text{-}2}$) . This is done by means of the formulae reported by [9] , p. n. .

The following below reported coefficients are calculated:

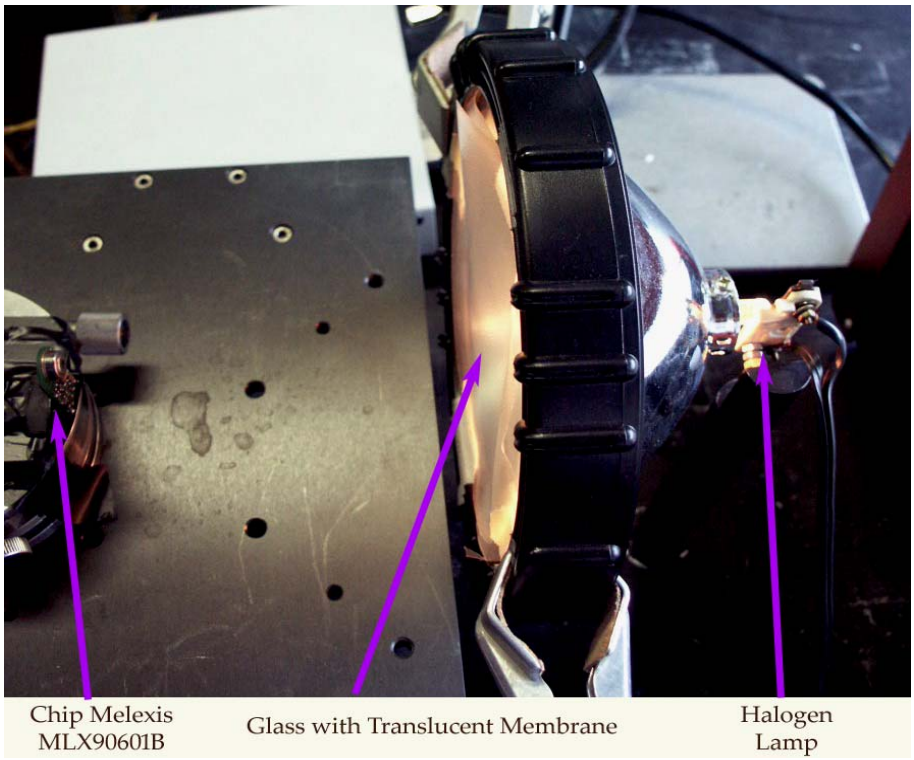

Figure 65: Measurement of the radiation with thermopile

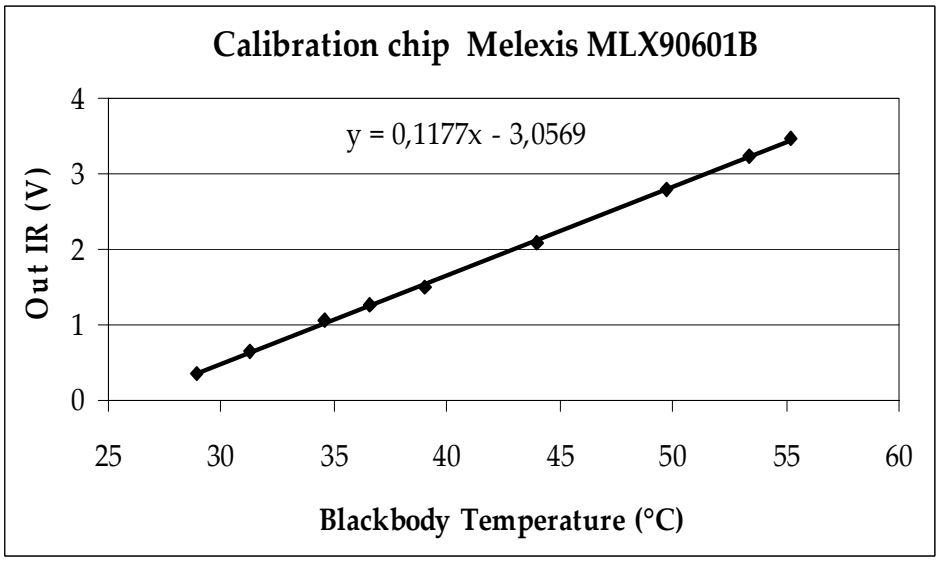

Figure 66: Calibration chip with blackbody “Tor Vergata”

The configuration factor depends clearly on the relative position of the sensor the glass plate position. (see fig 68). If it is calculated according to the rules gives by [9], the rectangular surface of each part of the sensor must be divided into four triangles, as can be see in Fig. 68. The configuration factors of all these triangles to the circle (plate with the translucent plastic) can be evaluated by the same formulas, again the C-33 of pag. 120-124 of [9](see fig 67).

The following quantities, according to [9], are then calculated:

$X=r/d$; $Y= d/l_1$; $Z=d/l_2$, F_{12}, F_{23}, F_{34} and F_{41}

With this factors it's possible to calculate

$F_{C-S} = F_{C-1} + F_{C-2} + F_{C-3} + F_{C-4}$ (25); (being C the circular glass plate)

Appling the reciprocity relation $A_s F_{S,C} = A_C F_{C;S}$ (26) we obtain:

$$T_{mr} = \sqrt[4]{F_{S,C}(T_C + 273)^4 + (1 - F_{S,C})(T_{amb} + 273)^4} - 273 \quad (27)$$

where :

$F_{C,S}$ radiation factor and A_C circle area

$F_{S,C}$ radiation factor and A_S flat sensor area

T_C the glass temperature (previous calculated with thermopile) [°C]

T_{amb} the ambient temperature [°C]

T_{mr} the mean radiant temperature [°C]

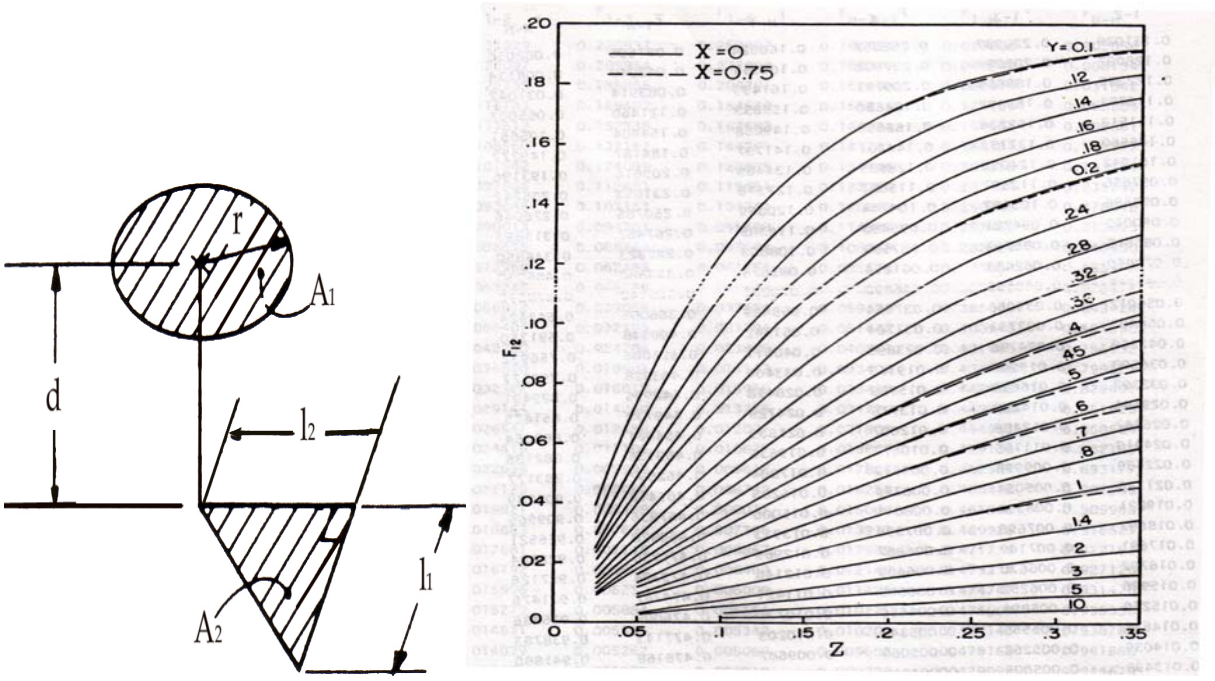

Figure 67: The configuration factors

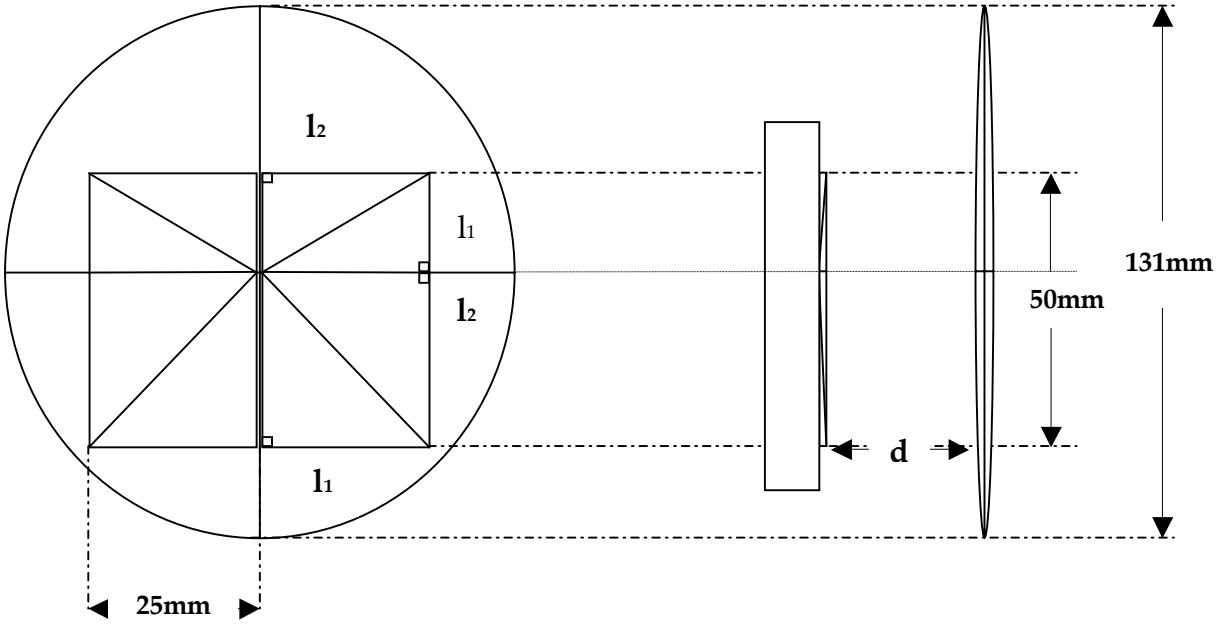

Figure 68: Relative positions of the sensor

C.4.6.2 Used Instrumentation for measurements

2700 Multimeter/Data Acquisition Systems -Keithley Integra series
Bipolar Operational Power supply/Amplifier –Kepco 100V/1A
Data Acquisition Systems and Control-Daqcard 6036 series E -National Instruments
DC power Supply 40V/1A-PE1537 Philips
Regulated Power Supply-BV170 40V/4.5A
Halogen 12V/50W Osram
Thermometer module Melexis MLX90601B

For the present tests two data acquisition systems were necessary, one (Keithley) for acquiring the sensor data , and the other (NI) for commanding with the DAC the constant current power supply.

C.4.6.3 Description and characteristics of the measurements

As for all the tests carried on the gold or platinum coated sensors, the measurements were made feeding the electric circuit with a current 900mA, in order to get a temperature increase of about 25-30°C. But in the present experiments, the glass temperature changed from the switching on of

the lamp(see Fig 69), till to a steady state value (as recorded by the thermopile output). Only when this value was reached, the heating of the sensor could begin, with the usual procedure.

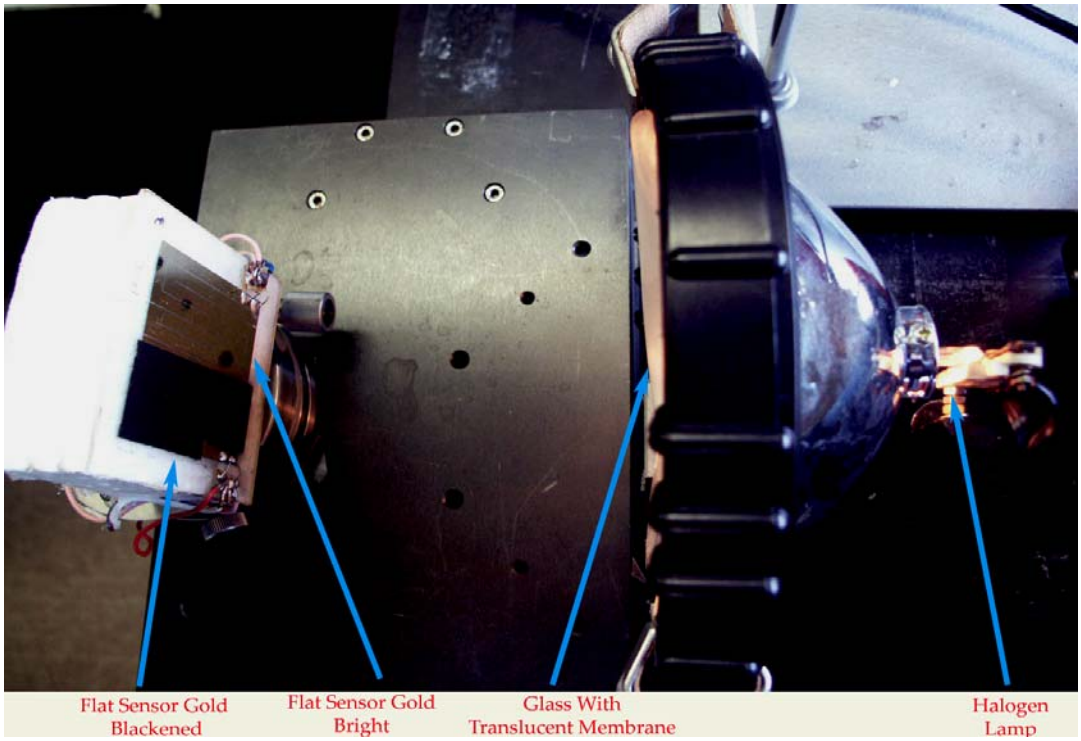

Figure 69: Test with flat sensor

C.4.6.4 Results for flat gold coated sensor

From the results of the tests (temperature behaviour versus time) first the convection coefficient is calculated with the least square regression procedure. Second the behaviours of the convection coefficients as a function of the mean radiant temperature (as measured with the thermopile and calculated as described in the previous subparagraph) are depicted .

Comparing the results of the two sensors, it appears immediately that two major differences exist:

- first, the temperature of the blackened sensor is always higher (from 2 to 3.5 °C) then the one of the bright (see Fig. 70)
- second, the sensitivity (i.e. the ratio between the convection coefficient increasing and the T_{mr} increasing) results almost the double for the blackened sensor (0.47 as regard 0.27)

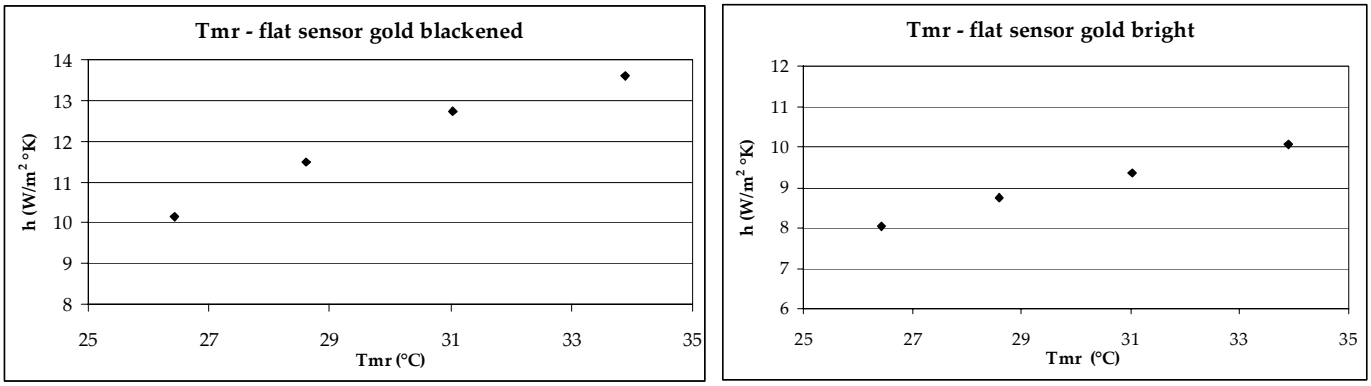

a. b.

Figure 70. The characteristic curves of convection coefficient versus the mean radiant temperature for flat sensor gold coated: a. Blackened, b. Bright

C.4.6.5 Results for flat sensor platinum coated

In the same way as for the air velocity dependence, platinum coated behaviour has been characterized by the maximum temperature reached during the test, computed fro the least square regression procedure. Clearly the mean radiant temperature has been evaluated in the same way. Results are shown in Fig. 71 a and b. Results agree completely with those of gold coated sensor, inasmuch sensitivity (now evaluated as ratio between decreasing of Δt_{max} and increasing of T_{mr}) varies from 0.46 for the blackened sensor to 0.25 for the bright one.

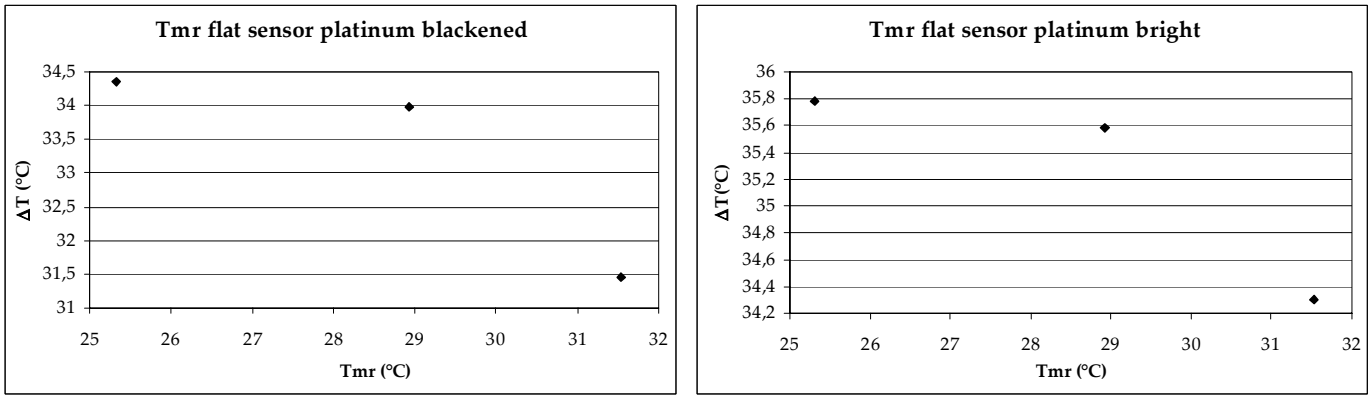

a. **b.**

Figure 71. The characteristic curves of temperature increase (ΔT_{max}) vs. r mean radiant temperature for flat sensor platinum coated: a. Blackened, b. Bright

C.5 Conclusions

- The gold coated flat sensors have the capacity of measuring al the three desired comfort variables: air temperature, air velocity and mean radiant temperature,. The first is measured through the initial value of the resistance, when ho heating of the metal deposition occurs. The second and the third quantities through the convective heat transfer coefficient. From the difference between the temperature behaviour of the blackened and the bright part of the sensor the mean radiant temperature can be deduced. The tests are easy to be conducted, only a stabilized power supply is needed. Test duration is about 25 s, and temperature increase lower than 30 °C (but there is no necessity for the sensor to be touched). The realized sensor is relatively easy to be fabricated, and the base material is rough (window glass) and very cheap, while the deposited gold is so thin that the necessary quantity represents a negligible cost increasing, at least in a large number of quantity. An improvement of the quality of the sensor, and also of its endurance, is the protection of the gold deposit with a thin layer (0.1 μm) of silicon oxide (vacuum deposited), or magnesium oxide, for avoiding metal contamination, abrasion, and facilitating cleaning.
- The platinum coated flat sensors have the capacity of measuring the same quantities through the same procedure. Compared to the results of the gold coated sensors, the temperature uncertainty in calibration is slightly higher, but the results of the dependence of the maximum temperature increase during the tests and the air velocity and the mean radiant temperature is quite good all the same. More efforts must be paid to get cheap sensors, inasmuch the realized ones have a silicon wafer base, having been impossible to deposit the platinum on glass. Other problems arise from contamination of platinum in temperature, which obliges to stabilize coating many hours (at least 48h) before using it. Also platinum coated sensors could profitable be covered by a thin layer of protective oxide.
- A practical use of the sensors to judge comfort conditions, as for instance in the car passenger compartment, as a medallion to be worn on the suit of the test driver, requires a more particular set up. For examples a cage of metal wire could be added to prevent heating by touching it, even if the maximum reached temperature is about 60°C. Connections with a portable power supply must be provided, and a data acquisition and processing data must be located near the test driver.

D. GENERAL CONCLUSIONS

- The overall activity of the described research has led to two different sensor.
- The first is an individual forehead skin temperature detector (low temperature pyrometer), which can be used to monitor temperature of people laid on a bed (in hospitals) or passing through the gate of an airport to recognize the presence of illness. e.g. SARS or Ebola virus. The accuracy of the instrument was about 0.15 °C. Unfortunately no correlation was found between the skin temperature and the declare vote of people in passenger compartment of cars, in order to develop an individual system for the climate control inside car. This lack of correlation was confirmed both during tests in a hot season (summer) and cold (winter).
- The second is a single sensor for detecting the three most influencing variables of comfort, i.e. air temperature, mean radiant temperature and air velocity. This device has been studied, designed, built, calibrated and tested. Again the temperature accuracy resulted about 0.15 °C, enough for the desired applications. It is constituted by a metal deposit (gold or platinum) on a flat support (glass or silicon wafer). An insulation from the underling ground is foreseen. The sensor is a medallion to be pointed on the suit of the car inspector. It is fed by a constant current and gives: the air temperature when the electric current supplied is so small to avoid self heating; the air velocity during the transient state when a current enough high to produce about 30 °C heating is supplied, and finally the mean radiant temperature from the difference between the two components of the sensor, a blackened art and a bright one. A good sensitivity to the above mentioned quantities has been tried and demonstrated.
- Industrialization of both sensor is still needed to get a device portable, reliable, without problem of contamination of the mirror or the sensible elements (coatings) from powder and pollution. This could be done by vacuum depositing a layer of SiO or MgO on the mirror and coatings. The working distance of the pyrometer could change in order to meet different requirements. In this case a proper optical designing (similar but not equal to the present one) should be provided. If also the relative humidity is desired, a semiconductor detector could be joined to the flat sensor to supply this further information. An electronic chip able to supply the most suited current to the flat sensor, to process data and to give an overall comfort evaluation could be realized.

Acknowledgements

I am especially grateful to Fiat Center of Research and Department of Electronic Engineering of Tor Vergata, for providing funds and for suggesting the research project.
I would like to express all my gratitude to my advisor Paolo Coppa, professor at the Department of Mechanical Engineering of the University of Rome – "Tor Vergata", for his grand support and humanity, never missing during these three years of research activity. Also, I want to thank Arnaldo D'Amico, professor at the Department of Electronic Engineering of Tor Vergata for his precious suggestions, Mr. Petrocco and the entire technical personnel of the National Council of the Research for their support during the sensor production stage, Ing. Malvicino of the FIAT Center of Research for the amicable cooperation, Dott. Tavernese for the vehicle experimental setup and tests. Finally, many thanks to all the PhD and graduating students at the Thermal-Fluid Dynamics laboratories at the Department of Mechanical Engineering of Tor Vergata and, of course, to all the friends sustaining and standing me during this formative and very amazing time at Tor Vergata.

References

[1] P. O. Fanger, Thermal Comfort, McGraw-Hill Book Company, New York, pp 243, 1973

[2] K. C. Wei, G. A. Dage, "An Intelligent Automotive Climate Control System",*IEEE Transaction* n.0-7803-2564-1/95,1995

[3] H.S. Carslaw, J.C. Jaeger, Conduction of heat in solids, Oxford university press second edition Great Bretain 1959

[4] R. Kingslake, *Optical System Design*, Academic Press Inc(London), 1983

[5] P. Godts, F. Raucoleus, S. Sakly, F .Polet, "A New self calibrating Radiation Planar Microsensor.Application to Contactless Temperature Measurement in a Car", *IEEE Instrumentation and Measurement Conference*, Brussel,1996,pp.778-781

[6] S. Brandt, Statistical and computational methods in data analysis,North-Holland,1976

[7] Y. Taniguchi, H. Aoki, K. Fujikake, H. Tanaka, M. Kitada, "Study on Car Air System Controlled by Car Occupants", *Development of a New Air Conditioning System*, SAE paper N.O.920887,1992

[8] J. P. Holman, Heat Transfer; McGraw-Hill International Book Company, New York, Fifth Edition 1981

[9] John R. Howell, Radiations Configuration Factors; McGraw-Hill International Book Company, New York.

[10] ISO Standard 7730: 1994

[11] P. Coppa, C. Corsaro, "Misura Radiante della temperatura della Pelle per il comfort termico all'interno degli autovehiculi", Università di Tor Vergata Roma

[12] R. Tmusic, A. Durisic, D. Stankovic, "Dynamic and Static Characteristics Investigation of Integrated Radiation Thermopile Sensor", *Proc. of the 21th Intern. Conf on Microelectronics (MIEL'97)*, Yugoslavia, 14-17 Sept. 1997, pp. 565-568

[13] H. Kataoka, H. Kano, H. Yoshida, A. Saijo, M. Yasuda, M. Osudi, "Development of a Skin Temperature measuring system for non-contact stress evaluation", *Proc. of the 20th International Annual Intern. Conf of The IEEE Engineering in Medicine and Biology Society*, **20**, pp. 940-943 ,1998

[14] H.Tanaka, M. Kitada, Y. Taniguchi, Y. Ohno, T. Shinagawa, H. Aoki, "Study on Car Air Conditioning System Controlled by Car Occuppants' Skin Temperatures – Part 2: Development of a New Air Conditioning System", SAE paper N.o 920170, 1992

[15] The International Temperature Scale of 1990 (ITS-90*). The official French text of the ITS-90 is published by the BIPM as part of the Prochès-verbaux of the Comité International des Poids et Mesures (CIPM).*

[16] Hak Min lee, Chang K, Cho, Myung Hwan Yun, Myun W. Lee, "Development of a Temperaure Control Procedure for a Room Air –Conditioner Using Concept of just Noticeable Difference (JND) in Thermal Sensation", *Industrial Ergonomics*, **22**, pp. 207-216,1998

[17] Fondamenti di Impianti di Climatizzazione per Autovetture, Volkswagen AG, aggiornamento tecnico 12/98

[18] Web site Melexis corporate- www.melexis.com

[19] Web site of the FIAT Center of Research (CRF) -http://www.crf.it/B/B1_4.html

Appendix

1. Thermo-regulatory System of a Human Being[1]

A human being has a nearly constant internal temperature ~37°C, and is not influenced even by large variations In ambient temperature. The internal temperature (core-temperature) can be kept constant only if there is balance between the heat which is produced by the body and the heat which is lost to the environment. In warm-blooded mammals, including man, the heat balance is controlled mainly by the hypothalamus, which is the part of the brain that acts like a thermostat.

The heat balance is controlled by the Information the temperature centre receives about the temperature conditions in the body. Thermo-receptors are situated both in the temperature centre in the brain and to a great extent in the skin. There are probably also thermo-receptors in other parts of the body as muscles, lungs and spinal-cord. There are both cold receptors and warm receptors. When the temperature, especially temperature changes, influence these receptors, nerve Impulses are transmitted to the temperature centre in the brain. Here the Information is co-ordinated, resulting In reactions which will keep the Internal body temperature constant.

Cold receptors start cold sensations if the temperature in a skin area decreases faster than approximately 0,004°C/s (14,4°C/h). Warm receptors start warm-sensations if the temperature in a skin area increases faster than approximately 0,001°C/s (3,6°C/h).

The heat production in the body takes place continuously by the metabolic process which converts chemical energy Into heat. This heat production (basal-metabolism) is of the order 1 W/kg (body weight), If It is measured at rest during certain standard conditions (fasting 8 hours after last meal, and lying relaxed at a neutral temperature). In cold environments the temperature centre starts tensions In the muscles, which start the metabolic process, and heat production Increases. In still colder environments, the muscle tensions will cause shivering, which can increase the heat production by a factor of three times the basal metabolism.
The greatest changes in heat production -are, however, the result of muscle work, which can change the heat production by a factor of 10 times the basal metabolism.

The heat Is transported from the warm core to the skin partly by conduction through the tissues and partly by blood flow to the skin.

In cold environments the nerve impulses from the cold receptors result in vaso-constriction i.e. contraction of the blood vessels, decreasing the blood flow and thus heat flow to the skin. To

maintain a high temperature (37°C) in the vital parts of the body, the blood flow is reduced first to the extremities (hands and feet), where the cold sensation is first experienced. When all blood vessels in the skin are completely closed, there will still be heat loss by conduction through the skin to the environment. This heat loss is dependent on the thermal insulation of the skin, which is in the range 0,1 to 1,0 clo depending on the thickness of the layer of fat.

In a hot environment the temperature of the skin is high, and the temperature gradient between the body core and the skin surface is small. Heat exchange by conduction from the core to the skin surface is therefore small. In warm environments however, the blood flow is increased due to vaso-dilation — opening of the blood vessels. For the skin as a whole the blood flow can increase as much as 10 times the minimum. The heat then produced is transported by the blood to the skin surface, where in hot environments it is lost mainly by evaporation of sweat. In hands and feet the blood flow may be changed by a factor of 30.

The regulation of heat loss by evaporation is achieved by secretion of water from the sweat glands. Uncontrolled evaporation of water diffused through the skin (perspiration insensibili) takes place continuously. Furthermore the water content of the air that we inhale Is less than that of the air we exhale. But the amount due to the evaporation when breathing Is however minimal, approximately 40 g/h, equivalent to a heat loss of approximately 28 W. The sweat glands can produce up to 2 to *3* litters of water per hour. Each gram or ml. which evaporates will remove 2,43 kJ from the skin surface. The sweat production, like the blood flow in the skin, is mainly controlled by the temperature centre in the hypothalamus.

Core Temperature and Skin Temperature

The above-mentioned thermo-regulation possibilities, i.e., in cold conditions decreased blood flow and shivering (increased metabolism), and in hot conditions increased blood flow and evaporation of sweat, attempt to maintain a core temperature within certain limits. The core temperature may change from approximately 36°C to 40 - 42°C, under certain circumstances, while the variation in mean skin temperature can be much greater, 17° to 40°C.

The normal core temperature in rest measured in the morning is approximately 37°C. However, there are significant individual differences (36° to 38°C). During a day the core temperature will normally vary by approximately 1°C. The temperature increases during the day and reach its maximum value late in the afternoon. Then it drops again and reaches the lowest temperature during the morning.

During muscle work the body temperature will increase to a higher level, depending on the amount of work. It is now generally believed that this increase is made to benefit the rate of the metabolic process in the working muscles. The core temperature is kept constant independent of great variation in the environmental conditions. But as the body's capacity for heat production and sweat production is limited, there exist upper and lower limits for keeping the heat balance.

If the ambient temperature rises above the upper limit for the regulation area, heat will be accummulated in the body and the core temperature will increase. Then the heat exchange between core and skin surface increases due to the increased blood flow and a new heat balance may be reached, but at a higher level of core temperature. If the environment is too hot the internal temperature will keep increasing up to a fatal level of 42° to 43°C.
In cold environments, where the heat loss even with maximum vaso-constriction is greater than the heat production, the core temperature will decrease. The first reaction is that shivering will start but at approximately 33°C shivering stops and at lower temperatures one reaches unconsciousness. A body temperature of approximately 25"C is fatal.

The skin temperature at different parts of the body tend to be uniform in hot environments. But in cold environments hands, feet, legs and arms in particular, become relatively colder than the head and torso (see Fig.1). The pain limit occurs at approximately 45°C skin temperature.

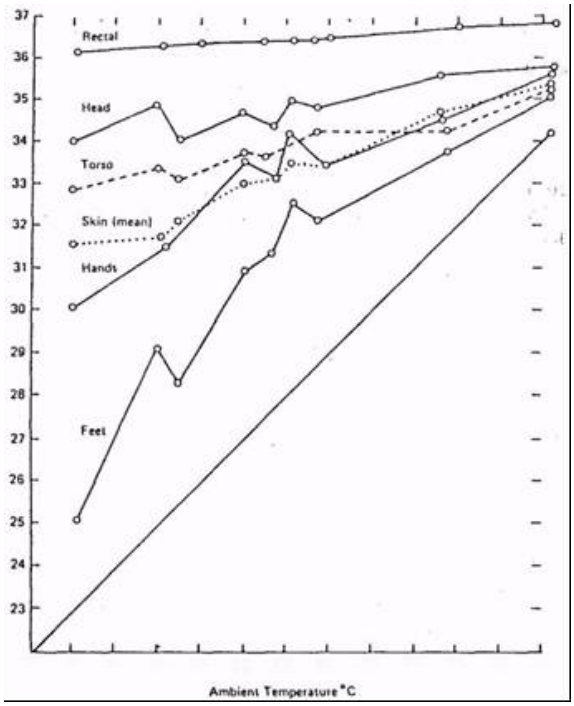

Fig.1

where S= Heat storage

M - Metabolism

W = External work

R = Heat exchange by radiation

C = Heat exchange by convection

K = Heat exchange by conduction

E = Heat loss by evaporation

RES = Heat exchange by respiration

Heat balance is reached if the storage S = 0.

The above heat balance equation is often used. However, when dealing with a person with clothing it is preferable to write the heat balance equation as (S = 0):

$$M \pm W - E - RES = \pm Kci = + R \pm C \qquad (2)$$

where $K_c i$ = Heat conduction through the clothing

The sign indicates that the parameter may be negative or positive i.e. heat loss or heat gain.

The double equation implies, that the metabolism *(M)* including the external work *(W)* minus the heat loss by evaporation *(E)* and respiration *(RES)* is equal to the heat conduction through the clothing *($K_c i$)* and equal to the heat loss by radiation *(R)* and convection *(C)* from the outer surface of the clothing.

The above equation does not take into account the heat exchange by conduction, for example, when loading sacks or the contact between feet and the floor. This amount is normally insignificant compared to the total heat exchange, but has of course a significant Influence on local heat exchange (warm fingers, cold toes).

A person seated in an armchair, will exchange heat by conduction to the chair across a substantial surface area. In this case the chair should be calculated as part of the clothing.

Conditions for Thermal Comfort

Thermal comfort Is defined as that state of mind in which satisfaction Is
expressed with the thermal environment.

The first condition for thermal comfort is that the heat balance equation (2), described in the previous section, is fulfilled.

At a given level of activity *(M),* mean skin temperature *(t_s)* and sweat loss *(E_{sw})* are the only physiological parameters which Influence the heat balance. For a given person at a given activity, clothing and environment, the heat balance will be established by a certain combination of mean skin temperature and sweat loss.

Heat balance is, however, not sufficient to establish thermal comfort: In the wide range of environmental conditions where heat balance can be obtained, there is only a narrow range which will provide thermal comfort. This range is then related to a narrow range for both mean skin temperature and sweat loss. It is assumed that for each Individual and at a given activity, there is a range of values of mean skin temperature (t_s) and sweat loss (E_{sw}) which will provide thermal comfort.

$$\mathbf{a} < \mathbf{r_s} < \boldsymbol{b} \qquad (16)$$

$$\mathbf{c} < \boldsymbol{E_{sw}} < \boldsymbol{d} \qquad (17)$$

These limits will vary with activity and individuals.

In tests with subjects in states of thermal comfort, relations between activity and mean skin temperature, and between activity and sweat loss, were established as shown in Fig.2 and Fig.3. From these Figures the individual differences are obvious and a mean value is used

when establishing the comfort equation.

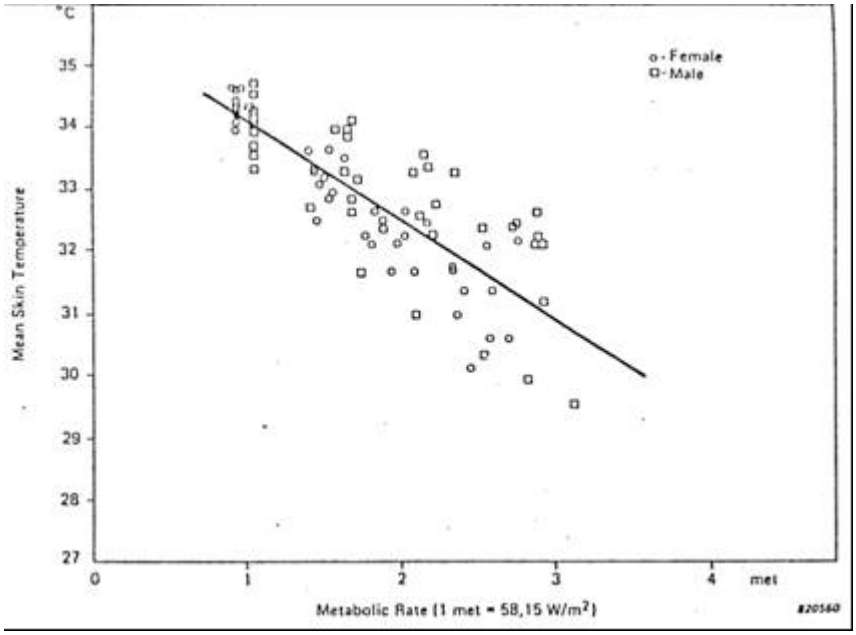

Fig. 2 Mean skin temperature as a function of the activity level for persons In thermal comfort. In order to maintain thermal comfort the ambient temperature is lower the higher the activity level [1]

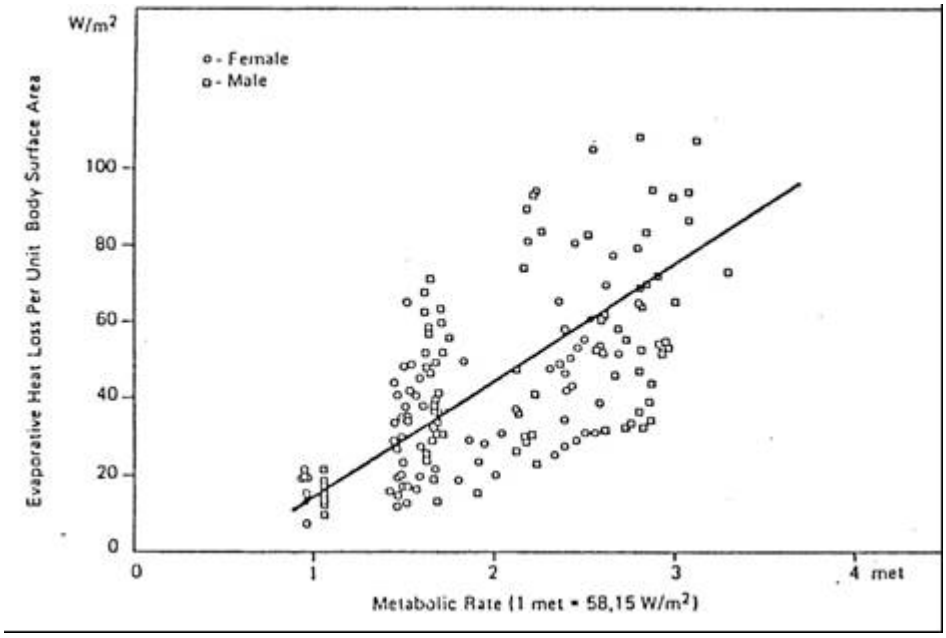

Fig. 3. Evaporative heat loss as a function of the activity level for persons in thermal comfort. In order to maintain thermal comfort the ambient temperature is lower the higher the activity level [1]

Using linear regression the following relations are found:

$$f_s = 35{,}7 - 0{,}0275\ (M - W)\ °C \qquad (18)$$

$$E_{sw} = 0{,}42\ (M - W - 58{,}15) \quad W/m^2 \qquad (19)$$

The mean skin temperature decreases at higher activities and the sweat loss increases. Both reactions will Increase the heat loss from the body core to the environment. For a person seated quietly (M = 58 W/m^2, W = 0) In a state of thermal comfort the mean skin temperature is 34,1°C and there Is no sweat loss. But there Is still evaporative heat loss from water vapour diffusion through the skin and respiration.

The Comfort Equation

If the equations for the heat loss derived In the previous section and the two equations for f_s and E_{sw} are inserted In the double sided heat balance equation (2) the comfort equation is established:

$$(M-W) - 3.05\text{-}10^{-3}\ \{\ 5733 - 6{,}99\ (M-W) - p_a\ \}$$

$$- 0{,}42\ \{\ (M-W) - 58{,}15\ \}\ -1{,}7\text{-}1 < r^5\ M(5867 - p_a) - 0{,}0014\ M\ (34 - t_a)$$

$$= 3.96\text{-}10^{-8}\ f_{cl}\ (t_c + 273)^4 - (f_r + 273)^4 + f_{cl}\ h_c\ (t_{cl} - t_a) \qquad (20)$$

where t_c, = 35,7 - 0,028 *(M-W)* - 0,155 $l_c i$ [*(M-W)*
-3.05-10-^{3} { 5733-6,99 *(M-W)*- p_a } -0,42{ *(M-W)*- 58,15 }
- 1.7-10-^{5} M(5867 - p_a) - 0,0014 *M* (34 - f_a)]

hc=2,38 ($f_{c;}$ - r_{aj})°-^{25} for 2,38 $(t_c, - t_a)°'^{25}$ > 12,1; or
hc=12,1 $\sqrt{Var}$ - for 2,38(f_c, - f_aj°'^{25} <12,1

fcl =1,00 + 0,2 $l_c i$ for /$_c$, < 0,5 clo; or
fcl =1,05 + 0,1 *Id* for *Id* > 0,5 clo

The Comfort Equation establishes those combinations of activity, clothing, and the four environmental variables (air temp., mean radiant temp., air velocity, humidity) which will provide thermal comfort. It has been known for a long time that these six variables influence the state of comfort. But the combined quantitative influence of all the parameters on man's comfort was not known until the Equation was introduced

PMV-PPD index

For technical or economical reasons a thermal environment which will provide optimal thermal comfort is not always possible. It is then often of value to quantify the degree of discomfort, and for this purpose an index has been devised [1] which gives the predicted mean vote (PMV) of a large group of subjects according to the following psycho-physical scale:

-3	Cold
-2	Cool
-1	**Slightly cool**
0	Neutral
+1	Slightly warm
+2	Warm
+3	Hot

The PMV value is determined from tables given in Ref. [1] or from the following equation.

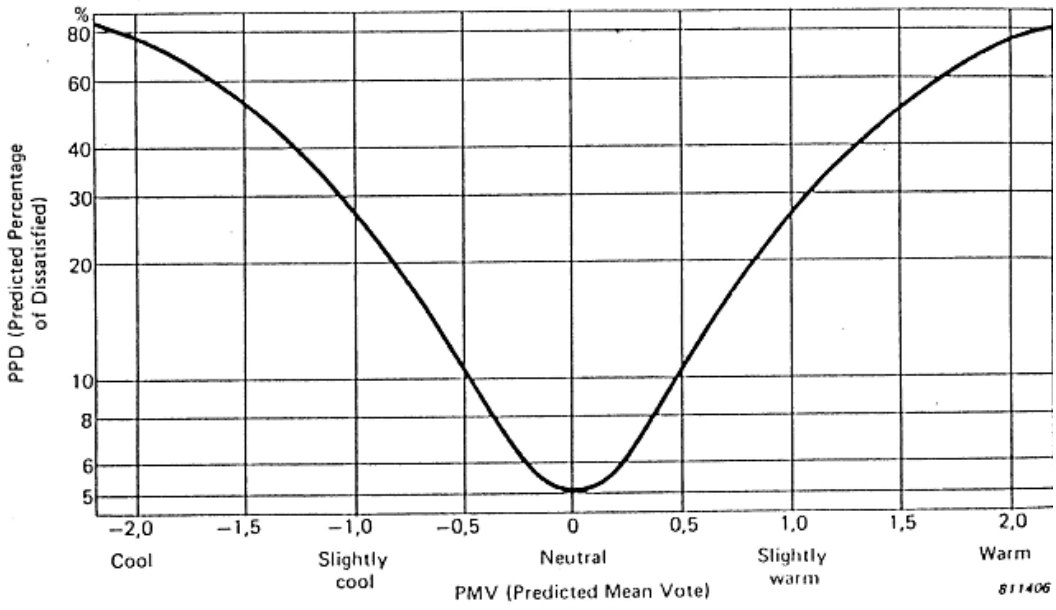

Fig. 4. The relationship between PPD (Predicted Percentage of dissatisfied) and PMV (Predicted Mean Vote)

The predicted percentage of dissatisfied (PPD), may then be estimated from Fig.4. When PMV is set to zero the comfort equation is established.
Fig.4 Is based on studies comprising a group of 1300 subjects. As mentioned earlier, 5% is the lowest percentage of dissatisfied which can be expected. The PPD value is an appropriate and easily understood expression for the quality of a given thermal environment.

The PMV-PPD index has now been suggested by ISO (DIS 7730) in a standard for evaluating moderate thermal environments. It has been recommended to use the limits

$$0,5 < PMV < 0,5 \quad PPD < 10\% \qquad (22)$$

for an acceptable thermal environment. The same range has also been adopted by the ASHRAE standard (or thermal environments and in a new proposal from NKB (Nordic Committee on Building regulations). In both standards the limits are however not specified directly In PMV-values but as a corresponding operative temperature interval depending on the given combination of clothing and activity.

2. General description of the Melexis MLX90247 [18]

The MLX90247family sensors are thermopile sensors IC which detects very small amounts of heat radiation. The sensors consist of a membrane with a thermopile on top of it.
The hot junctions of the thermopile are positioned near the center of the membrane and the cold junctions above the bulk silicon edge.
Due to the low thermal conductivity of the membrane, absorbed heat will cause the temperature to increase more at the center of the membrane than at the edge above the bulk.
This temperature difference is converted to an electric potential by the thermo-electric effect in the thermopile junctions. No supply voltage is needed.
The MLX90247DSG sensor IC is integrated together with a PTC thermistor. The thermopile sensor is grounded at the middle point, so that the output common-mode voltage is at ground potential. Using grounded thermopile sensor gives improved EMC susceptibility in some applications.
The MLX90247DSE sensor IC is packaged together with a 100k NTC chip thermistor. The sensor and thermistor can be used independent of each other if desired, as the thermopile potential is floating. This type of thermistor has better sensitivity than the PTC types, but must be used in smaller ambient ranges. Typical applications are ear thermometers or other medical equipment.
The MLX90247DSA sensor IC is integrated together with a PTC thermistor. The sensor and thermistor can be used independent of each other if desired, as the thermopile potential is floating.

3. General description of the Melexis MLX90601B [18]

In addition to the small amount of components like the sensor, ASIC etc there are also 2 RC protection circuits on the IROUT and TEMPOUT pins. This allows the module to be used in automotive environments. The Object temperature information is available at the IROUT pin. The ambient temperature information is available on the TEMPOUT pin. The resolution of the output D/A converter is 8bit. The output drivers have a maximum output voltage of 4.5V when the maximum calibrated temperature is reached. If the ambient temperature is out of the calibrated temperature range, the correct object temperature cannot be calculated. For applications where the ambient temperature can rise above the maximum calibrated temperature, the ambient temperature output must be monitored to make sure the object temperature is valid.

Next to the temperature outputs there is also a relay driver output. The relay driver has a threshold that is pre-set to 50 °C, with a hysteresis of 5 °C. Note that this module has no SPI interface connector available.

If the user wants to reconfigure this type of module, this can be done with the EVB board and a special test clip.

4. General description of the Melexis MLX90601KZA-BKA [18]

The sensor and the MLX90313 ASIC are placed on a flexible substrate. This allows the sensor to be bent in any direction. This may greatly simplify fitting in the module into the application.
The module has a 10 pole connector, which has all relevant interconnections to the ASIC. There are 2 temperature signals which are preset to provide analog output voltage. The Object temperature information is available at the IROUT pin. The ambient temperature information is available on the TEMPOUT pin. The resolution of the output D/A converter is 8bit. The output drivers have a maximum output voltage of 4.5V when the maximum calibrated temperature is reached.
If the ambient temperature is out of the calibrated temperature range, the correct object temperature cannot be calculated. For applications where the ambient temperature can rise above the maximum calibrated temperature, the ambient temperature output must be monitored to make sure the object temperature is valid.
The flex modules all have the SPI interface available. Next to reading the temperature information, the SPI interface also allows changing the module's settings and calibration.
The temperature as read by the SPI interface will not be equal to the temperature presented at the analog outputs. Refer to SPI interface description for details.
Next to the temperature outputs there is also a relay driver output. The relay driver has a threshold that is pre-set to 95°C, with a hysteresis of 5°C.

5. General description of the Melexis EVB90601 Configuration board[18]

The EVB90601 Configuration board is designed to support the MLX90601 based Infrared Thermometer modules. The hardware board acts as an interface between the USB port of a PC and the module's SPI interface. Power for the module and EVB board come from the computer USB port.

For example the MLX90601C Infrared Thermometer Module can be configured using the configuration board and software. The hardware board acts as an interface between the RS-232 computer link and the module's SPI interface. Also it supplies the supply voltages to the module. The accompanying software will greatly simplify the configuration of the module. It allows the user to change output options, use other temperature ranges, save and retrieve configuration settings to disk, set-up the comparators and more. For all inside information of the MLX90313 programmable IR sensor interface, please refer to the MLX90313 datasheet